NORSAR

NORSAR Scientific Report No. 1-2000/2001

Semiannual Technical Summary

1 April - 30 September 2000

Frode Ringdal (ed.)

Kjeller, November 2000

SECURITY CLASSIFICATION OF THIS PAGE

REPORT DOCUMENTATION PAGE

Form Approved OMB No. 0704-0188

1a. REPORT SECURITY CLASSIFICATION Unclassified	1b. RESTRICTIVE MARKINGS Not applicable
2a. SECURITY CLASSIFICATION AUTHORITY Not Applicable	3. DISTRIBUTION / AVAILABILITY OF REPORT Approved for public release; distribution unlimited
2b. DECLASSIFICATION / DOWNGRADING SCHEDULE	
4. PERFORMING ORGANIZATION REPORT NUMBER(S) Scientific Rep. 1-2000/2001	5. MONITORING ORGANIZATION REPORT NUMBER(S) Scientific Rep. 1-2000/2001
6a. NAME OF PERFORMING ORGANIZATION NORSAR 6b. OFFICE SYMBOL *(If applicable)*	7a. NAME OF MONITORING ORGANIZATION HQ/AFTAC/TTS
6c. ADDRESS *(City, State, and ZIP Code)* Post Box 51 N-2027 Kjeller, Norway	7b. ADDRESS *(City, State, and ZIP Code)* Patrick AFB, FL 32925-6001
8a. NAME OF FUNDING / SPONSORING ORGANIZATION Advanced Research Projects Agency/NTPO 8b. OFFICE SYMBOL *(If applicable)* NMRO/NTPO	9. PROCUREMENT INSTRUMENT IDENTIFICATION NUMBER Contract No. F08650-96-C-0001
8c. ADDRESS *(City, State, and ZIP Code)* 1515 Wilson Blvd., Suite 720 Arlington, VA 22209	10. SOURCE OF FUNDING NUMBERS PROGRAM ELEMENT NO. R&D PROJECT NO NORSAR Phase 3 TASK NO SOW Task 5.0 WORK UNIT ACCESSION NO. Sequence No. 004A2
11. TITLE *(Include Security Classification)* Semiannual Technical Summary, 1 April - 30 September 2000	
12. PERSONAL AUTHOR(S)	
13a. TYPE OF REPORT Scientific Summary 13b. TIME COVERED FROM 1 Apr TO 30 Sep 00 14. DATE OF REPORT *(Year, Month, Day)* 2000 Nov 15. PAGE COUNT 129	
16. SUPPLEMENTARY NOTATION	

17. COSATI CODES			18. SUBJECT TERMS *(Continue on reverse if necessary and identify by block number)*
FIELD	GROUP	SUB-GROUP	
8	11		NORSAR, Norwegian Seismic Array

19. ABSTRACT *(Continue on reverse if necessary and identify by block number)*

This Semiannual Technical Summary describes the operation, maintenance and research activities at the Norwegian Seismic Array (NORSAR) , the Norwegian Regional Seismic Array (NORES), the Arctic Regional Seismic Array (ARCES) and the Spitsbergen Regional Array for the period 1 April - 30 September 2000. Statistics are also presented for additional seismic stations, which through cooperative agreements with institutions in the host countries provide continuous data to the NORSAR Data processing Center (NDPC). These stations comprise the Finnish Regional Seismic Array (FINES), the Hagfors array in Sweden and the regional seismic array in Apatity, Russia.

(cont.)

20. DISTRIBUTION / AVAILABILITY OF ABSTRACT ☐ UNCLASSIFIED/UNLIMITED ☐ SAME AS RPT. ☐ DTIC USERS	21. ABSTRACT SECURITY CLASSIFICATION
22a. NAME OF RESPONSIBLE INDIVIDUAL Major William S. Jones	22b. TELEPHONE *(Include Area Code)* (407) 494-7985 22c. OFFICE SYMBOL AFTAC/TTS

DD Form 1473, JUN 86 *Previous editions are obsolete.* SECURITY CLASSIFICATION OF THIS PAGE

Abstract (cont.)

Beginning 1 January 1999, the responsibility for funding the operational activities of the seismic field systems and the Norwegian National Data Center (NDC) has been taken over by the Norwegian Government, with the understanding that the funding of IMS-related activities will gradually be arranged through the CTBTO/PTS. Research activities described in this report, as well as transmission of selected data to the United States NDC, are continuing to be funded by the United States Department of Defense.

The NOA Detection Processing system has been operated throughout the period with an average uptime of 99.85%. A total of 2670 seismic events have been reported in the NOA monthly seismic bulletin for April through September 2000. The performance of the continuous alarm system and the data transmission to AFTAC has been satisfactory. Processing of requests for full NOA and regional array data on magnetic tapes and through electronic transmission has progressed according to established schedules.

This Semiannual Report also presents statistics from operation of the Regional Monitoring System (RMS). The RMS has been operated in a limited capacity, with continuous automatic detection and location and with analyst review of selected events of special interest for regional monitoring of Fennoscandia and adjacent regions. Data sources for the RMS have comprised all the regional arrays processed at NORSAR. The Generalized Beamforming (GBF) program continues to be used as a pre-processor to RMS.

On-line detection processing and data recording at the NORSAR Data Processing Center (NDPC) of NORES, ARCES and FINES data have been conducted throughout the period. Data from two small-aperture arrays at sites in Spitsbergen and Apatity, Kola Peninsula, as well as the Hagfors array in Sweden, have also been recorded and processed. Processing statistics for the arrays as well as results of the RMS analysis for the reporting period are given.

The operation of the regional arrays has proceeded normally in the period. Maintenance activities in the period comprise preventive/corrective maintenance as required in connection with all of the NOA subarrays as well as the refurbished ARCES array. Other activities have involved repair of defective electronic equipment, cable repair and work in connection with the SPITS array. During the reporting period, the modifications required for formal certification of the NOA array were completed, and the NOA array was ceritified in August 2000.

A summary of the activities related to the GSETT-3 experiment and experience gained at the Norwegian NDC during the reporting period is provided in Section 4. Norway is now contributing primary station data from two seismic arrays: ARCES and NOA and one auxiliary array (SPITS). These data are being provided to the IDC via the global communications infrastructure (GCI). Continuous data from all three arrays are in addition being transmitted to the US NDC, and continuous data from SPITS are transmitted to the PIDC. Our link to the PIDC is also used to transmit data from the NORES array and the NIL station in Pakistan. The transmission speed of the NORSAR-PIDC link was reduced on 8 March 2000 from 256 Kbps to 128 Kbps.

During September 1999, the ARCES array was upgraded with completely new electronics, under a contract with the Provisional Technical Secretariat (PTS). The ARCES data transmission, which includes the conversion of data to the CD1-format used by the IDC, has continued to be carried out successfully during the period, and ARCES processing at the PIDC has been

proceeding normally after the installation was completed. The ARCES array is now in a testing and evaluation phase, and is expected to be considered for certification during 2001.

The PrepCom has encouraged states that operate IMS-designated stations to continue to do so on a voluntary basis and in the framework of the GSETT-3 experiment until the stations have been certified for formal inclusion in IMS. In line with this, we envisage continuing the provision of data from Norwegian IMS-designated stations in accordance with current procedures.

Summaries of six scientific and technical contributions are presented in Chapter 6 of this report.

Section 6.1 is entitled "Research in regional seismic monitoring". This paper, which was presented at the 22nd Annual Seismic Research Symposium, is a joint effort between Kola Regional Seismological Centre and NORSAR. The paper demonstrates that the regional array network in northern Europe, which comprises stations in Fennoscandia, Spitsbergen and NW Russia provides a detection capability for the European Arctic that is close to $m_b = 2.5$, using the Generalized Beamforming (GBF) method for automatic phase association and initial location estimates.

As part of an "event screening" study, we have assessed the seismicity (i.e. seismic events apart from confirmed nuclear explosions) of the Western Russia/Novaya Zemlya region during the past 25 years. We found an average of less than one seismic event per year exceeding m_b 3.5. Thus, the event occurrence in this region is so low that no event of m_b 3.5 and greater located in this region should be screened out in the IDC screening process. The same consideration could apply in some other regions of the world, and the study of detailed seismicity patterns is an important part of the further screening developments.

In the context of event location calibration, we have analyzed data from the Eurobridge profiling experiment which comprised a 1130 km seismic refraction profile crossing the Baltic Shield in the northwest and the Ukrainian Shield in the southeast. We have also analyzed data from some recent profiling experiments near the Spitsbergen array in order to improve the calibration of this station. Not unexpectedly, the study has demonstrated that the crust and uppermost mantle around the SPITS station is very heterogeneous. However, with the exact travel times available through this study for different azimuths in the range 0-3 degrees, the location and detection processing of local and near-regional events at SPITS will be considerably improved.

Section 6.2 is entitled "Optimized Threshold Monitoring", and was presented at the 22nd Annual Seismic Research Symposium. The main objective of this research is to develop and test a new, advanced method for applying regional seismic array technology to the field of nuclear test ban monitoring. To that end, we have addressed the development and testing of a method for optimized seismic monitoring of an extended geographical region, using a sparse network of regional arrays and three-component stations. We have applied the method to a temporary local network in northern Norway, and demonstrated that such a network can in certain cases be processed with a threshold monitoring capability that approaches that of a high-quality regional array (ARCES), located in the same area as the network. We emphasize that the experiments undertaken so far addresses the monitoring of a site that is within local distance (0-300 km) of the network (or array), and that a high-quality regional array will become progressively more capable than the network as the distance to the target site increases.

We believe that the results described in this paper as well as in earlier contributions demonstrate that the optimized threshold monitoring method has the potential to become an important tool in day-to-day monitoring of seismic activity. By this method, the full resources of the monitoring network will be brought to bear to focus on a specific target site in order to enable monitoring of this site with as high a capability as the network and available calibration information will allow.

Section 6.3 is a study of regional array recordings of signals associated with the accident of the Russian submarine "Kursk" on 12 August, 2000. On that day, signals from two presumed underwater explosions in the Barents Sea were recorded by Norwegian seismic stations. The first of these, at 07.28.27 GMT, was relatively small, measuring 1.5 on the Richter scale. The second explosion, 2 minutes and 15 seconds later, was much more powerful, with a Richter magnitude of 3.5. It soon became clear that these seismic events were associated with the "Kursk" accident, although the exact way in which this accident occurred has not yet been determined.

Using detection data from several arrays in northern Europe, the larger event was located fully automatically by NORSAR's Generalized Beamforming process (GBF) with an estimated location only 14 km from the known position of the submarine. The GBF process is running on-line at NORSAR for the purpose of providing trial epicenters of seismic events in Europe and the European Arctic. Later interactive analysis gave a position that was as close as 5 km from the site of the accident . This high accuracy is due to the travel-time calibration available for the Barents region, as provided by the Fennoscandian/Barents velocity model. The paper also lists a sequence of detected explosions (carried out by the Russian Navy) in the Kursk area during September and October 2000.

The recordings by seismic stations in the IMS network form the only publicly available evidence of the presumed explosions associated with the Kursk accident. This information has been important in contributing to the study of the cause of the accident, although no definite conclusions can be drawn from these recordings alone.

The recording of numerous small explosions during September and October 2000 confirm the value of the IMS stations in monitoring seismic activity in the Barents Sea at very low magnitude levels. These explosions, although their magnitudes were only about 2.0 on the Richter scale, were particularly well recorded by the ARCES array (distance 500 km), while the FINES, SPITS and NORES array also detected many of the events. In addition, the Apatity array station in the Kola Peninsula (not an IMS station) provided useful recordings.

Section 6.4 is a study of synthetic travel times for regional crustal transects across the Barents Sea and the adjacent western continental margin. We have calculated synthetic travel times for the first arrivals along four regional crustal transects across the Barents Sea and the adjacent western continental margin and compared these with the corresponding travel times predicted by the Barents regional velocity model which today is used to locate earthquakes in this area. Along one of the transects, between the spreading axis in the Greenland Sea and SPITS on Svalbard, we have also carried out a sensitivity study concerning the effects of uncertainties in the Moho topography on the calculated travel times.

Depending on the offset, travel time differences of up to 2 - 3 seconds are found when comparing travel time curves from the four transects to the standard 1D model (Barents Sea crustal

model). This reveals that the Barents Sea crustal model needs to be refined in order to fit the velocity structure established along the regional transects. Because most of the observed events in this region are only observable at regional distances, it will be particularly important within this context to address upper mantle velocities, as a basis for Pn travel times.

Section 6.5 describes results from tuning of the Threshold Monitoring processing parameters for IMS stations PDYAR and ARCES. In general, the processing parameters for all stations in the IMS Threshold Monitoring System processing must be tuned for reliable estimation of the detection capability. The IMS array stations PDYAR and ARCES, discussed in this contribution, have recently been incorporated into the pIDC processing (in the case of ARCES, following a complete refurbishment), and therefore need such tuning.

The tuning study requires events with good SNR's, preferably occurring at a range of distances from the stations. This was done by searching the pIDC data base for good SNR events at various distances, and then requesting and receiving the data intervals. More than 30 events were used for the station PDYAR and more than 50 for ARCES, with a large range of epicentral distances in both cases.

The general procedure in the tuning study has been in accordance with the Threshold Monitoring Operations Manual, and has included studies of short-term-averages (STAs) in various frequency bands, SNR as a function of frequency and epicentral distance, effects of beamsteering losses, and evaluation of the number of beams required for a given "worst-case" missteering loss. The results of this study have been communicated to the pIDC and the IDC for operational implementation.

Section 6.6 contains a study of the source properties and focal depth of the M_S 4.2 Revda earthquake of August 17, 1999. This was the strongest of the local and regional earthquakes observed during the Masi-1999 field experiment, described in a previous Semiannual Report, and was in fact the largest seismic event in the Kola Peninsula during the past 20 years.

Full waveform modelling of this event was conducted using two different methods, a precise frequency-wavenumber (f-k) method and the reflectivity method. The main target of the modelling was the dispersed surface waves and the goal was to resolve the 1D crustal shear wave velocity model and the source depth of the Revda event. The paper presents a few selected modelling results pointing out the effect of different source depths and crustal structure. We considered various velocity models in order to fit the observed waveforms. Our final double-couple solution was obtained through a systematic search over mechanism parameter space during the waveform modelling.

From the waveform modelling of the surface waves of the Revda earthquake we conclude that the source depth of the event was deeper than 2.5 km, probably between 4 and 7 km, and that there must be a relatively strong velocity gradient in the uppermost crust.

Frode Ringdal

AFTAC Project Authorization	:	T/6141/NORSAR
ARPA Order No.	:	4138 AMD # 53
Program Code No.	:	0F10
Name of Contractor	:	The Norwegian Research Council (NFR)
Effective Date of Contract	:	1 Oct 1995
Contract Expiration Date	:	31 December 2000
Project Manager	:	Frode Ringdal +47 63 80 59 00
Title of Work	:	The Norwegian Seismic Array (NORSAR) Phase 3
Amount of Contract	:	$ 3,083,528
Contract Period Covered by Report	:	1 April - 30 September 2000

The views and conclusions contained in this document are those of the authors and should not be interpreted as necessarily representing the official policies, either expressed or implied, of the Advanced Research Projects Agency, the Air Force Technical Applications Center or the U.S. Government.

The research presented in this report was supported by the Advanced Research Projects Agency of the Department of Defense and was monitored by AFTAC, Patrick AFB, FL32925, under contract no. F08650-96-C-0001.

Beginning 1 January 1999, the responsibility for funding the operational activities of the seismic field systems and the Norwegian National Data Center (NDC) has been taken over by the Norwegian Government, with the understanding that the funding of IMS-related activities will gradually be arranged through the CTBTO/PTS.

NORSAR Contribution No. 714

Table of Contents

1 Summary

This Semiannual Technical Summary describes the operation, maintenance and research activities at the Norwegian Seismic Array (NOA), the Norwegian Regional Seismic Array (NORES), the Arctic Regional Seismic Array (ARCES) and the Spitsbergen Regional Array (SPITS) for the period 1 April - 30 September 2000. Statistics are also presented for additional seismic stations, which through cooperative agreements with institutions in the host countries provide continuous data to the NORSAR Data Processing Center (NPDC). These stations comprise the Finnish Regional Seismic Array (FINES), the Hagfors array in Sweden and the regional seismic array in Apatity, Russia.

Beginning 1 January 1999, the responsibility for funding the operational activities of the seismic field systems and the Norwegian National Data Center (NDC) has been taken over by the Norwegian Government, with the understanding that the funding of IMS-related activities will gradually be arranged through the CTBTO/PTS. Research activities described in this report, as well as transmission of selected data to the United States NDC, are continuing to be funded by the United States Department of Defense.

The NOA Detection Processing system has been operated throughout the period with an average uptime of 99.85%. A total of 2670 seismic events have been reported in the NOA monthly seismic bulletin for April through September 2000. The performance of the continuous alarm system and the data transmission to AFTAC has been satisfactory. Processing of requests for full NOA and regional array data on magnetic tapes and through electronic transmission has progressed according to established schedules.

This Semiannual Report also presents statistics from operation of the Regional Monitoring System (RMS). The RMS has been operated in a limited capacity, with continuous automatic detection and location and with analyst review of selected events of special interest for regional monitoring of Fennoscandia and adjacent regions. Data sources for the RMS have comprised all the regional arrays processed at NORSAR. The Generalized Beamforming (GBF) program continues to be used as a pre-processor to RMS.

On-line detection processing and data recording at the NORSAR Data Processing Center (NDPC) of NORES, ARCES and FINES data have been conducted throughout the period. Data from two small-aperture arrays at sites in Spitsbergen and Apatity, Kola Peninsula, as well as the Hagfors array in Sweden, have also been recorded and processed. Processing statistics for the arrays as well as results of the RMS analysis for the reporting period are given.

The operation of the regional arrays has proceeded normally in the period. Maintenance activities in the period comprise preventive/corrective maintenance as required in connection with all of the NOA subarrays as well as the refurbished ARCES array. Other activities have involved repair of defective electronic equipment, cable repair and work in connection with the SPITS array. During the reporting period, the modifications required for formal certification of the NOA array were completed, and the NOA array was ceritified in August 2000.

A summary of the activities related to the GSETT-3 experiment and experience gained at the Norwegian NDC during the reporting period is provided in Section 4. Norway is now contributing primary station data from two seismic arrays: ARCES and NOA and one auxiliary array (SPITS). These data are being provided to the IDC via the global communications infrastructure (GCI). Continuous data from all three arrays are in addition being transmitted to the US NDC,

and continuous data from SPITS are transmitted to the PIDC. Our link to the PIDC is also used to transmit data from the NORES array and the NIL station in Pakistan. The transmission speed of the NORSAR-PIDC link was reduced on 8 March 2000 from 256 Kbps to 128 Kbps.

During September 1999, the ARCES array was upgraded with completely new electronics, under a contract with the Provisional Technical Secretariat (PTS). The ARCES data transmission, which includes the conversion of data to the CD1-format used by the IDC, has continued to be carried out successfully during the period, and ARCES processing at the PIDC has been proceeding normally after the installation was completed. The ARCES array is now in a testing and evaluation phase, and is expected to be considered for certification during 2001.

The PrepCom has encouraged states that operate IMS-designated stations to continue to do so on a voluntary basis and in the framework of the GSETT-3 experiment until the stations have been certified for formal inclusion in IMS. In line with this, we envisage continuing the provision of data from Norwegian IMS-designated stations in accordance with current procedures.

Summaries of six scientific and technical contributions are presented in Chapter 6 of this report.

Section 6.1 is entitled "Research in regional seismic monitoring". This paper, which was presented at the 22nd Annual Seismic Research Symposium, is a joint effort between Kola Regional Seismological Centre and NORSAR. The paper demonstrates that the regional array network in northern Europe, which comprises stations in Fennoscandia, Spitsbergen and NW Russia provides a detection capability for the European Arctic that is close to $m_b = 2.5$, using the Generalized Beamforming (GBF) method for automatic phase association and initial location estimates.

As part of an "event screening" study, we have assessed the seismicity (i.e. seismic events apart from confirmed nuclear explosions) of the Western Russia/Novaya Zemlya region during the past 25 years. We found an average of less than one seismic event per year exceeding m_b 3.5. Thus, the event occurrence in this region is so low that no event of m_b 3.5 and greater located in this region should be screened out in the IDC screening process. The same consideration could apply in some other regions of the world, and the study of detailed seismicity patterns is an important part of the further screening developments.

In the context of event location calibration, we have analyzed data from the Eurobridge profiling experiment which comprised a 1130 km seismic refraction profile crossing the Baltic Shield in the northwest and the Ukrainian Shield in the southeast. We have also analyzed data from some recent profiling experiments near the Spitsbergen array in order to improve the calibration of this station. Not unexpectedly, the study has demonstrated that the crust and uppermost mantle around the SPITS station is very heterogeneous. However, with the exact travel times available through this study for different azimuths in the range 0-3 degrees, the location and detection processing of local and near-regional events at SPITS will be considerably improved.

Section 6.2 is entitled "Optimized Threshold Monitoring", and was presented at the 22nd Annual Seismic Research Symposium. The main objective of this research is to develop and test a new, advanced method for applying regional seismic array technology to the field of nuclear test ban monitoring. To that end, we have addressed the development and testing of a method for optimized seismic monitoring of an extended geographical region, using a sparse network of regional arrays and three-component stations. We have applied the method to a temporary local network in northern Norway, and demonstrated that such a network can in certain cases be processed with a threshold monitoring capability that approaches that of a high-quality regional array (ARCES),

located in the same area as the network. We emphasize that the experiments undertaken so far addresses the monitoring of a site that is within local distance (0-300 km) of the network (or array), and that a high-quality regional array will become progressively more capable than the network as the distance to the target site increases.

We believe that the results described in this paper as well as in earlier contributions demonstrate that the optimized threshold monitoring method has the potential to become an important tool in day-to-day monitoring of seismic activity. By this method, the full resources of the monitoring network will be brought to bear to focus on a specific target site in order to enable monitoring of this site with as high a capability as the network and available calibration information will allow.

Section 6.3 is a study of regional array recordings of signals associated with the accident of the Russian submarine "Kursk" on 12 August, 2000. On that day, signals from two presumed underwater explosions in the Barents Sea were recorded by Norwegian seismic stations. The first of these, at 07.28.27 GMT, was relatively small, measuring 1.5 on the Richter scale. The second explosion, 2 minutes and 15 seconds later, was much more powerful, with a Richter magnitude of 3.5. It soon became clear that these seismic events were associated with the "Kursk" accident, although the exact way in which this accident occurred has not yet been determined.

Using detection data from several arrays in northern Europe, the larger event was located fully automatically by NORSAR's Generalized Beamforming process (GBF) with an estimated location only 14 km from the known position of the submarine. The GBF process is running on-line at NORSAR for the purpose of providing trial epicenters of seismic events in Europe and the European Arctic. Later interactive analysis gave a position that was as close as 5 km from the site of the accident . This high accuracy is due to the travel-time calibration available for the Barents region, as provided by the Fennoscandian/Barents velocity model. The paper also lists a sequence of detected explosions (carried out by the Russian Navy) in the Kursk area during September and October 2000.

The recordings by seismic stations in the IMS network form the only publicly available evidence of the presumed explosions associated with the Kursk accident. This information has been important in contributing to the study of the cause of the accident, although no definite conclusions can be drawn from these recordings alone.

The recording of numerous small explosions during September and October 2000 confirm the value of the IMS stations in monitoring seismic activity in the Barents Sea at very low magnitude levels. These explosions, although their magnitudes were only about 2.0 on the Richter scale, were particularly well recorded by the ARCES array (distance 500 km), while the FINES, SPITS and NORES array also detected many of the events. In addition, the Apatity array station in the Kola Peninsula (not an IMS station) provided useful recordings.

Section 6.4 is a study of synthetic travel times for regional crustal transects across the Barents Sea and the adjacent western continental margin. We have calculated synthetic travel times for the first arrivals along four regional crustal transects across the Barents Sea and the adjacent western continental margin and compared these with the corresponding travel times predicted by the Barents regional velocity model which today is used to locate earthquakes in this area. Along one of the transects, between the spreading axis in the Greenland Sea and SPITS on Svalbard,

we have also carried out a sensitivity study concerning the effects of uncertainties in the Moho topography on the calculated travel times.

Depending on the offset, travel time differences of up to 2 - 3 seconds are found when comparing travel time curves from the four transects to the standard 1D model (Barents Sea crustal model). This reveals that the Barents Sea crustal model needs to be refined in order to fit the velocity structure established along the regional transects. Because most of the observed events in this region are only observable at regional distances, it will be particularly important within this context to address upper mantle velocities, as a basis for Pn travel times.

Section 6.5 describes results from tuning of the Threshold Monitoring processing parameters for IMS stations PDYAR and ARCES. In general, the processing parameters for all stations in the IMS Threshold Monitoring System processing must be tuned for reliable estimation of the detection capability. The IMS array stations PDYAR and ARCES, discussed in this contribution, have recently been incorporated into the pIDC processing (in the case of ARCES, following a complete refurbishment), and therefore need such tuning.

The tuning study requires events with good SNR's, preferably occurring at a range of distances from the stations. This was done by searching the pIDC data base for good SNR events at various distances, and then requesting and receiving the data intervals. More than 30 events were used for the station PDYAR and more than 50 for ARCES, with a large range of epicentral distances in both cases.

The general procedure in the tuning study has been in accordance with the Threshold Monitoring Operations Manual, and has included studies of short-term-averages (STAs) in various frequency bands, SNR as a function of frequency and epicentral distance, effects of beamsteering losses, and evaluation of the number of beams required for a given "worst-case" missteering loss. The results of this study have been communicated to the pIDC and the IDC for operational implementation.

Section 6.6 contains a study of the source properties and focal depth of the M_S 4.2 Revda earthquake of August 17, 1999. This was the strongest of the local and regional earthquakes observed during the Masi-1999 field experiment, described in a previous Semiannual Report, and was in fact the largest seismic event in the Kola Peninsula during the past 20 years.

Full waveform modelling of this event was conducted using two different methods, a precise frequency-wavenumber (f-k) method and the reflectivity method. The main target of the modelling was the dispersed surface waves and the goal was to resolve the 1D crustal shear wave velocity model and the source depth of the Revda event. The paper presents a few selected modelling results pointing out the effect of different source depths and crustal structure. We considered various velocity models in order to fit the observed waveforms. Our final double-couple solution was obtained through a systematic search over mechanism parameter space during the waveform modelling.

From the waveform modelling of the surface waves of the Revda earthquake we conclude that the source depth of the event was deeper than 2.5 km, probably between 4 and 7 km, and that there must be a relatively strong velocity gradient in the uppermost crust.

Frode Ringdal

2 Operation of International Monitoring System (IMS) Stations in Norway

2.1 PS27 — Primary Seismic Station NOA

The average recording time was 99.85% as compared to 99.93% for the previous reporting period.

Table 2.1.1 lists the reasons for and times of the main outages in the reporting period.

Date	Time	Cause
13 May	1319 - 1914	Hardware failure NDPC
31 May	0849 - 0931	Maintenance NDPC

Table 2.1.1. *The major downtimes in the period 1 April - 30 September 2000.*

Monthly uptimes for the NORSAR on-line data recording task, taking into account all factors (field installations, transmissions line, data center operation) affecting this task were as follows:

April	:	99.99%
May	:	99.11%
June	:	100.00%
July	:	99.99%
August	:	100.00%
September	:	100.00%

J. Torstveit

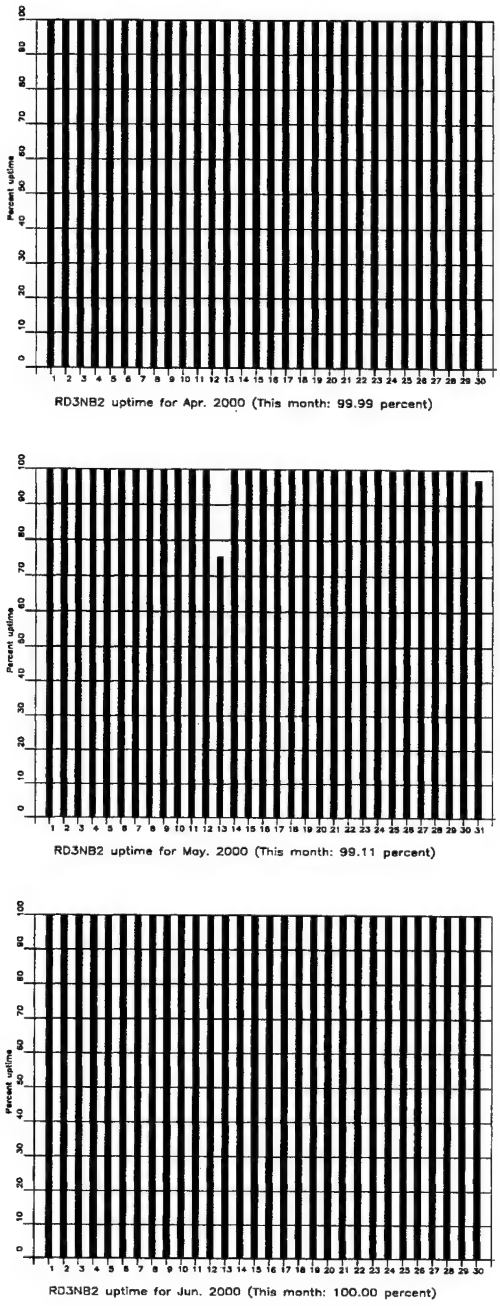

Fig. 2.1.1. *The figure shows the uptime for the data recording task, or equivalently, the availability of NOA data in our tape archive, on a day-by-day basis, for the reporting period. (Page 1 of 2, Apr-Jun 2000).*

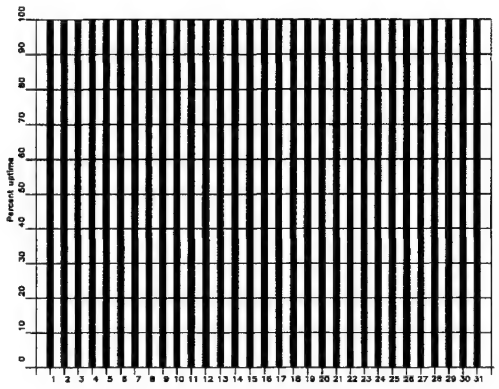

RD3NB2 uptime for Jul., 2000 (This month: 99.99 percent)

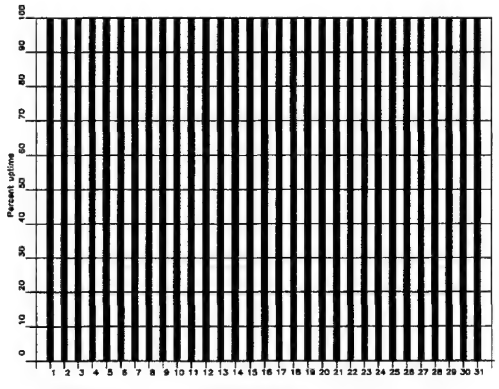

RD3NB2 uptime for Aug. 2000 (This month: 100.00 percent)

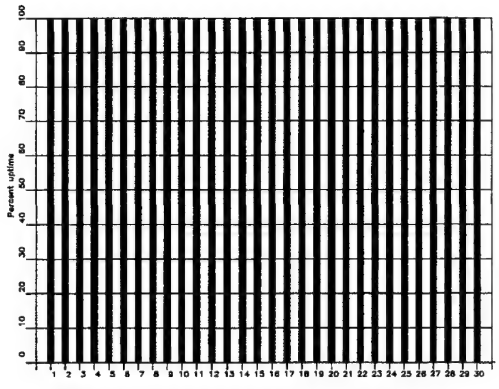

RD3NB2 uptime for Sep. 2000 (This month: 100.00 percent)

Fig. 2.1.1. *(cont.) (Page 2 of 2, Jul-Sep 2000).*

NOA Event Detection Operation

In Table 2.1.2 some monthly statistics of the Detection and Event Processor operation are given. The table lists the total number of detections (DPX) triggered by the on-line detector, the total number of detections processed by the automatic event processor (EPX) and the total number of events accepted after analyst review (teleseismic phases, core phases and total).

	Total DPX	Total EPX	Accepted Events		Sum	Daily
			P-phases	Core Phases		
Apr	9,445	820	265	63	328	10.9
May	4,796	718	257	71	328	10.6
Jun	9,609	1,046	358	48	406	13.5
Jul	7,124	1,147	671	60	731	23.6
Aug	8,519	1,098	484	88	572	18.5
Sep	9,180	849	250	55	305	10.2
	48,673	5.678	2,285	385	2,670	14.55

Table 2.1.2. *Detection and Event Processor statistics, 1 April - 30 September 2000.*

NOA detections

The number of detections (phases) reported by the NORSAR detector during day 092, 2000, through day 274 , 2000, was 48,673, giving an average of 266 detections per processed day (183 days processed).

B. Paulsen

U. Baadshaug

2.2 PS28 — Primary Seismic Station ARCES

The average recording time was 100% as compared to 94.84% for the previous period.

Monthly uptimes for the ARCESS on-line data recording task, taking into account all factors (field installations, transmission lines, data center operation) affecting this task were as follows:

April	:	100%
May	:	100%
June	:	100%
July	:	100%
August	:	100%
September	:	100%

J. Torstveit

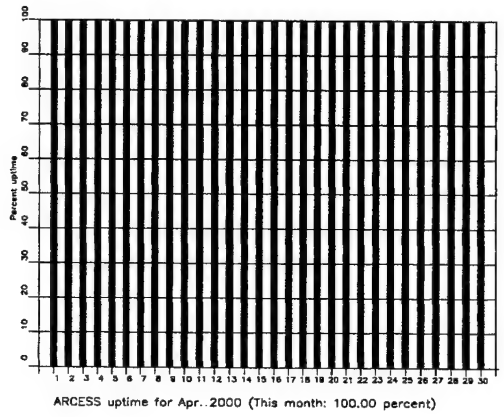

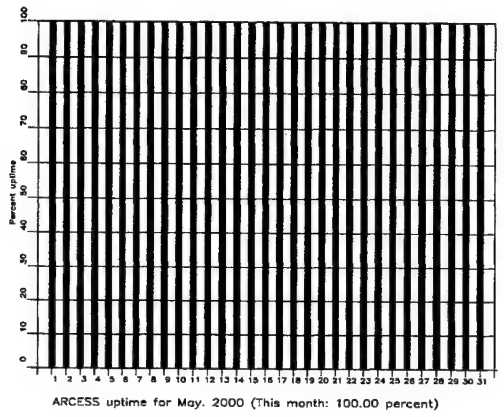

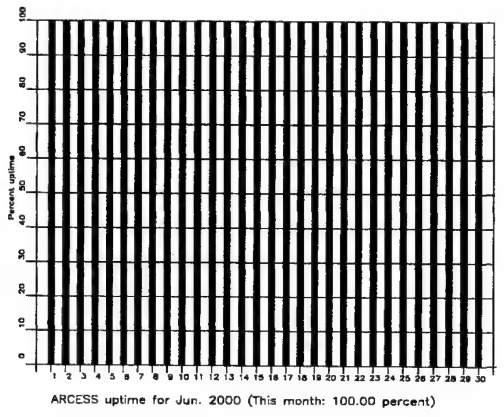

Fig. 2.2.1. *The figure shows the uptime for the data recording task, or equivalently, the availability of ARCES data in our tape archive, on a day-by-day basis, for the reporting period. (Page 1 of 2, Apr-Jun 2000)*

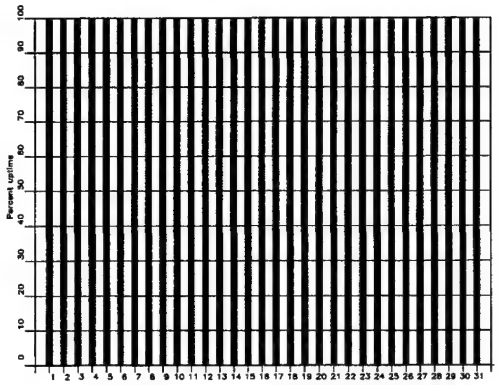

ARCESS uptime for Jul. 2000 (This month: 100.00 percent)

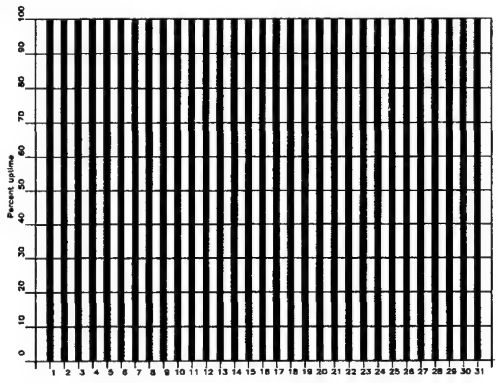

ARCESS uptime for Aug. 2000 (This month: 100.00 percent)

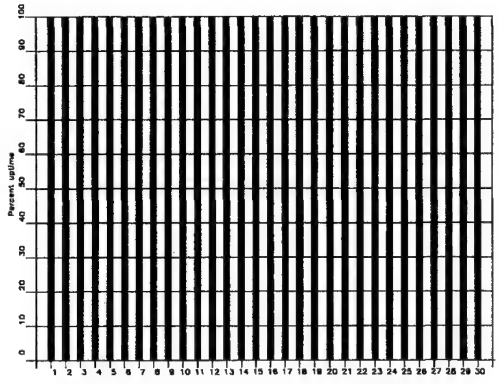

ARCESS uptime for Sep. 2000 (This month: 100.00 percent)

Fig. 2.2.1 *(cont.) (Page 2 of 2, Jul-Sep 2000).*

Event Detection Operation

ARCES detections

The number of detections (phases) reported during day 092, 2000, through day 274, 2000, was 117,396, giving an average of 642 detections per processed day (183 days processed).

Events automatically located by ARCES

During days 092, 2000, through 274, 2000, 7284 local and regional events were located by ARCES, based on automatic association of P- and S-type arrivals. This gives an average of 39.8 events per processed day (183 days processed). 57% of these events are within 300 km, and 85% of these events are within 1000 km.

U. Baadshaug

2.3 AS72 — Auxiliary Seismic Station Spitsbergen

The average recording time was 90.64% as compared to 95.50% for the previous reporting period.

Table 2.3.1 lists the reasons for and time periods of the main downtimes in the reporting period.

Date		Time		Cause
16 Jun	1502	-		NORAC failure
03 Jul		-	0915	

Table 2.3.1. *The main interruptions in recording of Spitsbergen data at NDPC, 1 April - 30 September 2000.*

Monthly uptimes for the Spitsbergen on-line data recording task, taking into account all factors (field installations, transmissions line, data center operation) affecting this task were as follows:

April	:	99.59%
May	:	99.98%
June	:	52.07%
July	:	92.28%
August	:	99.90%
September	:	100.00%

J. Torstveit

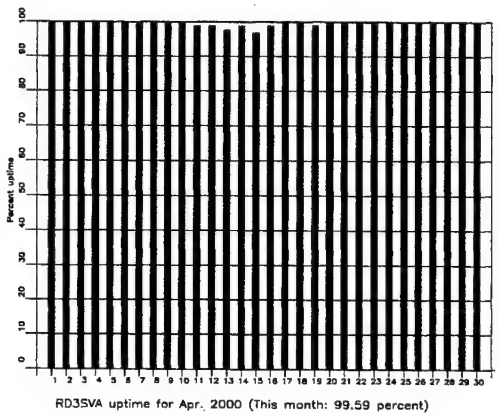

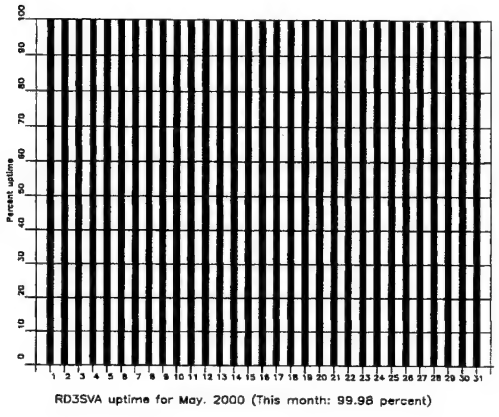

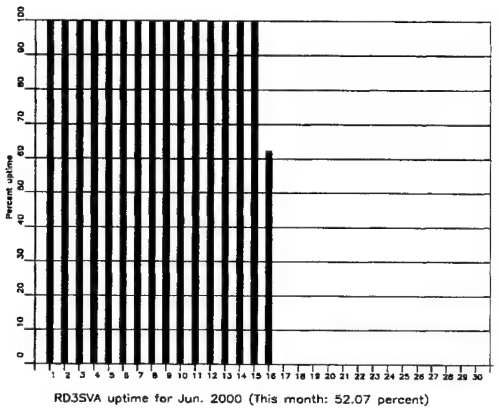

Fig. 2.3.1. *The figure shows the uptime for the data recording task, or equivalently, the availability of Spitsbergen data in our tape archive, on a day-by-day basis, for the reporting period. (Page 1 of 2, Apr-Jun 2000).*

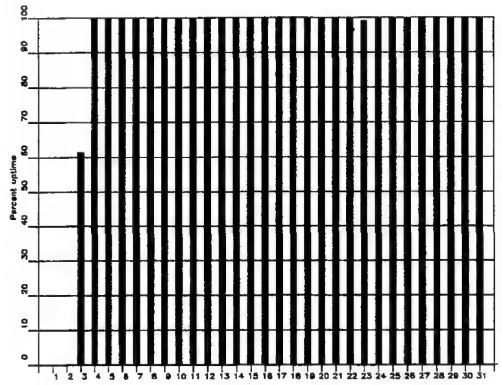

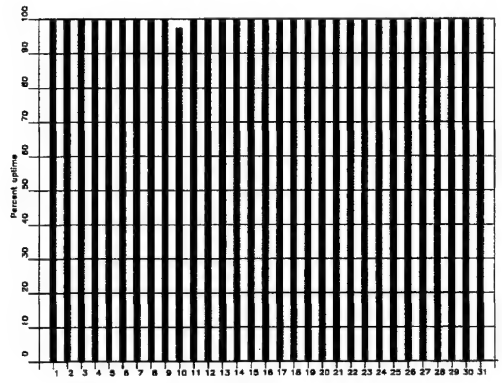

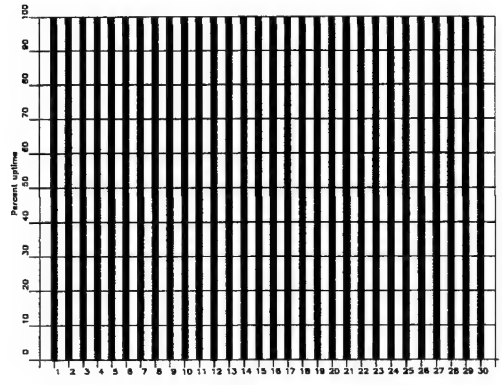

Fig. 2.3.1 *(cont.) (Page 2 of 2, Jul-Sep 2000).*

Event Detection Operation

Spitsbergen array detections

The number of detections (phases) reported from day 092, 2000, through day 274, 2000, was 217,978, giving an average of 1290 detections per processed day (169 days processed).

Events automatically located by the Spitsbergen array

During days 092, 2000, through 274, 2000, 22,560 local and regional events were located by the Spitsbergen array, based on automatic association of P- and S-type arrivals. This gives an average of 133.5 events per processed day (169 days processed). 66% of these events are within 300 km, and 83% of these events are within 1000 km.

U. Baadshaug

2.4 AS73 — Auxiliary Seismic Station Jan Mayen

The IMS auxiliary seismic network will include a three-component station at the Norwegian island of Jan Mayen. The station location given in the protocol to the Comprehensive Nuclear Test-Ban Treaty is 70.9°N, 8.7°W.

The University of Bergen has operated a seismic station at this location since 1970. An investment in the new station at Jan Mayen will be made in due course and in accordance with PrepCom budget decisions. In the meanwhile, NORSAR has, in cooperation with the University of Bergen, investigated technical possibilities of transmitting data from the existing station at Jan Mayen, and a VSAT link for this purpose was installed in April 2000. Data from the existing seismic station at Jan Mayen are now transmitted to the NDC at Kjeller and to the University of Bergen.

S. Mykkeltveit

2.5 IS37 — Infrasound Station at Karasjok

The IMS infrasound network will include a station at Karasjok in northern Norway. The coordinates given for this station are 69.5°N, 25.5°E. These coordinates coincide with those of the primary seismic station PS28.

A site survey for this station was carried out during June/July 1998 as a cooperative effort between the Provisional Technical Secretariat of the CTBTO and NORSAR. Analysis of the data collected at several potential locations for this station in and around Karasjok has been completed. The results of this analysis have lead to a recommendation on the exact location of the infrasound station. Planning work for installation at this site has commenced, and will result in an application to the relevant local authorities to obtain the permissions required in this regard. We expect station installation to take place in the year 2001.

S. Mykkeltveit

2.6 RN49 — Radionuclide Station on Spitsbergen

The IMS radionuclide network will include a station at Longyearbyen on the island of Spitsbergen, at location 78.2°N, 16.4°E. These coordinates coincide with those of the auxiliary seismic station AS72. According to PrepCom decision, this station will also be among those IMS radionuclide stations that will have a capability of monitoring for the presence of relevant noble gases upon entry into force of the CTBT.

A site survey for this station was carried out in August of 1999 by NORSAR, in cooperation with the Norwegian Radiation Protection Authority. The site survey report to the PTS contained a recommendation to establish this station at Platåberget, some 20 km away from the Treaty location. The PrepCom approved the corresponding coordinate change in its meeting in May 2000. The station installation is part of PrepCom's work program for the year 2000, and work is now in progress to prepare the infrastructure for receipt and installation of station equipment (both noble gas and particulate station equipment) during the first half of 2001.

S. Mykkeltveit

3 Operation of Regional Seismic Arrays

3.1 NORES

Average recording time was 92.41 as compared to 98.67 for the previous period.

Table 3.1.1 lists the reasons for and times of the main outages in the reporting period.

Date	Time			Cause
14 May	1544	-		Computer failure field installation
15 May		-	0659	
16 May	2229	-		Computer failure field installation
17 May		-	0802	
24 May	2229	-		Field inst. hit by lightning
02 Jun		-	0919	
04 Jun	0334	-	0813	Computer failure field installation
04 Jun	2103	-		Computer failure field installation
05 Jun		-	0611	
06 Jun	0330	-	0537	Computer failure field installation
09 Jun	2019	-		Computer failure field installation
10 Jun		-	0831	
11 Jun	0943	-		Computer failure field installation
12 Jun		-	1800	
21 Jun	1236	-		Field inst. hit by lightning
22 Jun		-	1359	

Table 3.1.1. *The main interruptions in recording of NORES data at the NDC 1 April - 30 September 2000.*

Monthly uptimes for the NORES on-line data recording task, taking into account all factors (field installations, transmissions line, data center operation) affecting this task were as follows

April	:	100.00%
May	:	72.76%
June	:	81.71%
July	:	100.00%
August	:	100.00%
September	:	100.00%

J. Torstveit

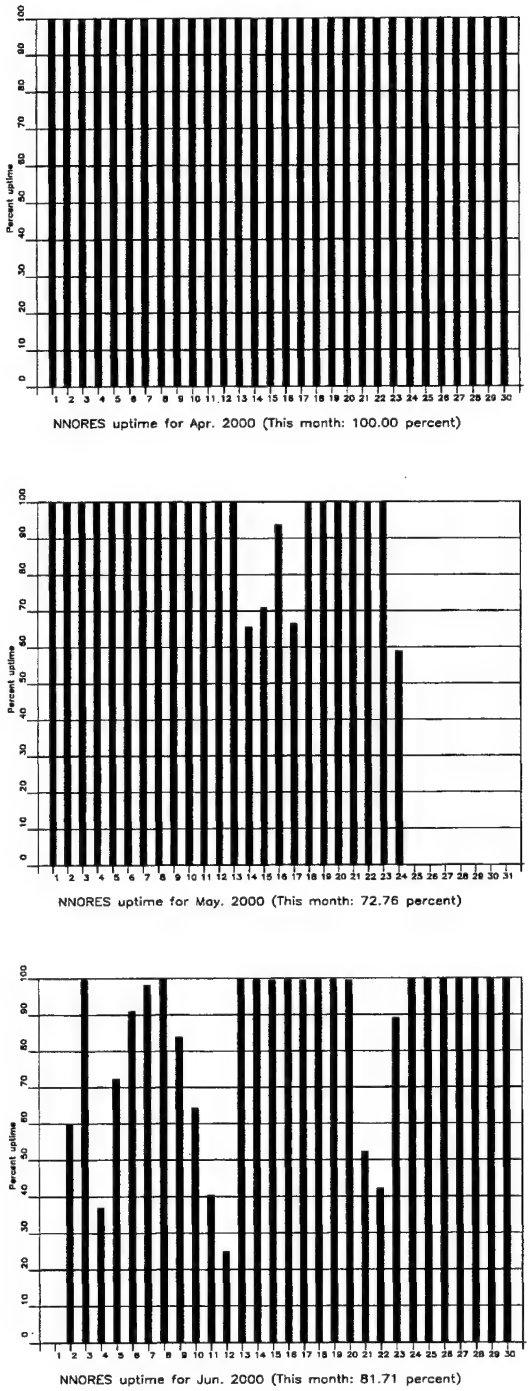

Fig. 3.1.1. *The figure shows the uptime for the data recording task, or equivalently, the availability of NORES data in our tape archive, on a day-by-day basis, for the reporting period (Page 1 of 2, Apr-Jun 2000).*

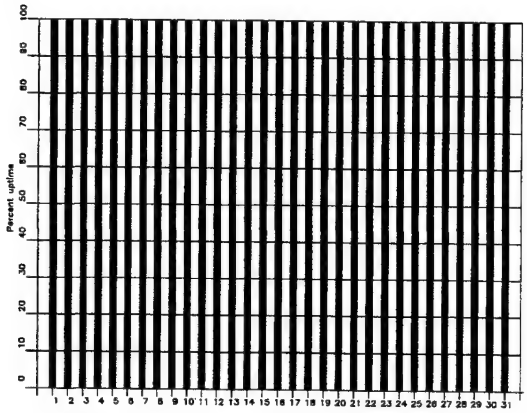

NNORES uptime for Jul. 2000 (This month: 100.00 percent)

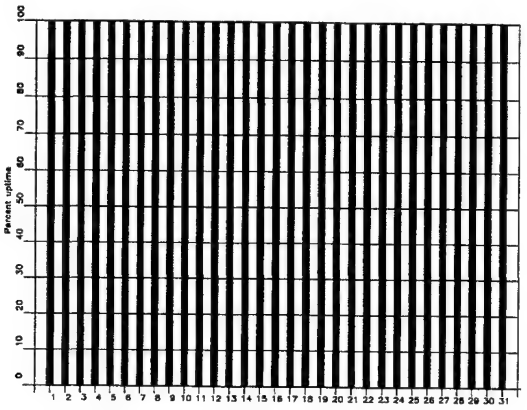

NNORES uptime for Aug. 2000 (This month: 100.00 percent)

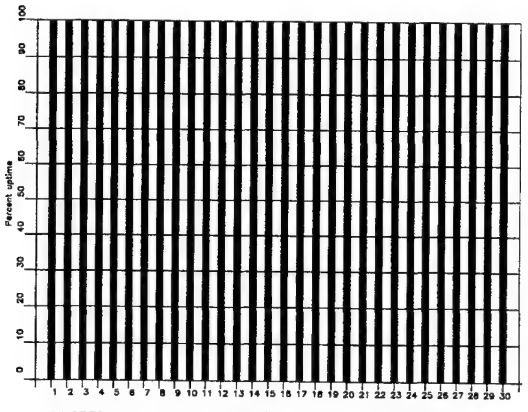

NNORES uptime for Sep. 2000 (This month: 100.00 percent)

Fig. 3.1.1 *(cont.) (Page 2 of 2, Jul-Sep 2000).*

NORES Event Detection Operation

NORES detections

The number of detections (phases) reported from day 092, 2000, through day 274, 2000, was 70,190, giving an average of 401 detections per processed day (175 days processed).

Events automatically located by NORES

During days 092, 2000, through 274, 2000, 5626 local and regional events were located by NORES, based on automatic association of P- and S-type arrivals. This gives an average of 34.1 events per processed day (165 days processed). 55% of these events are within 300 km, and 84% of these events are within 1000 km.

U. Baadshaug

3.2 Hagfors (IMS Station AS101)

The average recording time was 98.49% as compared to 97.02% for the previous reporting period.

Table 3.2.1 lists the reasons for and times of the main outages in the reporting period.

Date	Time	Cause
13 Jun	1432 -	Digitizer failure, corrupted data
14 Jun	- 0714	
11 Aug	1410 -	NORAC failure
13 Aug	- 1751	

Table 3.2.1. *The main interruptions in Hagfors recordings at the NDC, 1 April - 30 September 2000.*

Monthly uptimes for the Hagfors on-line data recording task, taking into account all factors (field installations, transmissions line, data center operation) affecting this task were as follows:

April	:	100.00%
May	:	100.00%
June	:	98.05%
July	:	100.00%
August	:	92.86%
September	:	100.00%

J. Torstveit

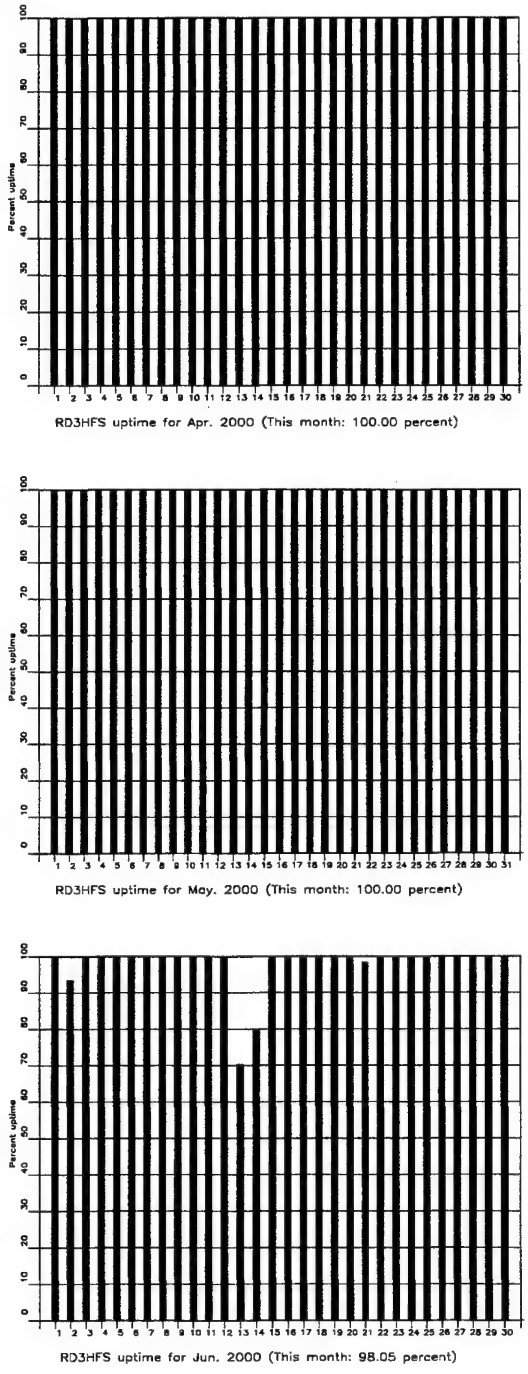

Fig. 3.2.1. *The figure shows the uptime for the data recording task, or equivalently, the availability of Hagfors data in our tape archive, on a day-by-day basis, for the reporting period (Page 1 of 2, Apr-Jun 2000).*

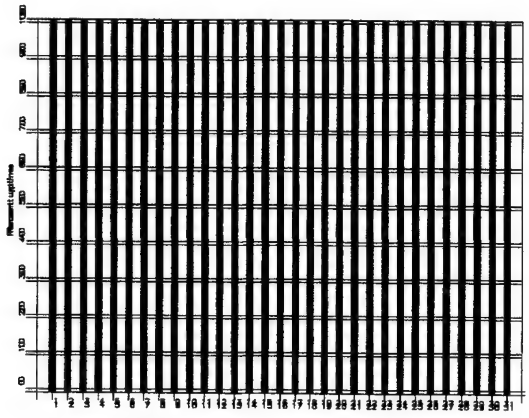

RD3HFS uptime for Jul. 2000 (This month: 100.00 percent)

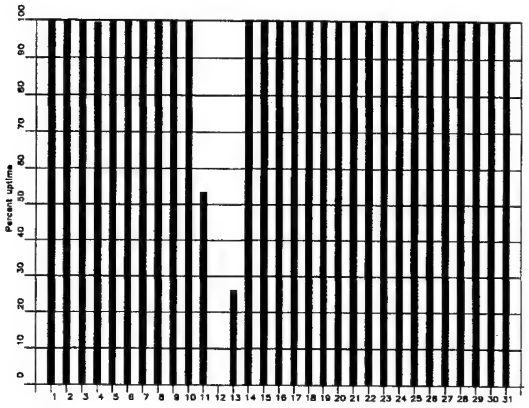

RD3HFS uptime for Aug. 2000 (This month: 92.86 percent)

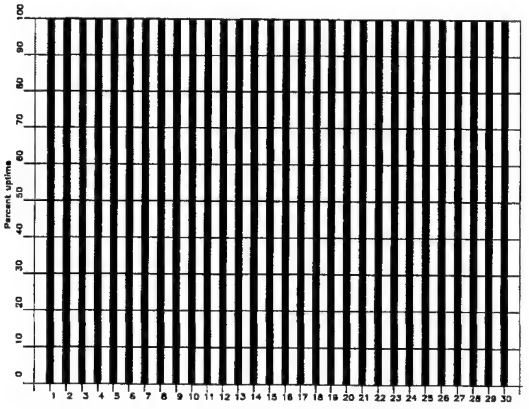

RD3HFS uptime for Sep. 2000 (This month: 100.00 percent)

Fig. 3.2.1 *(cont.) (Page 2 of 2, Jul-Sep 2000).*

Hagfors Event Detection Operation

Hagfors array detections

The number of detections (phases) reported from day 092, 2000, through day 274, 2000, was 62,998, giving an average of 346 detections per processed day (182 days processed).

Events automatically located by the Hagfors array

During days 092, 2000, through 274, 2000, 1927 local and regional events were located by the Hagfors array, based on automatic association of P- and S-type arrivals. This gives an average of 10.6 events per processed day (182 days processed). 56% of these events are within 300 km, and 83% of these events are within 1000 km.

U. Baadshaug

3.3 FINES

The average recording time was 98.94% as compared to 93.67% for the previous reporting period.

Table 3.3.1 lists the reasons for and times of the main outages during the reporting period.

Date	Time	Cause
29 Jun	1706-	Hardware failure in Helsinki
30 Jun	-1400	
19 Jul	1304-	Problems in Helsinki
20 Jul	-1315	

Table 3.3.1. *The main interruptions in FINES recordings at the NDC, 1 April - 30 September 2000.*

Monthly uptimes for the FINES on-line data recording task, taking into account all factors (field installations, transmissions line, data center operation) affecting this task were as follows:

April	:	100.00%
May	:	100.00%
June	:	97.09%
July	:	96.57%
August	:	100.00%
September	:	100.00%

J. Torstveit

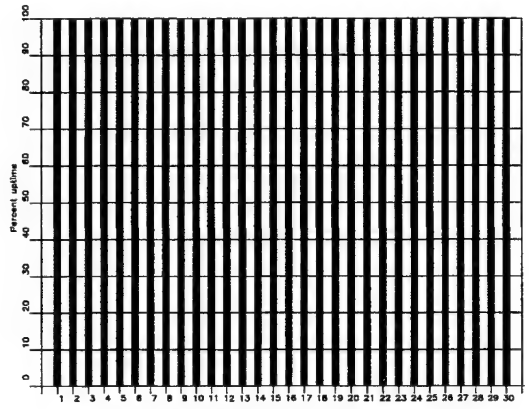

FINESS uptime for Apr. 2000 (This month: 100.00 percent)

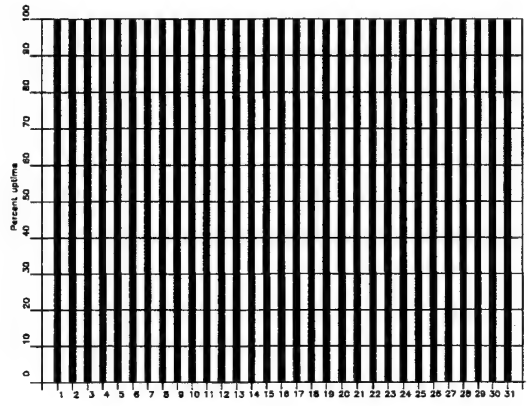

FINESS uptime for May. 2000 (This month: 100.00 percent)

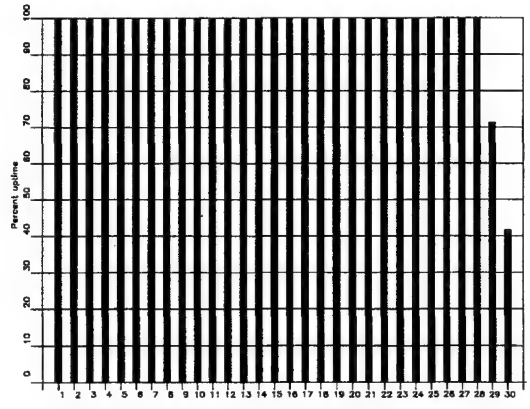

FINESS uptime for Jun. 2000 (This month: 97.09 percent)

Fig. 3.3.1. *The figure shows the uptime for the data recording task, or equivalently, the availability of FINES data in our tape archive, on a day-by-day basis, for the reporting period (Page 1 of 2, Apr-Jun 2000).*

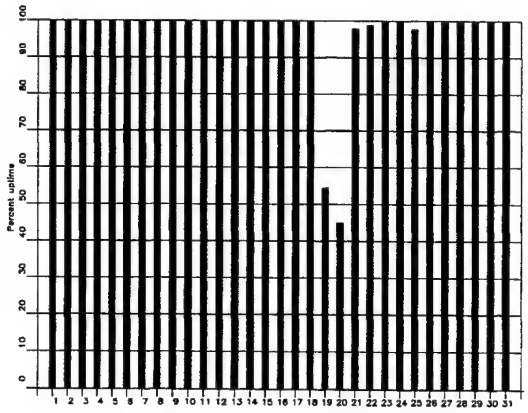

FINESS uptime for Jul. 2000 (This month: 96.57 percent)

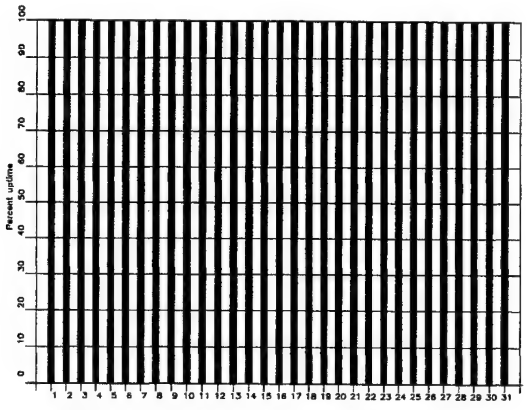

FINESS uptime for Aug. 2000 (This month: 100.00 percent)

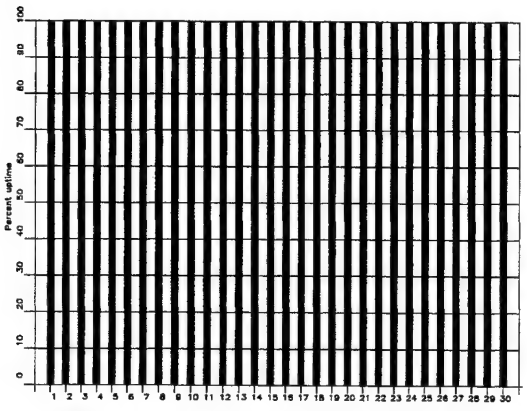

FINESS uptime for Sep. 2000 (This month: 100.00 percent)

Fig. 3.3.1 *(cont.) (Page 2 of 2, Jul-Sep 2000)*

FINES Event Detection Operation

FINES detections

The number of detections (phases) reported during day 092, 2000, through day 274, 2000, was 42,189, giving an average of 231 detections per processed day (183 days processed).

Events automatically located by FINES

During days 092, 2000, through 274, 2000, 2320 local and regional events were located by FINESS, based on automatic association of P- and S-type arrivals. This gives an average of 12.7 events per processed day (183 days processed). 76% of these events are within 300 km, and 89% of these events are within 1000 km.

U. Baadshaug

3.4 Apatity

The average recording time was 96.14% in the reporting period compared to 99.01% during the previous period.

Table 3.4.1 lists the reasons for and times of the main outages during the reporting period

.

Date	Time	Cause
30 May	1004-1040	Problems in Apatity
29 Jun	1656-	Problems in Apatity
30 Jun	-0455	
15 Jul	2357-	Power failure in Apatity
16 Jul	-0427	
28 Jul	0942-1032	Timing problems in Apatity
30 Jul	0030-0057	Problems in Apatity
10 Aug	1325-	Power failure in Apatity
11 Aug	-0443	
14 Aug	1446-1523	Problems in Apatity
01 Sep	1419-1439	Problems in Apatity
13 Sep	1501-	Timing problems in Apatity
14 Sep	-0704	

Table 3.4.1. *The main interruptions in Apatity recordings at the NDC, 1 April - 30 September 2000.*

Monthly uptimes for the Apatity on-line data recording task, taking into account all factors (field installations, transmissions line, data center operation) affecting this task were as follows:

April	:	100.00%
May	:	99.92%
June	:	98.30%
July	:	99.03%
August	:	97.88%
September	:	97.63%

J. Torstveit

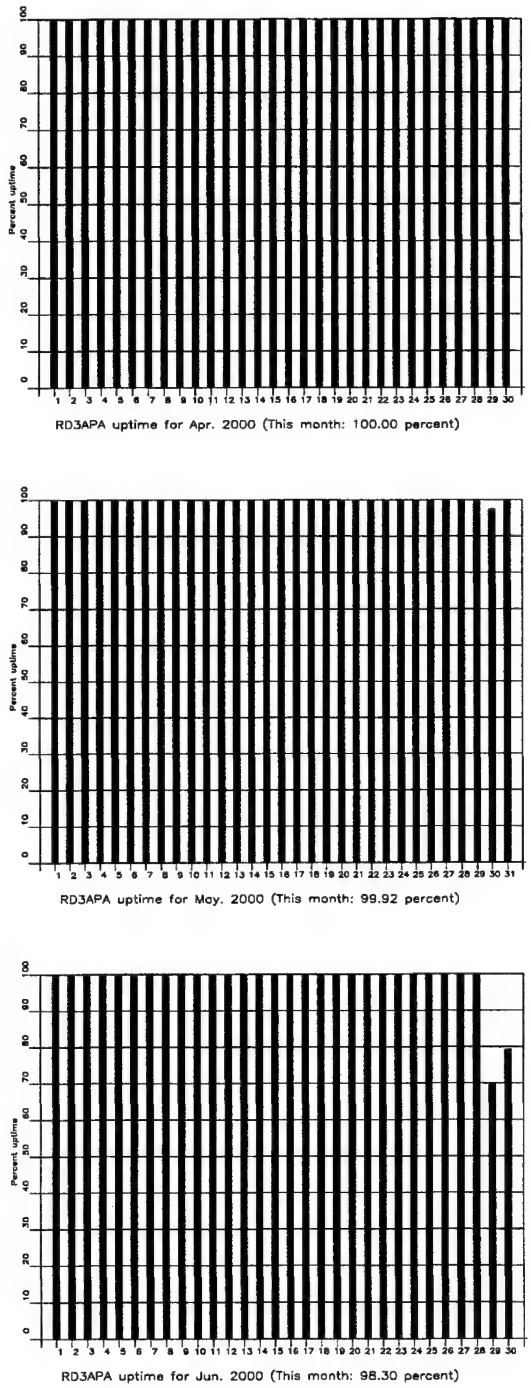

Fig. 3.4.1. *The figure shows the uptime for the data recording task, or equivalently, the availability of Apatity data in our tape archive, on a day-by-day basis, for the reporting period (Page 1 of 2, Apr-Jun 2000).*

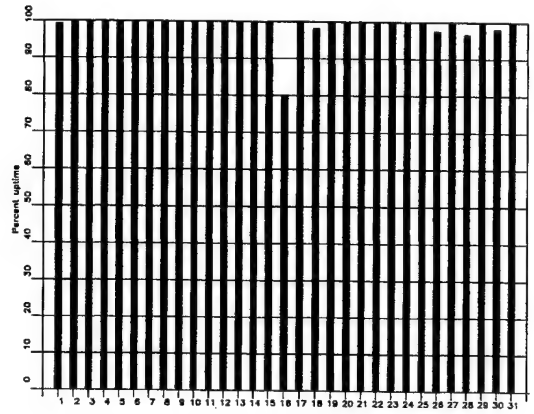

RD3APA uptime for Jul. 2000 (This month: 99.03 percent)

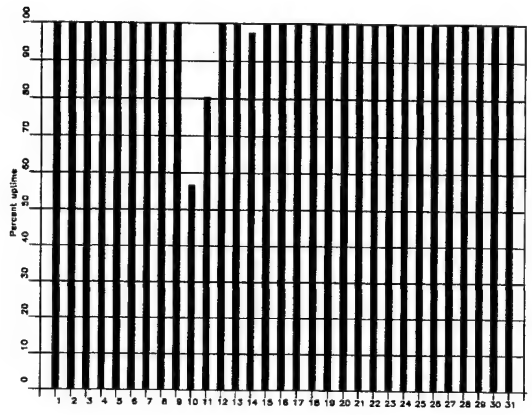

RD3APA uptime for Aug. 2000 (This month: 97.88 percent)

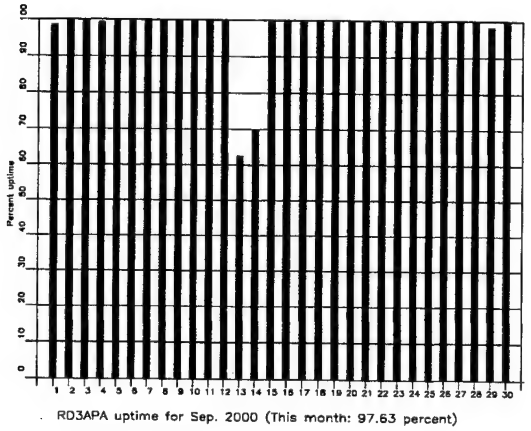

RD3APA uptime for Sep. 2000 (This month: 97.63 percent)

Fig. 3.4.1 *(cont.) (Page 2 of 2, Jul-Sep 2000)*

Apatity Event Detection Operation

Apatity array detections

The number of detections (phases) reported from day 092, 2000, through day 274, 2000, was 191,434, giving an average of 1058 detections per processed day (181 days processed).

As described in earlier reports, the data from the Apatity array are transferred by one-way (simplex) radio links to Apatity city. The transmission suffers from radio disturbances that occasionally result in a large number of small data gaps and spikes in the data. In order for the communication protocol to correct such errors by requesting retransmission of data, a two-way radio link would be needed (duplex radio). However, it should be noted that noise from cultural activities and from the nearby lakes cause most of the unwanted detections. These unwanted detections are "filtered" in the signal processing, as they give seismic velocities that are outside accepted limits for regional and teleseismic phase velocities.

Events automatically located by the Apatity array

During days 092, 2000, through 274, 2000, 1954 local and regional events were located by the Apatity array, based on automatic association of P- and S-type arrivals. This gives an average of 10.9 events per processed day (180 days processed). 41% of these events are within 300 km, and 77% of these events are within 1000 km.

U. Baadshaug

3.5 Regional Monitoring System Operation and Analysis

The Regional Monitoring System (RMS) was installed at NORSAR in December 1989 and was operated at NORSAR from 1 January 1990 for automatic processing of data from ARCES and NORES. A second version of RMS that accepts data from an arbitrary number of arrays and single 3-component stations was installed at NORSAR in October 1991, and regular operation of the system comprising analysis of data from the 4 arrays ARCES, NORES, FINES and GERES started on 15 October 1991. As opposed to the first version of RMS, the one in current operation also has the capability of locating events at teleseismic distance.

Data from the Apatity array were included on 14 December 1992, and from the Spitsbergen array on 12 January 1994. Detections from the Hagfors array were available to the analysts and could be added manually during analysis from 6 December 1994. After 2 February 1995, Hagfors detections were also used in the automatic phase association.

Since 24 April 1999, RMS has processed data from all the seven regional arrays ARCES, NORES, FINES, GERES (until January 2000), Apatity, Spitsbergen, and Hagfors. Starting 19 September 1999, waveforms and detections from the NORSAR array have also been available to the analyst.

Phase and event statistics

Table 3.5.1 gives a summary of phase detections and events declared by RMS. From top to bottom the table gives the total number of detections by the RMS, the number of detections that are associated with events automatically declared by the RMS, the number of detections that are not associated with any events, the number of events automatically declared by the RMS, the total number of events defined by the analyst, and finally the number of events accepted by the analyst without any changes (i.e., from the set of events automatically declared by the RMS).

New criteria for interactive event analysis were introduced from 1 January 1994. Since that date, only regional events in areas of special interest (e.g, Spitsbergen, since it is necessary to acquire new knowledge in this region) or other significant events (e.g, felt earthquakes and large industrial explosions) were thoroughly analyzed. Teleseismic events of special interest are also analyzed.

To further reduce the workload on the analysts and to focus on regional events in preparation for Gamma-data submission during GSETT-3, a new processing scheme was introduced on 2 February 1995. The GBF (Generalized Beamforming) program is used as a pre-processor to RMS, and only phases associated to selected events in northern Europe are considered in the automatic RMS phase association. All detections, however, are still available to the analysts and can be added manually during analysis.

	Apr 00	May 00	Jun 00	Jul 00	Aug 00	Sep 00	Total
Phase detections	89737	91895	97279	124466	139611	149274	692262
- Associated phases	4338	4029	3389	3354	4471	5313	24884
- Unassociated phases	85399	87876	93890	121112	135140	143961	667378
Events automatically declared by RMS	660	678	576	623	790	1003	4330
No. of events defined by the analyst	109	84	68	67	87	118	533

Table 3.5.1. *RMS phase detections and event summary.*

U. Baadshaug
B. Paulsen

4 NDC and Field Activities

4.1 NDC Activitities

NORSAR is functioning as the Norwegian National Data Center (NDC) for treaty verification. Six monitoring stations, comprising altogether 119 field instruments, will be located on Norwegian territory as part of the future IMS as described elsewhere in this report. The four seismic IMS stations are all in operation today, with three of them contributing data to GSETT-3. The infrasound station in northern Norway and the radionuclide station at Spitsbergen will need to be established within the next few years. Data recorded by the Norwegian stations is being transmitted in real time to the Norwegian NDC, and provided to the IDC through the Global Communications Infrastructure (GCI). Norway is connected to the GCI with a frame relay link to Vienna.

Operating the Norwegian IMS stations will require increased resources and additional personnel both at the NDC and in the field. It will require establishing new and strictly defined procedures as well as increased emphasis on regularity of data recording and timely data transmission to the IDC in Vienna. Anticipating these requirements, a new organizational unit has been established at NORSAR to form a core group for the future Norwegian NDC for treaty monitoring. The NDC will carry out all the technical tasks required in support of Norway's treaty obligations. NORSAR will also carry out assessments of events of special interest, and advise the Norwegian authorities in technical matters relating to treaty compliance.

Verification functions

After the CTBT enters into force, the IDC will provide data for a large number of events each day, but will not assess whether any of them are likely to be nuclear explosions. Such assessments will be the task of the States Parties, and it is important to develop the necessary national expertise in the participating countries.

Monitoring the Arctic region

Norway will have monitoring stations of key importance for covering the Arctic, including Novaya Zemlya, and Norwegian experts have a unique competence in assessing events in this region. On several occasions in the past, seismic events near Novaya Zemlya have caused political concern, and NORSAR specialists have contributed to clarifying these issues.

Information received from IDC

The IDC will provide regular bulletins of detected events as well as numerous other products, but will not assess the nature of each individual event. An important task for the Norwegian NDC will be to make independent assessments of events of particular interest to Norway, and to communicate the results of these analyses to the Norwegian Ministry of Foreign Affairs.

International cooperation

After entry into force of the treaty, a number of countries are expected to establish national expertise to contribute to the treaty verification on a global basis. Norwegian experts have been in contact with experts from several countries with the aim to establish bilateral or multilateral

cooperation in this field. One interesting possibility for the future is to establish NORSAR as a regional center for European cooperation in the CTBT verification activities.

NORSAR event processing

The automatic routine processing of NORSAR events as described in NORSAR Sci. Rep. No. 2-93/94, has been running satisfactorily. The analyst tools for reviewing and updating the solutions have been continuously modified to simplify operations and improve results. NORSAR is currently applying teleseismic detection and event processing using the large-aperture NORSAR array as well as regional monitoring using the network of small-aperture arrays in Fennoscandia and adjacent areas.

Certification of PS27

On 28 July 2000 the IMS station PS27-NOA was formally certified. PTS personnel visited the station in June 1998, and carried out a detailed technical evaluation. As a result of this inspection and subsequent discussions between NORSAR and the PTS, and following further discussions of the certification requirements during Working Group B meetings, it was concluded that PS27 needed the following enhancements, which all have been implemented:

- A tamper detector has been emplaced at every seismometer and at the subarray central vaults.
- A centralized authentication process in each subarray as well as at the central array recording facility has been installed.
- Connection to the GCI frame-relay link at the central array facility has been established.
- A Guralp CMG-3T seismometer has been installed at site NC602 in accordance with the certification requirements.

Communication topology

Norway has elected to use the option for an independent subnetwork, which will connect the IMS stations AS72, AS73, PS28, IS37 and RN49 operated by NORSAR to the GCI at NOR_NDC. A contract has been concluded and VSAT antennas have been installed at each station in the network. Under the same contract, VSAT antennas for 6 of the PS27 subarrays have been installed for intra-array communication. The seventh subarray is connected to the central recording facility via a leased land line. The central recording facility is connected directly to the GCI (Basic Topology). All the VSAT communication is functioning satisfactorily.

The Norwegian NDC has been cooperating with several institutions in other countries for transmission of IMS data to the Prototype IDC during GSETT-3. During the reporting period, several changes were made to these arrangements. Details on this can be found in Section 4.2.

Upgrade of PS28

IMS station PS28-ARCES was selected by the PrepCom for hardware upgrade in 1999, and this effort has been concluded. All the digitizers and data acquisition equipment have been replaced. Data from the upgraded array are now being transmitted from the NDC to PIDC, IDC

and US_NDC. PS28 will now undergo a testing and evaluation phase, leading up to certification of this station, perhaps by mid-2001.

Jan Fyen

4.2 Status Report: Norway's Participation in GSETT-3

Introduction

This contribution is a report for the period April - September 2000 on activities associated with Norway's participation in the GSETT-3 experiment, which is now being coordinated by PrepCom's Working Group B. This report represents an update of contributions that can be found in previous editions of NORSAR's Semiannual Technical Summary.

Norwegian GSETT-3 stations and communications arrangements

During the reporting interval 1 April - 30 September 2000, Norway has provided data to the GSETT-3 experiment from the three seismic stations shown in Fig. 4.2.1. The NORSAR array (PS27, station code NOA) is a 60 km aperture teleseismic array, comprised of 7 subarrays, each containing six vertical short period sensors and a three-component broadband instrument. ARCES is a 25-element regional array with an aperture of 3 km, whereas the Spitsbergen array (station code SPITS) has 9 elements within a 1-km aperture. ARCES and SPITS both have a broadband three-component seismometer at the array center.

The intra-array communication for NOA has been achieved by a mixture of land lines and newly installed VSAT links in the following way.

During April and June the NOA data have been transmitted using dedicated land lines as before, but six new VSAT satellite links, based on TDMA technology, and one 64 kps land line were used in a test mode in parallel with the land lines. The land lines were discontinued on 1 June, when transmission via the new VSAT links and the new land line from the various subarrays of NOA had been verified with respect to the appropriate technical requirements. The central recording facility of NOA is at NOR_NDC.

Continuous ARCES data have been transmitted since late September 1999 from the ARCES site to NOR_NDC using a new 64 kbits/s VSAT satellite link, based on BOD technology.

Continuous SPITS data are still transmitted to NOR_NDC using the same arrangements that have existed for several years (terrestrial line to Isfjord Radio at the west coast of Spitsbergen, and a VSAT satellite link from there to NOR_NDC). A modification to this system is expected in early 2001.

Seven-day station buffers have been established at the ARCES and SPITS sites and at all subarray sites, as well as at NOR_NDC for ARCES, SPITS and NOA (central array station buffer).

The NOA and ARCES arrays are primary stations in the GSETT-3 network, which implies that data from these stations are transmitted continuously to the receiving international data center. Since October 1999, these data have been transmitted (from NOR_NDC) via the Global Communications Infrastructure (GCI) to the IDC in Vienna, whereas transmission of the same data to the PIDC was discontinued on 7 February 2000. The SPITS array is an auxiliary station in GSETT-3, and the SPITS data have been available to both the IDC and the PIDC throughout

the reporting period on a request basis via use of the AutoDRM protocol (Kradolfer, 1993; Kradolfer, 1996). The Norwegian stations are thus participating in GSETT-3 with the same status (primary/auxiliary seismic stations) they have in the International Monitoring System (IMS) defined in the protocol to the Comprehensive Nuclear-Test-Ban Treaty. In addition, continuous data from all three arrays are being transmitted to the US NDC.

Uptimes and data availability

Figs. 4.2.2 - 4.2.3 show the monthly uptimes for the Norwegian GSETT-3 primary stations ARCES and NOA, respectively, for the period 1 April - 30 September 2000, given as the hatched (taller) bars in these figures. These barplots reflect the percentage of the waveform data that are available in the NOR_NDC tape archives for these two arrays. The downtimes inferred from these figures thus represent the cumulative effect of field equipment outages, station site to NOR_NDC communication outage, and NOR_NDC data acquisition outages.

Figs. 4.2.2-4.2.3 also give the data availability for these two stations as reported by the PIDC in the PIDC Station Status reports. The main reason for the discrepancies between the NOR_NDC and PIDC data availabilities as observed from these figures is the difference in the ways the two data centers report data availability for arrays: Whereas NOR_NDC reports an array station to be up and available if at least one channel produces useful data, the PIDC uses weights where the reported availability (capability) is based on the number of actually operating channels. On 7 February 2000, NOR_NDC stopped sending ARCES and NOA data directly to the PIDC, and the PIDC receives its ARCES and NOA data via the IDC in Vienna.

Experience with the AutoDRM protocol

NOR_NDC's AutoDRM has been operational since November 1995 (Mykkeltveit & Baadshaug, 1996).

The PIDC started actively and routinely using NOR_NDC's AutoDRM service after SPITS changed its station status from primary to auxiliary on 1 October 1996. For the month of October 1996, the NOR_NDC AutoDRM responded to 12338 requests for SPITS waveforms from two different accounts at the PIDC: 9555 response messages were sent to the "pipeline" account and 2783 to "testbed". Following this initial burst of activity, the number of "pipeline" requests stabilized at a level between 5000 and 7000 per month. Requests from the "testbed" account show large variations. More recently, the number of requests has decreased further. "Pipeline" requests for the reporting period range between 1000 and 1500 per month.

The monthly number of requests by PIDC for SPITS data for the period April - September 2000 is shown in Fig. 4.2.4.

NDC automatic processing and data analysis

These tasks have proceeded in accordance with the descriptions given in Mykkeltveit and Baadshaug (1996). For the period April - September 2000, NOR_NDC derived information on 568 supplementary events in northern Europe and submitted this information to the Finnish NDC as the NOR_NDC contribution to the joint Nordic Supplementary (Gamma) Bulletin, which in turn is forwarded to the PIDC. These events are plotted in Fig. 4.2.5.

Data forwarding for GSETT-3 stations in other countries

NOR_NDC continued to forward data to the PIDC from GSETT-3 primary stations in several countries until 31 December 1999. These included FINESS (Finland), GERESS (Germany) and Sonseca (Spain). From 1 January 2000 data from these stations are sent directly to the IDC in Vienna via new links of the GCI. We are continuing to provide communications for the GSETT-3 auxiliary station at Nilore, Pakistan, through a VSAT satellite link between NOR_NDC and Pakistan's NDC in Nilore. The PIDC as well as the IDC obtain data from the Hagfors array (HFS) in Sweden through requests to the AutoDRM server at NOR_NDC (in the same way requests for Spitsbergen array data are handled, see above). Fig. 4.2.6 shows the monthly number of requests for HFS data from the two PIDC accounts "pipeline" and "test-bed".

Current developments and future plans

NOR_NDC is continuing the efforts towards improvements and hardening of all critical data acquisition and data forwarding hardware and software components, so as to meet future requirements related to operation of IMS stations to the maximum extent possible.

The PrepCom has tasked its Working Group B with overseeing, coordinating, and evaluating the GSETT-3 experiment. The PrepCom has also encouraged states that operate IMS-designated stations to continue to do so on a voluntary basis and in the framework of the GSETT-experiment until such time that the stations have been certified for formal inclusion in IMS. The NOA array was formally certified by the PTS on 28 July 2000, and negotiations on a contract with the PTS in Vienna for operation and maintenance of this station are in progress. This formalizes the responsibility of the PTS for funding of the operation and maintenance of PS27. Provided that adequate funding continues to be made available, we envisage also continuing the provision of data from other Norwegian IMS-designated stations without interruption to the IDC in Vienna.

U. Baadshaug
S. Mykkeltveit
J. Fyen

References

Kradolfer, U. (1993): Automating the exchange of earthquake information. *EOS, Trans., AGU*, 74, 442.

Kradolfer, U. (1996): AutoDRM — The first five years, *Seism. Res. Lett.*, 67, 4, 30-33.

Mykkeltveit, S. & U. Baadshaug (1996): Norway's NDC: Experience from the first eighteen months of the full-scale phase of GSETT-3. *Semiann. Tech. Summ., 1 October 1995 - 31 March 1996*, NORSAR Sci. Rep. No. 2-95/96, Kjeller, Norway.

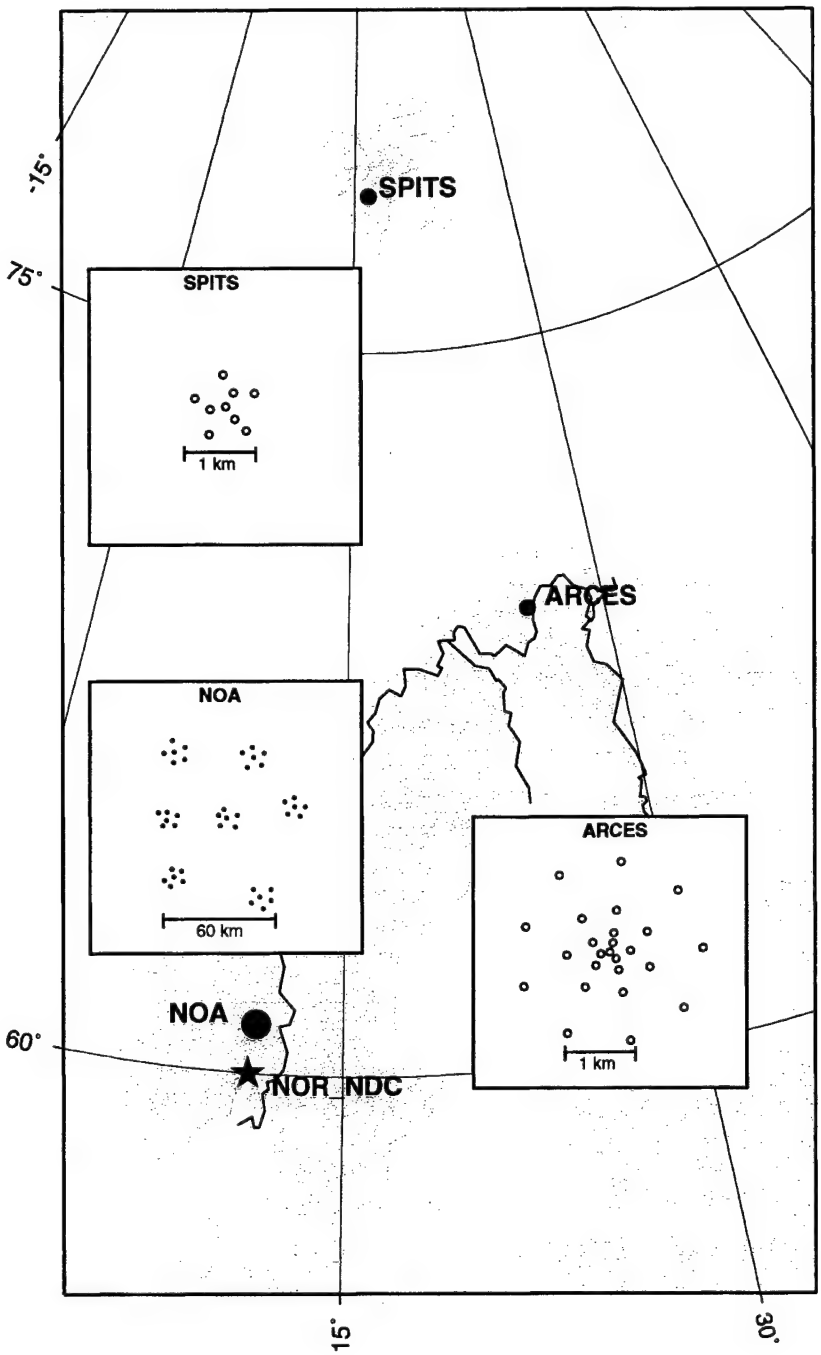

Fig. 4.2.1. The figure shows the locations and configurations of the three Norwegian seismic array stations that have provided data to the GSETT-3 experiment during the period 1 April - 30 September 2000. The data from these stations are transmitted continuously and in real time to the Norwegian NDC (NOR_NDC). The stations NOA and ARCES have participated in GSETT-3 as primary stations, whereas SPITS has contributed as an auxiliary station.

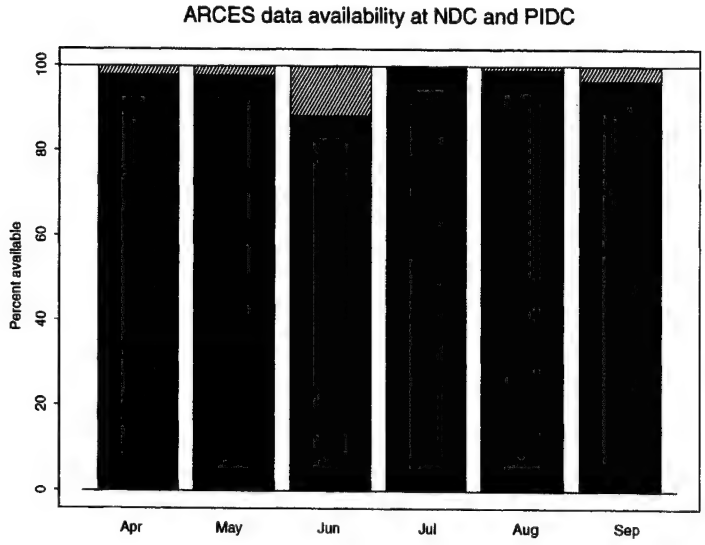

Fig. 4.2.2. The figure shows the monthly availability of ARCES array data for the period April - September 2000 at NOR_NDC and the PIDC. See the text for explanation of differences in definition of the term "data availability" between the two centers. The higher values (hatched bars) represent the NOR_NDC data availability.

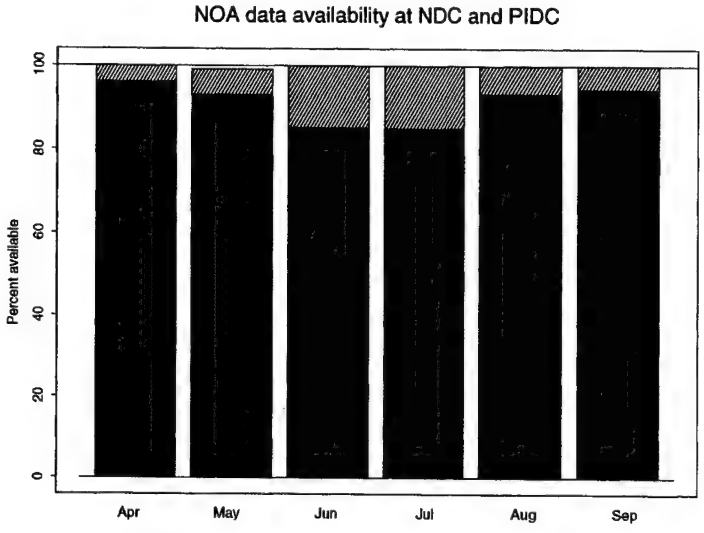

Fig. 4.2.3. The figure shows the monthly availability of NORSAR array data for the period April - September 2000 at NOR_NDC and the PIDC. See the text for explanation of differences in definition of the term "data availability" between the two centers. The higher values (hatched bars) represent the NOR_NDC data availability.

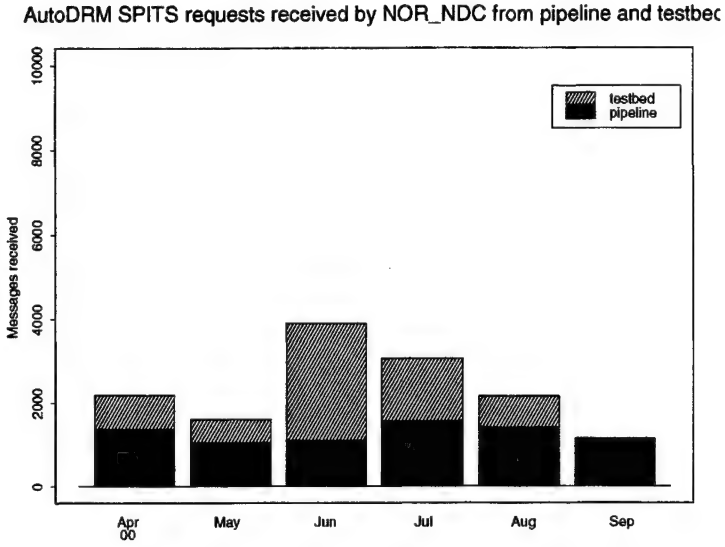

Fig. 4.2.4. The figure shows the monthly number of requests received by NOR_NDC from the PIDC for SPITS waveform segments during April - September 2000.

Reviewed Supplementary events

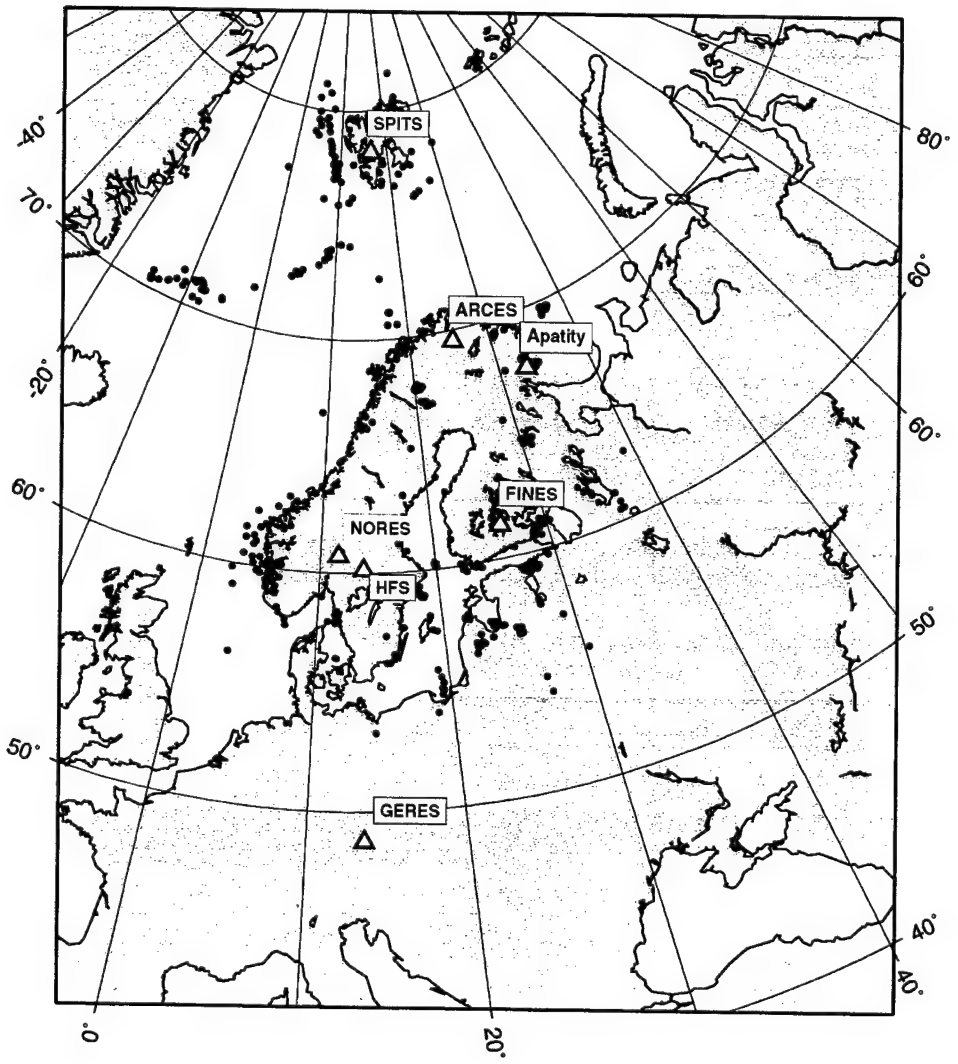

Fig. 4.2.5. The map shows the 568 events in and around Norway contributed by NOR_NDC during April - September 2000 as supplementary (Gamma) events to the PIDC, as part of the Nordic supplementary data compiled by the Finnish NDC. The map also shows the seismic stations used in the data analysis to define these events.

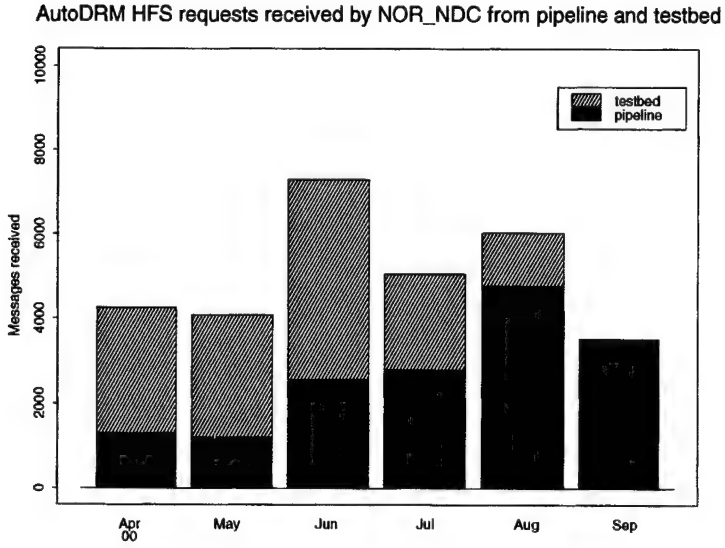

Fig. 4.2.6. The figure shows the monthly number of requests received by NOR_NDC from the PIDC for HFS waveform segments during April - September 2000.

4.3 Field Activities

Activities in the field and at the Maintenance Center

This section summarizes the activities at the Maintenance Center (NMC) Hamar, and includes activities related to monitoring and control of the NORSAR teleseismic array, as well as the NORES, ARCES, FINES, Apatity, Spitsbergen, and Hagfors small-aperture arrays.

Activities also involve preventive and corrective maintenance, planning and activities related to the refurbishment of the NORSAR teleseismic array.

Details for the reporting period are provided in Table 4.3.1 below.

P.W. Larsen
K.A. Løken

Subarray/ area	Task	Date
	April 2000	
NORSAR		April
06C	Installed Guralp broadband seismometer	3/4
02B	Transmission line failure	13/4
02B	VSAT adjustment	17/4
01B	VSAT adjustment	18/4
02C	VSAT adjustment	18/4
03C	VSAT adjustment	25/4
04C	VSAT adjustment	25/4
01A	Replaced authentication device	28/4
NMC	Repair of defective electronic equipment	April
	May 2000	
NORSAR		May
01A	Installated tamper-detector switches in CTV and LPV	24/5
01B	Installated tamper-detector switches in CTV and LPV	25/5
03C	Installed tamper-detector switches in CTV and LPV	29/5
04C	Installed tamper-detector switches in CTV and LPV	30/5

Subarray/ area	Task	Date
06C	Installed tamper-detector switches in CTV and LPV	31/5
ARCES	Replaced Guralp broadband instrument	3-4/5
Hagfors	Replaced DC/DC converter at B1	15/5
NMC	Repair of defective electronic equipment.	May
	June 2000	
NORSAR		June
01A	Tamper-detector adjustment	6/6
01B	Tamper-detector adjustment	6/6
02C	Tamper-detector adjustment	6/6
02B	Tamper-detector adjustment	7/6
03C	Tamper-detector adjustment	7/6
04C	Tamper-detector adjustment	7/6
06C	Tamper-detector adjustment	7/6
02C	Installed tamper-detector switches in CTV and LPV	9/6
02B	Installed tamper-detector switches in CTV and LPV	13/6
01A	Testing of tamper-detector switches with PTS	15/6
01B	Testing of tamper-detector switches with PTS	15/6
03C	Testing of tamper-detector switches with PTS	15/6
04C-01	Replaced surge protection card	21/6
03C-00	Replaced surge protection card	21/6
NORES	Transmission problems NORES-NDC. Repaired HUB unit Repaired power supply units at C4 and C7 Repaired fiber optic card B3 and C5	2/6 3/6 5/6 6/6
Hagfors	Replaced DC/DC converter card at B1 and B2 Replaced RD3 digitizer at C2	30/6

Subarray/ area	Task	Date
NMC	Repair of defective electronic equipment.	June
	July 2000	
NORSAR		July
03C	220 VAC power line failure	1/7
04C	220 VAC power line failure	1/7
02C	220 VAC power line failure	2/7
02B	220 VAC power line failure	3/7
02C	220 VAC power line failure	3/7
04C-01,02,03	Replaced protection diodes	11/7
03C-01,02	Replaced surge protection cards	12/7
04C-03,04	Replaced surge protection cards	12/7
02C-01,03,05	Replaced surge protection cards	14/7
02B-03	Replaced surge protection cards	14/7
02C-03,05,00	Replaced protection diodes	20/7
02C-04	Replaced SP seismometer	24/7
04C-04	Replaced protection diodes	25/7
NMC	Repair of defective electronic equipment.	July
	August 2000	
NORSAR		August
04C-05	Repaired surge protection card	1/8
01B-00	Installed new software in AIM-24 digitizer	1/8
02B-03	Cable failure due to lightning	2/8

Subarray/ area	Task	Date
01A-03	Repaired junction box	2/8
02C	Repaired broken broadband seismometer	11,14 & 16/8
04C	Reinstalled broadband seismometer	18/8
04C-02	Installed new software in AIM-24 digitizer	21/8
02B-03	Splicing of cable	24,25 & 28/8
02B-05	Preventive maintenance of vault, including installation of pole for GPS	30/8
02B-03	Splicing of cable	31/8
NMC	Repair of defective electronic equipment	August
	September 2000	
NORSAR		Sept.
02B-03	Splicing of cable	5,8,18 & 19/9
04C-01	Replaced tamper indicator switch	20/9
04C-02	Installed new software in AIM-24 digitizer	20/9
01B-05	Splicing of cable	21/9
ARCES	Installed tamper-indication switch in the central building. Replaced Guralp broadband instrument	11,12 & 13/9
NMC	Repaird of defective electronic equipment	Sept.

Table 4.3.1. *Activities in the field and the NORSAR Maintenance Center during 1 April - 30 September 2000.*

5 Documentation Developed

Bungum, H., C. Lindholm, A. Dahle, G. Woo, F. Nadim, J.K. Holme, O.T. Gudmestad, T. Hagberg & K. Karthigeyan (2000): New seismic zoning maps for Norway, the North Sea and the U.K., *Seism. Res. Lett.*, 71(6), 687-697.

Faleide, J.I., J. Schweitzer, H. Bungum & E. Møllegaard (2000): Synthetic travel times for regional crustal transects across the Barents Sea and the adjacent western continental margin, **In**: *Semiannual Tech. Summ., 1 April - 30 September 2000*, NORSAR Sci. Rep. 1-2000/2001, Kjeller, Norway.

Fejerskov, M., C. Lindholm, A. Myrvang & H. Bungum (2000): Crustal stress in and around Norway: a compilation of in situ stress observations. *Geol. Soc., London*, Special Publ., 167, 441-449.

Hicks, E., H. Bungum, C. Lindholm & O. Olesen (2000): Seismic activity, inferred crustal stresses and seismotectonics in the Rana region, northern Norway. **In**: I.S. Stewart, J. Sauber & J. Rose (eds.): Glacio-seismotectonics: Ice sheets, crustal deformation and seismicity, *Quaternary Sci. Rev.*, 19, 1423-1436.

Hicks, E., H. Bungum & F. Ringdal (2000): Earthquake location accuracies in Norway based on a comparison between local and regional networks. *Pure Appl. Geophys.*, in press.

Hicks, E., H. Bungum & C. Lindholm (2000): Stress inversions of earthquake focal mechanism solutions from onshore and offshore Norway. *Nor. Geol. Tidsskr.*, in press.

Holden, L., B. Natvig, S. Sannan, P. Abrahamsen & H. Bungum (2000): Modelling spatial and temporal dependencies between earthquakes. *Proc. 6th Int. Geostatistics Conf.*, Cape Town, South Africa, 10-14 April 2000.

Kværna, T. & L. Taylor (2000): Threshold Monitoring processing parameters for IMS stations PDYAR and ARCES, **In**: *Semiannual Tech. Summ., 1 April - 30 September 2000*, NORSAR Sci. Rep. 1-2000/2001, Kjeller, Norway.

Kværna, T., F. Ringdal, J. Schweitzer & L. Taylor (2000): Regional Threshold Monitoring, **In**: *Semiannual Tech. Summ., 1 April - 30 September 2000*, NORSAR Sci. Rep. 1-2000/2001, Kjeller, Norway.

Kværna, T., F. Ringdal, J. Schweitzer & L. Taylor (2000): Regional seismic Threshold Monitoring , Ext. Abstract, 22nd Annual DOD/DOE Seismic Research Symposium, 12-15 Sept 2000.

Lindholm, C., & H. Bungum (2000): Probabilistic seismic hazard: A review of the seismological frame of reference with examples from Norway. *Soil Dyn. Earth. Eng.*, in press.

Mykkeltveit, S., F. Ringdal, C. Lindholm & E. Kremenetskaya (2000): Seismic calibration of the European Arctic, Ext. Abstract, 22nd Annual DOD/DOE Seismic Research Symposium, 12-15 Sept 2000.

Ringdal, F., E. Kremenetskaya, V. Asming, T. Kværna & J. Schweitzer (2000): Research in regional seismic monitoring, Ext. Abstract, 22nd Annual DOD/DOE Seismic Research Symposium, 12-15 Sept 2000.

Ringdal, F., E. Kremenetskaya, V. Asming, T. Kværna & J. Schweitzer (2000): Research in regional seismic monitoring, **In**: *Semiannual Tech. Summ., 1 April - 30 September 2000*, NORSAR Sci. Rep. 1-2000/2001, Kjeller, Norway.

Ringdal, F., T. Kværna & B. Paulsen (2000): Seismic events in the Barents Sea at and near the site of the Kursk submarine accident on 12 August 2000, **In:** *Semiannual Tech. Summ., 1 April - 30 September 2000*, NORSAR Sci. Rep. 1-2000/2001, Kjeller, Norway.

Roth, M., H. Bungum & R.A.W. Haddon (2000): Source properties and focal depth of the M_S 4.2 Revda (Lovozero) earthquake of August 17, 1999, **In**: *Semiannual Tech. Summ., 1 April - 30 September 2000*, NORSAR Sci. Rep. 1-2000/2001, Kjeller, Norway.

Schweitzer, J., F. Krueger, G. Richter, E. Hicks, C. Lindholm & H. Bungum (2000): The 1999 Finnmark seismic field experiment. **In**: J. Dehls & E. Olesen (eds.): *Neotectonics in Norway*, Annual Report 2000.001, 89-97.

6 Summary of Technical Reports / Papers Published

6.1 Research in regional seismic monitoring

(Paper presented at the 22nd Annual Seismic Research Symposium)

Abstract

During the last decades, a network of sensitive regional arrays has been installed in northern Europe in preparation for the global seismic monitoring network under the Comprehensive Nuclear-Test-Ban treaty (CTBT). This regional network, which comprises stations in Fennoscandia, Spitsbergen and NW Russia provides a detection capability for the European Arctic that is close to $m_b = 2.5$, using the Generalized Beamforming (GBF) method for automatic phase association and initial location estimates. We have continued our studies to use data from the regional networks operated by the Kola Regional Seismological Centre (KRSC) and NORSAR to assess the seismicity and characteristics of regional phases of the Barents/Kara Sea region, as well as the application to seismic event screening.

We have studied the seismicity (i.e. seismic events apart from confirmed nuclear explosions) of the Western Russia/Novaya Zemlya region for the past 25 years, and found an average of less than one seismic event per year exceeding m_b 3.5. Thus, the event occurrence in this region is so low that no event of m_b 3.5 and greater located in this region should be screened out in the IDC screening process. The same consideration could apply in some other regions of the world, and the study of detailed seismicity patterns is an important part of the further screening developments.

In discrimination studies, our results for the European Arctic show that the P/S discriminant should be applied with great caution in this region, and further research is required. The regional M_S:m_b discriminant has considerable promise, and the shorter-period energy available in surface waves recorded at regional distances can be exploited in improving the monitoring capabilities during periods with strong interfering surface waves from large distant earthquakes.

We recommend that the current efforts to improve m_b determinations and to reconcile the current m_b values with the "historic" magnitude scale be continued. A project to apply maximum-likelihood techniques to reassess the m_b of past seismic events should be undertaken.

We have analyzed data from the Eurobridge profiling experiment which comprised a 1130 km seismic refraction profile crossing the Baltic Shield in the northwest and the Ukrainian Shield in the southeast. We have investigated in detail observed deviations in P-wave travel times from those predictions by the Fennoscandian crustal and upper mantle velocity model. Our study has revealed several instances of documented timing errors at the various arrays. An important outcome of this study is the development of a method to identify possible timing anomalies at IMS stations. This method could be useful both in validating calibration data and in providing a tool for continuously checking the timing accuracy and consistency of IMS stations.

We have also analyzed data from some recent profiling experiments near the Spitsbergen array in order to improve the calibration of this station. Not unexpectedly, the study has demonstrated that the crust and uppermost mantle around the SPITS station is very heterogeneous. However, with the exact travel times available through this study for different azimuths in the

range 0-3 degrees, the location and detection processing of local and near-regional events at SPITS will be considerably improved.

The location calibration effort will continue to be an important part of our work. The recommendations provided in the paper CTBT/WGB/TL-2/49 should be followed up by the international community, and the progress of this work will be reviewed in a planned workshop in Oslo in 2001.

Objective

This work represents a continued effort in seismic monitoring, with emphasis on studying earthquakes and explosions in the Barents/Kara Sea region, which includes the Russian nuclear test site at Novaya Zemlya. The overall objective is to characterize the seismicity of this region, to investigate the detection and location capability of regional seismic networks and to study various methods for screening and identifying seismic events in order to improve monitoring of the Comprehensive Test Ban Treaty. An important part of the work is contributions toward the international effort to provide regional location calibration of the International Monitoring System.

Research accomplished

Introduction

NORSAR and Kola Regional Seismological Centre (KRSC) of the Russian Academy of Sciences have for many years cooperated in the continuous monitoring of seismic events in North-West Russia and adjacent sea areas. The research has been based on data from a network of sensitive regional arrays which has been installed in northern Europe during the last decade in preparation for the CTBT monitoring network. This regional network, which comprises stations in Fennoscandia, Spitsbergen and NW Russia (see Fig. 6.1.1) provides a detection capability for the Barents/Kara Sea region that is close to $m_b = 2.5$ (Ringdal, 1997).

The research carried out during this effort is documented in detail in several contributions contained in the NORSAR Semiannual Technical Summaries. In the present paper we will limit the discussions to some recent results of interest in the context of applying screening criteria to seismic events in the European Arctic and within the location calibration effort currently underway for the International Monitoring System (IMS). We also report on some recent developments in monitoring mining events in the Kola Peninsula.

Screening

The development of event screening criteria is one of the main tasks of the expert work currently conducted by Working Group B of the Preparatory Commission for the Comprehensive Nuclear-Test-Ban Treaty (CTBT). The purpose of event screening is to "screen out" events that are thought to be consistent with natural causes (such as earthquakes), so that detailed analysis can be focused on those events that are truly of interest for monitoring purposes. The current seismic screening procedure employed at the International Data Centre (IDC) is applied only for seismic events exceeding a m_b threshold of 3.5, and focuses on two criteria: event focal depth and M_s:m_b. These are considered to be the most robust criteria currently available, but have the disadvantage that they are difficult to apply to small events or events recorded only by few stations. Other criteria, such as the high-frequency P/S ratio, hold the promise of being

applicable at much lower event magnitudes, and this is currently an area of active research (see e.g. Ringdal et.al., 2000).

The purpose of screening is not to identify events, but rather to limit as far as possible the number of events that need to be subjected to special analysis. It might be argued that in some regions of the world, seismic events exceeding m_b 3.5 are so infrequent that any particular screening criteria based on signal characteristics may be superfluous. We have studied the region comprising Western Russia and Novaya Zemlya, including the surrounding parts of the Barents and Kara Seas in this perspective. Our recommendation, as detailed below, is that the event occurrence in this region is so low that no event of m_b 3.5 and greater located in this region should be screened out. This would exclude the possibility of accidentally missing events of potential monitoring interest, and at the same time improve confidence that the treaty is adhered to.

Seismicity of the European Arctic

The seismicity of the Barents/Kara sea region has previously been discussed by Ringdal (1997). Nuclear and chemical explosions were conducted at Novaya Zemlya until 1990, and in addition a number of PNEs were carried out in Western Russia until 1988. We have carried out a detailed study of the seismicity of Western Russia, including the Ural Mountains and the Novaya Zemlya region. Our emphasis has been on collecting information on available seismic events (in addition to the confirmed nuclear explosions) for a region bounded by 50-78 deg North, 30-65 deg East, and with m_b of 3.5 or greater. This is of interest in the screening process at the IDC, since the current event screening criteria are applied only to events above this magnitude.

Table 6.1.1: Seismic events with m_b at least 3.5 during 1975-2000 in the region 50-78N, 30-65E. Confirmed nuclear explosions are not included.

No	Date/time	Location	m_b (MLE)	Comment/Reference
1	15.11.78/ 08.30.00	73.40 N, 55.00 E	3.6	Probably chemical explosion, Novaya Zemlya (Ringdal, 1997)
2	10.04.81/ 19.43.33	68.76 N, 36.96 E	4.4	Earthquake, felt in Murmansk, Kola Peninsula
3	01.08.86/ 13.56.38	72.945 N, 56.549 E	4.3	Classified as earthquake by Marshall et.al. (1989)
4	26.02.87/ 00.18.21	60.10N, 60.20 E	4.1	Rockburst in Sevuralboksitruda mine, 50m of tunnel destroyed, 150 cubic m rock volume (VNIMI, 1989)
5	16.04.89/ 06.34.42	67.67 N, 33.73 E	3.5	Earthquake in Kirovsk mine, faulting observed, 3 floors of tunnels (total 200m) destroyed (Kremenetskaya and Asming, 1995)
6	14.05.89/ 11.46.56	50.84 N, 51.24 E	4.3	NEIC/PDE

Table 6.1.1: Seismic events with m_b at least 3.5 during 1975-2000 in the region 50-78N, 30-65E. Confirmed nuclear explosions are not included.

No	Date/time	Location	m_b (MLE)	Comment/Reference
7	28.05.90/ 00.35.48	55.17 N, 58.72 E	4.3	Collapse of Kurbazakskaya mine of Jushnouralboksitruda, 450 000 sq. m area affected (Lomakin and Yunusov, 1993)
8	28.05.90/ 02.41.28	55.17 N, 58.72 E	4.4	See preceding event. Reference: Lomakin and Yunusov (1993)
9	16.06.90/ 12.43.28	68.52 N, 33.09 E	4.0	Earthquake, felt in Murmansk, Kola Peninsula
10	05.01.95/ 12.46.01	59.60 N, 56.65 E	4.5	Collapse at the Silvinit salt mine near Solikamsk. 300 000 sq.m. area affected.
11	10.06.96/ 17.16.47	59.74 N, 43.11 E	3.7	REB (PIDC)
12	13.06.96/ 19.22.38	75.2 N, 56.7 E	3.5	Located by Ringdal et. al. (1997)
13	16.08.97/ 02.11.00	72.510 N, 57.550 E	3.5	Classified as earthquake by Richards and Kim (1997)
14	17.08.99/ 04.44.36	67.885 N, 34.532 E	4.3	Earthquake/collapse, mine Umbozero of Sevredmet, 650 000 sq.m area affected. 50 cubic m rock volume, river changed course
15	18.01.00/ 04.05.32	58.06 N, 49.42 E	3.5	REB (PIDC)

In this compilation, we have used available international bulletins (ISC, USGS/NEIC, PIDC) together with the regional bulletins issued by NORSAR and KRSC. We have re-assessed the m_b estimates, making use of the maximum-likelihood method developed by Ringdal (1986) as well as the regional magnitudes provided by NORSAR and KRSC, adjusted to world-wide m_b. We have attempted to make our magnitude estimates consistent with "historic" world-wide m_b, as opposed to the current values which have been shown to have a slight negative bias relative to the traditional estimates.

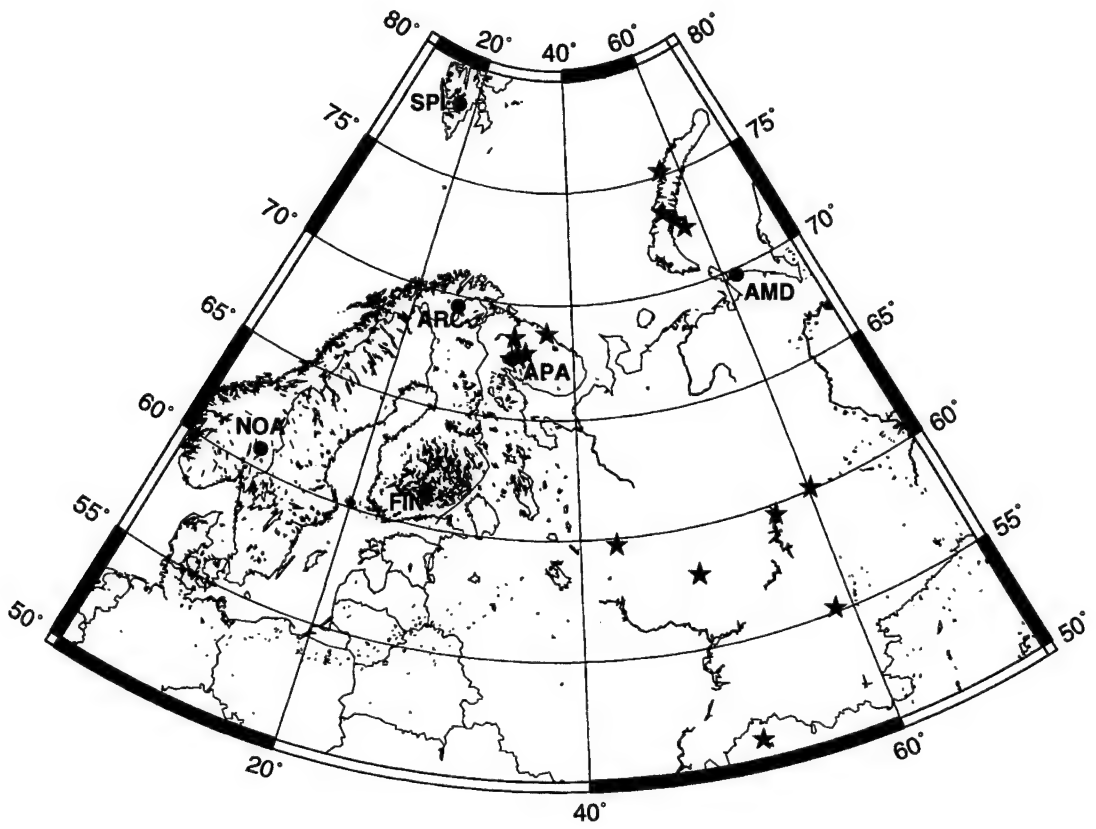

Fig.6.1.1 Map showing the regional network operated by NORSAR and KRSC. The map also shows the location of the events in Table 1, which comprises all known events 1975-2000 (apart from nuclear explosions) with m_b of 3.5 or greater in a region bounded by 50-78 deg North, 30-65 deg East.

The result of this compilation is listed in Table 1, which covers the 25-year time interval 1975-2000 (see also Fig. 6.1.1). Only 15 reported seismic events (not counting confirmed nuclear explosions) have exceeded magnitude 3.5 in this period, i.e. less than one event per year on the average. We note that the detectability of the current global network is sufficiently high so that we consider this catalog to be essentially complete since 1990, but a few small events may certainly have been missed for the earlier years. Nevertheless, the average occurrence of events of m_b=3.5 or greater in this region seems to be at most 1 event per year. It thus appears that any screening of seismic events above magnitude 3.5 in this region is superfluous, so it is currently not necessary to develop screening criteria for this region. This could of course change if the screening is applied at a lower magnitude threshold in the future.

It is interesting to note, as explained in Table 1, that many of the events are associated with mining activity (i.e. collapses, rockbursts or earthquakes inside known mines). This means that true tectonic earthquakes of m_b=3.5 or greater in this region are very rare indeed. Any significant seismic event located by the IDC inside this region should in our opinion be subject to special analysis, as part of the confidence-building process that is essential in CTBT verification.

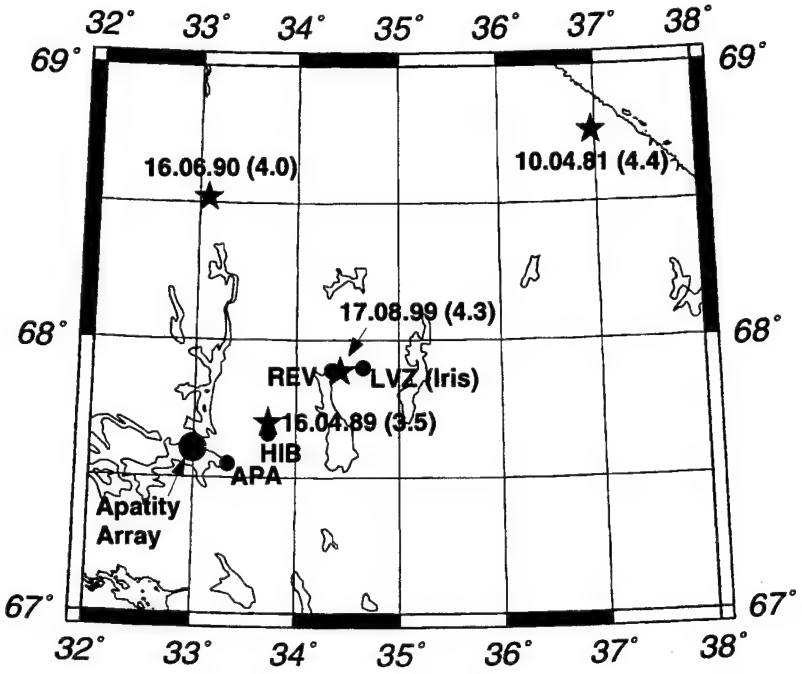

Fig .6.1.2. Station network operated by KRSC in the Kola Peninsula. Two new stations (HIB and REV) have been deployed in 2000. The locations of those seismic events in Table 1 which occurred in the Kola Peninsula are also indicated.

We might note that other parts of the European Arctic have a much higher level of natural seismicity than the Western Russia/Novaya Zemlya region discussed above. For example, there are many significant earthquakes in the intraplate areas of Fennoscandia, and the seismicity is of course even higher along the tectonic plate boundary areas, such as the North Atlantic Ridge, Spitsbergen and the Lomonosov Ridge.

Study of P/S ratios

A paper by Ringdal et. al. (2000) discusses the application of the P/S ratio for discriminating seismic events in the European Arctic. It is shown that the P/S ratios of Novaya Zemlya nuclear explosions measured in the 1-3 Hz filter band scale with magnitude, indicating a need for caution and further research when applying P/S discriminants. Using mainly data from the large NORSAR array, the authors note that observed P/S amplitude ratios in the European Arctic shows large variability for the same source type and similar propagation paths, even when considering closely spaced observation points. This effect is most pronounced at far-regional distances and relatively low frequencies (typically 1-3 Hz), but it is also significant on closer recordings (around 10 degrees) and at higher frequencies (up to about 8 Hz). The conclusion from the study is that the P/S ratio at high frequencies (e.g. 6-8 Hz) shows promise as a discriminant between low-magnitude earthquakes and explosions in the European Arctic, but its application will require further research, including extensive regional calibration and detailed station-source corrections. Such research should also focus on combining the P/S ratio with other short-period discriminant, such as complexity and spectral ratios.

Study of Regional M_s:m_b

A paper by Kremenetskaya et. al. (2000) describes the historical archive of regional long-period data (on analog form) available at KRSC since 1970 for the station APA in Apatity, Kola Peninsula. Since the station APA is situated at a regional distance from the Novaya Zemlya test site, these recordings provide a unique source for studying the performance of M_s:m_b at regional distances for the European Arctic. Selected seismograms from APA have been digitized, and the quality of the analog recordings at this station is demonstrated by comparing recordings from a modern broad-band seismometer at the same place to signals digitized from the analog equipment.

In the paper, it is further shown that the APA surface wave recordings, normalized for distance and magnitude, provide an encouraging degree of separation between earthquakes and explosions in the European Arctic. It is demonstrated that this separation can be achieved in a wide frequency band (at least 10-25 seconds period), and the authors note that this gives promise for applying the M_s:m_b discriminant down to lower magnitudes and at lower signal periods than is possible using teleseismic recordings. They also note that the shorter-period energy available in surface waves recorded at regional distances can be exploited in improving the monitoring capabilities during periods with strong interfering surface waves from large distant earthquakes.

Network developments

Kola network and earthquake studies

On 17 August 1999, only 4 hours after the large earthquake in Turkey, an earthquake of m_b=4.3 occurred in a mining area in Revda, Kola Peninsula. This is the largest seismic event in Kola for almost 20 years, and has been the subject of considerable interest. The earthquake, which was associated with a large mine collapse in the Lovozero Massif, was preceded by numerous foreshocks several months in advance, and was followed by several aftershocks

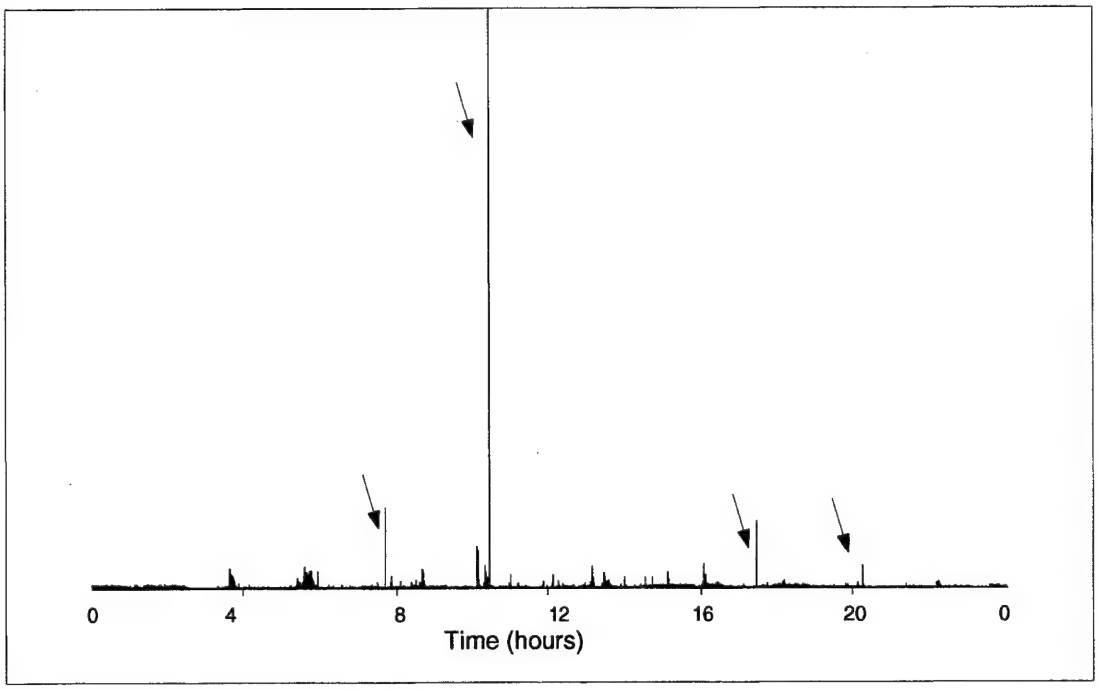

Fig 6.1.3. STA trace (filter 4-12 Hz) for station REV in the Kola Peninsula. The data cover the 24 hours of 12 April 2000. The arrows mark detected microearthquakes in the Revda mine (magnitudes 0.0-1.0)

KRSC installed in early 2000 3-component seismic stations in the Khibiny Massif (HIB) and in Revda (REV) - see Fig. 6.1.2. The station at Revda was deployed for the purpose of studying the aftershocks of the 17 August 1999 event, and the station in Khibiny had as its main purpose to enable improved locations and origin times for seismic events in the Khibiny mines. An example of a one-day STA trace for the Revda station is shown in Fig. 6.1.3. This trace could be seen as a simple version of the Threshold Monitoring technique applied to this mining site, and most of the peaks on the trace are in fact associated with the Revda mine. Examples of recordings for two of the peaks are shown in Fig. 6.1.4 (for an aftershock at Revda and a mining explosion in Olenegorsk).

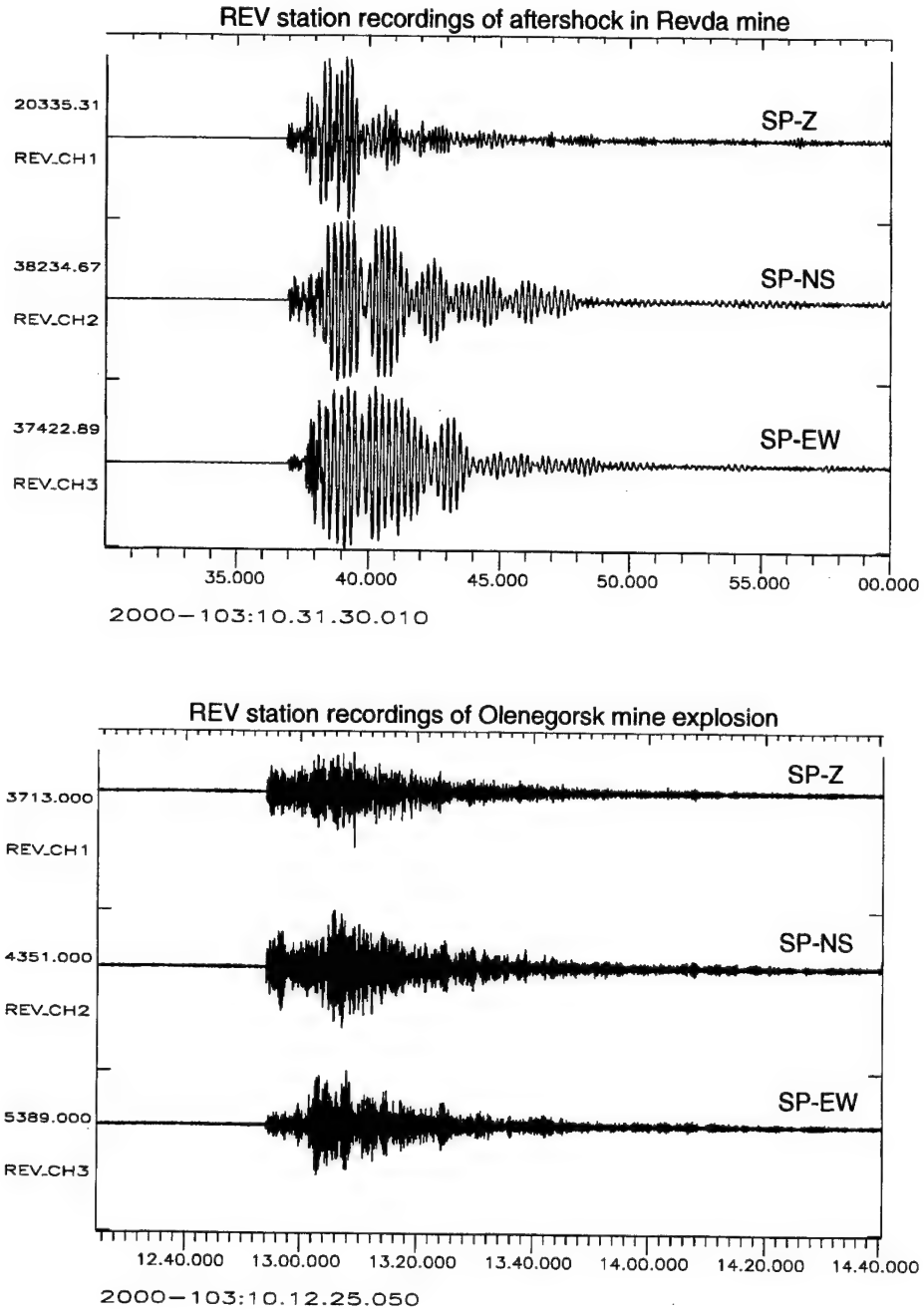

Fig.6.1.4. REV 3-component short period recordings on an aftershock in the Revda mine (top) and a mining explosion in the Olenegorsk mine 50 km away (bottom). Note the strong Rg phases on the top traces.

Amderma station

The seismic station at Amderma is a key monitoring resource for the Kara Sea region. In 1999, KRSC installed a broadband 3-component seismometer (Guralp) at this site, and implemented a dial-up mechanism to enable rapid retrieval of data of special interest. An example of data retrieved in this way for the 17 August 1999 Revda event is shown in Fig. 6.1.5. We note the strong surface waves recorded for this event, and in particular the high Rayleigh wave energy in the frequency band near 0.1 Hz (10 seconds period) is noteworthy. The prominence of energy at these high frequencies and their possible usefulness in regional M_s:m_b discrimination has been pointed out by Kremenetskaya et al (2000). Otherwise, the traces show a feature which is common for many paths in the European Arctic: The Pn and Sn phase are dominant at frequencies above 2 Hz, whereas the Lg phase is strongest near 1 Hz.

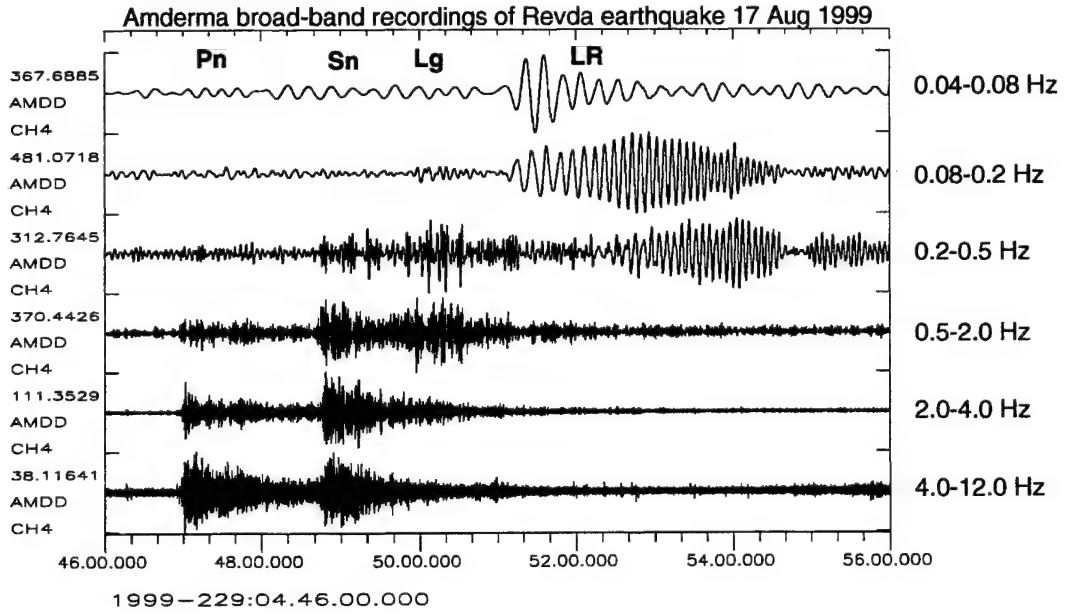

Fig.6.1.5. Amderma broad-band vertical channel recording of the Revda earthquake of 17 August 1999. The traces are filtered in several different bands. The distance from the event to the station is approximately 10 degrees.

Location Calibration

Eurobridge profile

We have analyzed data from the Eurobridge profiling experiment which comprised a 1130 km seismic refraction profile crossing the Baltic Shield in the northwest and the Ukrainian Shield in the southeast. There were three series of shots, one in 1995 and two in 1996. Observations of these explosions at the Fennoscandian arrays provide an opportunity to check the accuracy of the travel-time tables in use at NORSAR for Fennoscandia. At the same time, these refraction

shots provide a useful extension to the pIDC ground-truth database. P-phases from most of the Eurobridge shots were observed at the FINES, HAGFORS and NORES arrays, and even at the more distant ARCES array as many as 12 out of the 29 events were seen. We have investigated in detail observed deviations in P-wave travel times from those predictions by the Fennoscandian crustal and upper mantle velocity model. Our study has revealed several instances of documented timing errors at the various arrays. Even when accounting for these timing errors, there remains a considerable scatter in the travel times as compared to the theoretical model. The interpretation of these anomalies in terms of crustal and upper mantle structure is not obvious. An important outcome of this study is the development of a method to identify possible timing anomalies at IMS stations. This method could be useful both in validating calibration data and in providing a tool for continuously checking the timing accuracy and consistency of IMS stations.

Calibrating the Spitsbergen array

We have analyzed data from some recent profiling experiments near the Spitsbergen array in order to improve the calibration of this station. Data from airgun shots in the water as well as small underwater explosions of 25 to 50 kg conventional explosives could be observed at distances up to 350 km when using the double-beam technique for SNR enhancement. Not unexpectedly, the study has demonstrated that the crust and uppermost mantle around the SPITS station is very heterogeneous. However, with the exact travel times available through this study for different azimuths in the range 0-3 degrees, the location and detection processing of local and near-regional events at SPITS will be considerably improved. This is particularly important because there are large numbers of local events recorded at SPITS every day, and a correct location and phase identification will help eliminate these phases from interfering in the GBF process for network association and event definition analysis.

Oslo Workshop on location calibration

A workshop was held in Oslo, Norway during 20-24 March 2000 in support of the global seismic event location calibration effort currently being undertaken by PrepCom's Working Group B in Vienna. Among the contributions were recent results provided by NORSAR and KRSC of our joint regional calibration effort in the European Arctic, which has resulted in much improved travel-time models for the Barents region. We show that the Barents model, which is known to give accurate locations in the Fennoscandian and NW Russia area, can be successfully applied to the more general northern Eurasia region. The recommendations from this workshop have been provided in the paper CTBT/WGB/TL-2/49, issued by Working Group B of the CTBTO Preparatory Commission.

Conclusions and recommendations

The seismicity of the Western Russia/Novaya Zemlya region is very low, with an average of less than one seismic event per year exceeding m_b 3.5. Thus, the event occurrence in this region is so low that no event of m_b 3.5 and greater located in this region should be screened out in the IDC event screening process. This would exclude the possibility of accidentally missing events of potential monitoring interest, and at the same time allow for special analysis of all significant events in this region. This would contribute to improved confidence building with respect to treaty adherence. We consider that the same consideration could apply in some other regions

of the world, and the study of detailed seismicity patterns is an important part of the further screening developments.

Our results for the European Arctic show that the P/S discriminant should be applied with great caution in this region, and further research is required. The regional M_S:m_b discriminant has considerable promise, and the shorter-period energy available in surface waves recorded at regional distances can be exploited in improving the monitoring capabilities during periods with strong interfering surface waves from large distant earthquakes.

We recommend that the current efforts to improve m_b determinations and to reconcile the current m_b values with "historic" magnitude scale be continued. A project to apply maximum-likelihood techniques to reassess the m_b of past seismic events should be undertaken.

The location calibration effort will continue to be an important part of our work. The recommendations provided in the paper CTBT/WGB/TL-2/49 should be followed up by the international community, and the progress of this work will be reviewed in a planned workshop in Oslo in 2001.

F. Ringdal
E. Kremenetskaya, KRSC
V. Asming, KRSC
T. Kværna
J. Schweitzer

Sponsored by DoD, Contract No. F08650-06-C-0001

References

Kremenetskaya, E. and V. Asming (1995). Induced seismicity in the Khibiny Massif (Kola Peninsula). *PAGEOPH, 145 No. 1,* 29-37.

Kremenetskaya, E.Asming, V. and F. Ringdal (1999). Seismic location calibration of the Barents region. *Semiannual Technical Summary 1 October 1998 - 31 March 1999,* NORSAR Sci. Rep. 2-98/99, Kjeller, Norway.

Lomakin,V.S. and Ph.Ph.Yunusov (1993). Effective methods for seismological observations in mines. In: *Prediction and prevention of rock bursts in ore deposit.* Apatity, Kola Science Centre, Mining Institute, pp.73-76 (in Russian).

Kremenetskaya, E.Asming, V. and F. Ringdal (2000). Study of regional surface waves and frequency-dependent Ms:mb discrimination in the European Arctic, submitted to *PAGEOPH Special Issue on CTBT Monitoring.*

Marshall, P.D., R.C. Stewart and R.C. Lilwall (1989): The seismic disturbance on 1986 August 1 near Novaya Zemlya: a source of concern? *Geophys. J.*, 98, 565-573.

Richards, P.G. and Won-Young Kim (1997). Test-ban Treaty monitoring tested, *Nature*, 389, 781-782.

Ringdal, F. (1986). Study of magnitudes, seismicity and earthquake detectability using a global network, *Bull. Seism. Soc. Am.* 76, 1641-1659.

Ringdal, F. (1997): Study of low-magnitude seismic events near the Novaya Zemlya nuclear test site, *Bull. Seism. Soc. Am. 87 No. 6,* 1563-1575.

Ringdal, F., E.Kremenetskaya, V.Asming, T.Kvœrna, J. Fyen, J. Schweitzer (1998). Seismic monitoring of the Barents/Kara Sea Region. *Proceedings from the 20th Annual Seismic Research Symposium on CTBT Monitoring, September 21-23, 1998*

Ringdal, F., T.Kvœrna, E.Kremenetskaya, V.Asming (1997). The seismic event near Novaya Zemlya on 16 August 1997. *Semiannual Technical Summary 1 April - 30 September 1997*, NORSAR Sci. Rep. 1-97/98, Kjeller, Norway.

Ringdal, F., E.Kremenetskaya and V. Asming (2000): Observed characteristics of regional seismic phases and implications for P/S discrimination in the European Arctic, submitted to *PAGEOPH Special Issue on CTBT Monitoring.*

VNIMI - State Scientific Research Institute for Mining Geomechanics (1989): Catalog of rockbursts in ore and non-ore deposits. Leningrad, VNIMI, 1989, 189pp (in Russian).

6.2 Regional Seismic Threshold Monitoring

(Paper presented at the 22nd Annual Seismic Research Symposium)

We are starting a project to develop an optimized, automatic capability to monitor seismic events originating in an extended geographical region, using data from a sparse network of regional arrays and three-component stations. The work will build on the site-specific threshold monitoring technique developed under previous contracts. As an integral part of the method development, we plan to apply and evaluate the method in several practical applications. Our focus will be on using IMS and selected non-IMS stations to experimentally investigate the performance of regional threshold monitoring of a grid system covering the entire Novaya Zemlya region, and an area with high mining activity (e.g. the Kola Peninsula).

The basic approach in the project will be:

- To apply a regional travel time model for the paths between each station and grid node, possibly with source-station specific corrections.
- To apply wave attenuation relationships based primarily on regional calibration events, as available.
- To apply optimized bandpass filters for the grid nodes to be monitored, also considering the use of several bandpass filters in parallel if sufficient calibration information is not available.
- To provide automatic "explanation facilities" to assist the analyst in assessing the results

An important consideration in the project work will be to lay the foundation for its actual implementation in an operational monitoring system. Thus, the software will be developed using the general framework already provided by the prototype IDC, and the examples of applications will to a large extent (although not exclusively) be based on data from the emerging IMS. To facilitate a possible future implementation of this method in the IDC operational environment, the data formats will be made compatible with those of the global Threshold Monitoring system now operational at the Vienna International Data Centre.

Objective

The objective of this work has been to assess the applicability of a temporary three-component network for Threshold Monitoring (Kværna and Ringdal, 1999; Ringdal and Kværna, 1989, 1992) of a small mining area located within local/regional distances. In particular, we have focused on comparing the performance of such a network with the performance of a single IMS array with respect to background noise levels and suppression of signals from interfering events. These results will be important when considering strategies for permanent monitoring of a larger region.

Research Accomplished

Station network and data

In the time period May-October 1999, 13 Lennartz MARSlite data loggers equipped with three-component LE-3D/5s were deployed in Finnmark, northern Norway. The project was a cooperative project between NORSAR and the University in Potsdam, Germany, primarily initiated for studying the local seismicity of the neotectonic Masi fault system (Schweitzer, 1999).

This instrument deployment, denoted the "MASI network", provided continuous data for the entire period of operation. A map with the sensor sites is shown in Fig. 6.2.1. Within the same area we also find the ARCES array (IMS station PS 28) and the IRIS three-component station Kevo (KEV) in northern Finland that is also a part of the finnish national seismic network. Continuous data from both ARCES and KEV were stored together with the data from the MASI network on CDs for subsequent analysis.

A quarry with an areal extent of approximately 2 km across is located on the Kola Peninsula, between the towns of Nikel and Zapolarnyi near the Russian-Norwegian border. Relatively large blasts (~100 tons) are regularly detonated in this quarry, providing strong signals at the nearby stations. An example of such an event as recorded at three of the MASI stations and at ARCES is shown in Figs. 6.2.2 and 6.2.3. Clear P- and S-, and Rg-phases are observed at many of the closest stations.

For the purpose of optimizing the SNR of the phases to be used for threshold monitoring, the three-component observations were rotated into the L, Q, and T ray oriented coordinate system, where P generally had the largest SNR in the L direction and S in the Q or T directions, as seen from Fig. 6.2.2. For ARCES, the best SNRs were found on array beams steered with either P or S velocities, But as seen from Fig. 6.2.3, where the center three-component ARA0 has been rotated into the L, Q, T coordinate system, the largest P amplitude is found on the L component and the largest S amplitude is found on the T component. Most of the P energy on the horizontal components is in this way projected into the L component. This effect will usually be observable for local and regional P phases where the rays approach the Earth's surface at relatively large incidence angles.

For the purpose of testing the performance of the MASI network for monitoring of the quarry near Nikel, we derived processing parameters for Threshold Monitoring from the event shown in Figs. 6.2.2 and 6.2.3. This event had an announced yield of 98 tons and were assigned a local magnitude of 1.97 based on the S-phase recordings at ARCES and Apatity. Details on the processing parameters are given in Table 6.2.1.

Threshold monitoring of the mine near Nikel, Russia

In a practical monitoring situation, a variety of seismic stations at local distances may be available for monitoring a given target site of interest. Usually, such local networks are of a lower quality and sensitivity than IMS stations, but this is to some extent compensated for by the proximity of the network stations to the target site. This tradeoff is in fact one of the main topics for study under the present project.

The IMS network in Fennoscandia is composed of high-quality regional arrays. In addition, we have access to experimental data from local stations such as the MASI network, and this gives us the possibility to test the concept of optimized site-specific seismic monitoring using dense local networks and comparing the results to monitoring using a sparse network of high-quality seismic arrays.

We have carried out a monitoring experiment focusing on the mining site near Nikel, Kola Peninsula. Our purpose has been to compare the results from site-specific monitoring in the following two cases:

- Optimized threshold monitoring using P and S waves from the ARCES array
- Optimized threshold monitoring using P and S waves a local network composed of the MASI stations supplemented by the Kevo station in Finland

We note that the ARCES array is at a distance of about 200 km from the target site, whereas the local network stations are at distances ranging from 30 km to about 300 km. The closest station (MA05) should in theory be able to provide the best recording of mining events at Nikel. In practice, this station is not ideally situated, and its capability is therefore not quite as good as expected. We will return to this point in the following discussion.

Monitoring example for 2 June 1999

Figs. 6.2.4 and 6.2.5 show the results from optimized site-specific threshold monitoring for the two cases mentioned above (ARCES array and the local network) for a typical 24-hour period (2 June 1999). In the following, we provide some comments to these plots, which in fact illustrate many of the most important conclusions from this preliminary study:

The ARCES plot (Fig. 6.2.4) shows three traces: The two bottom traces correspond to the P-phase and the S-phase. We note that the threshold monitoring technique can be used on individual phases as well as on a combination of phases from one or several stations. In this particular case, the ARCES P-phase monitoring result shows a general "background" noise level of about magnitude 0. This simply means that the background noise level for an ARCES P-beam steered to the Nikel site, with an optimized filter setting, and compensated for wave attenuation, is close to magnitude 0. We can easily translate this to a detectability estimate, simply by adding a detection threshold (typically a factor of 4.0 in SNR, or 0.5 in magnitude units). In a detectability context, it would thus mean that the ARCES P-wave detectability for this site is around magnitude 0.5.

The S-phase plot for ARCES (Fig. 6.2.4) is interpreted in the same way as the P-wave trace. The background level for the S-phase is slightly lower than for the P-phase (about magnitude -0.5). This reflects the fact that the ARCES S-phase is stronger than the P-phase for events from this mine. We recall that the threshold monitoring trace shows the "upper limit" of an event that could possibly have occurred at a given instance in time. Thus the "absence" of an S-phase on the recorded trace is a stronger indication of a low upper limit than the "absence" of a P-phase.

The combined P and S threshold trace for ARCES (upper trace in Fig. 6.2.4) shows the overall threshold monitoring result using all the available information from the ARCES array. The background level is about magnitude -0.6, and the number of "spurious" peaks due to interfering events and other noise bursts is reduced compared to either the P-wave trace or the S-wave trace. The actual events at the mining sites, as well as the other main peaks on the trace, are indicated. Note that all the peaks exceeding magnitude 0 can be either associated with events in the mine or explained as a result of other causes. Thus, the monitoring capability of the ARCES array for the Nikel mining site is close to magnitude 0.

Fig. 6.2.5 is a threshold plot for the local network defined earlier. In this case, 5 station traces are shown (5 bottom traces), with the combined network trace on the top. Note that each of the 5 station traces have been generated using a combination of the P and S phase for that station, so that we have not displayed the individual phase traces in each case.

First we will briefly comment on the performance of the individual stations. The best station is the "permanent" station Kevo, which has a background threshold of about magnitude 0. Kevo is known to be an excellent station for local as well as regional/teleseismic recording, and is situated on hard rock in a low-noise environment. It is therefore not surprising that it is performing well, especially taken into account that the temporary MASI stations were, due to logistic considerations, placed near populated areas, and some also on sediments. Nevertheless, the performance of Kevo is encouraging. Compared to ARCES, KEV is at about the same distance from the target site (actually slightly nearer). The fact that ARCES has a better performance than KEV is not surprising, since the ARCES array has the advantage of noise suppression through beamforming of 25 sensors. This is sufficient to explain the performance difference of about 0.6 magnitude units.

For the stations in the MASI network, the most pronounced feature is the high variability of the background noise. While we have not attempted to study this in detail, we attribute it to the siting of the instruments and the proximity to man-made noise sources (roads, buildings etc.). Nevertheless, these stations have a threshold (background noise) between 0 and 1 on the magnitude scale, which means that they will contribute to lowering the overall network threshold. Thus, the combined thresholds (top of Fig. 6.2.5) is well below magnitude 0, although not quite as low as for the ARCES array. The number of spurious peaks is reduced compared to the ARCES plot, and this is in fact one of the main benefits of having a distributed network available rather than a concentrated array. The geographical distribution of the network enables spurious noise bursts or interfering signals to be more effectively suppressed.

Monitoring example for 17 August 1999

Our second example is from the day 17 August 1999 (Figs. 6.2.6 and 6.2.7). This is the day of the large Turkey earthquake (occurring early in the morning GMT), and during the same day (at about 4.40 GMT a relatively large earthquake occurred in Revda, Kola Peninsula. These "interfering" events naturally stand out on the plots, both for the ARCES array (Fig. 6.2.6) and the network (Fig. 6.2.7). Otherwise, the same considerations as were previously made for the 2 June example also apply in this case: The ARCES threshold is slightly lower than the network threshold, but the network has a reduced occurrence of spurious peaks ton the combined threshold trace.

We note that the closest network station (MA05) was not in operation on 17 August 1999. This seems to have had little effect on the network threshold. This is encouraging, since it indicates a robustness to failure of one or a few individual network stations.

Conclusions and recommendations

The main objective of the research described here is to develop and test a new, advanced method for applying regional seismic array technology to the field of nuclear test ban monitoring. To that end, we have addressed the development and testing of a method for optimized seismic monitoring of an extended geographical region, using a sparse network of regional arrays and three-component stations. We have applied the method to a temporary local network in northern Norway, and demonstrated that such a network can in certain cases be processed with a threshold monitoring capability that approaches that of a high-quality regional array (ARCES). We emphasize that the experiments undertaken so far addresses the monitoring of a

site that is within local distance (0-300 km) of the network, and that a high-quality regional array will become progressively more capable than the network as the distance from the network to the target site increases.

We believe that the results described in this paper as well as in earlier contributions demonstrate that the optimized threshold monitoring method has the potential to become an important tool in day-to-day monitoring of seismic activity. By this method, the full resources of the monitoring network will be brought to bear to focus on a specific target site in order to enable monitoring of this target site with as high a capability as the network and available calibration information will allow.

In future research we plan to develop the site-specific method further to enable monitoring of a larger area, and it will then be necessary to apply a number of "optimized" beams. This is simple in principle, but in practice, the number of such beams may easily become too large to be reasonably manageable by the analyst, calling for an additional level of data reduction. We will develop a semi-automated method to form a (potentially large) number of optimized beams to cover a given region, and to process jointly, by automatic means, the resulting threshold traces so as to provide the analyst with a suitable "composite" result for review. We believe that in this way the threshold monitoring technique can be developed into a powerful tool for practical seismic CTBT monitoring.

Acknowledgements

We would like to acknowledge Frank Krüger and Daniel Vollmer of the Institute for Geosciences at the University of Potsdam, Germany for their extensive support during planning and field work of the MASI experiment. The University of Potsdam also provided the 13 mobile stations of the temporary network.

T. Kværna
F. Ringdal
J. Schweitzer
L. Taylor

(Sponsored by The Defense Threat Reduction Agency, Arms Control Technology Division, Nuclear Treaties Branch)

References

Kværna, T. and F. Ringdal (1999): Seismic Threshold Monitoring for Continuous Assessment of Global Detection Capability, accepted for publication in BSSA.

Kværna, T., J. Schweitzer, L. Taylor and F. Ringdal (1999): Monitoring of the European Arctic using regional generalized beamforming. In: *NORSAR Semiannual Tech. Summ. 1 October 1998 - 31 March 1999, NORSAR Sci. Rep. 2-98/99*, Kjeller, Norway

Ringdal, F. & T. Kværna (1989): A multichannel processing approach to real time network detection, phase association and threshold monitoring, *Bull. Seism. Soc. Am.*, 79, 1927-1940.

Ringdal, F. & T. Kværna (1992): Continuous seismic threshold monitoring, *Geophys. J. Int.*, 111, 505-514.

Schweitzer, J. (1999): The MASI-1999 field experiment. In: *NORSAR Semiannual Tech. Summ. 1 April - 30 September 1999, NORSAR Sci. Rep. 1-1999/2000*, Kjeller, Norway

Table 6.2.1: Parameter processing for Threshold Monitoring of the mine near Nikel.

Station	Phase	Flow	Fhigh	Azimuth	Inc/ Vel	Comp	STA len	Travel time	STA calib	Dis-tance (km)
MA05	P	3.0	8.0	89.0	84.2	l	0.6	5.46	-2.016	27.58
MA05	S	3.0	8.0	89.0	-	t	0.5	8.86	-2.856	27.58
MA04	P	4.5	9.0	109.09	34.42	l	1.0	12.95	-0.835	59.01
MA04	S	3.0	6.0	110.23	60.87	t	1.0	17.76	-1.661	59.01
MA03	P	4.0	8.0	88.2	78.3	l	0.5	25.06	-1.283	146.50
MA03	S	4.0	8.0	88.2	78.3	t	1.0	42.33	-1.883	146.50
KEV	P	3.0	6.0	95.75	42.18	l	1.0	28.14	-1.308	150.40
KEV	S	3.0	8.0	110.17	63.70	t	1.0	45.14	-1.634	150.40
MA02	P	4.5	9.0	83.69	73.46	l	1.0	33.68	-1.447	199.96
MA02	S	3.5	7.0	124.06	62.56	t	1.0	57.54	-1.531	199.96
ARCES	P	4.0	8.0	92.70	7.99	z	1.0	34.75	-1.737	205.23
ARCES	S	4.0	8.0	94.12	4.81	z	1.0	60.31	-2.183	205.23
MA12	P	4.0	8.0	98.3	65.0	l	0.5	37.39	-1.728	225.01
MA12	S	4.0	8.0	98.3	65.0	q	1.5	64.23	-2.486	225.01
MA13	S	2.0	4.0	103.84	65.62	q	1.0	64.43	-1.221	225.11
MA06	P	3.5	8.0	126.99	27.72	l	1.0	41.00	-0.873	248.46
MA06	S	1.5	3.0	124.06	62.56	t	1.0	69.46	-1.198	248.46
MA10	P	2.0	5.0	71.63	60.18	l	1.0	46.57	-0.858	282.62
MA10	S	1.5	5.0	60.59	63.18	t	1.0	78.45	-1.305	282.62
MA08	P	4.0	8.0	75.0	53.0	l	1.0	49.01	-0.686	295.58
MA08	S	4.0	8.0	75.0	53.0	q	1.0	81.61	-1.210	295.58

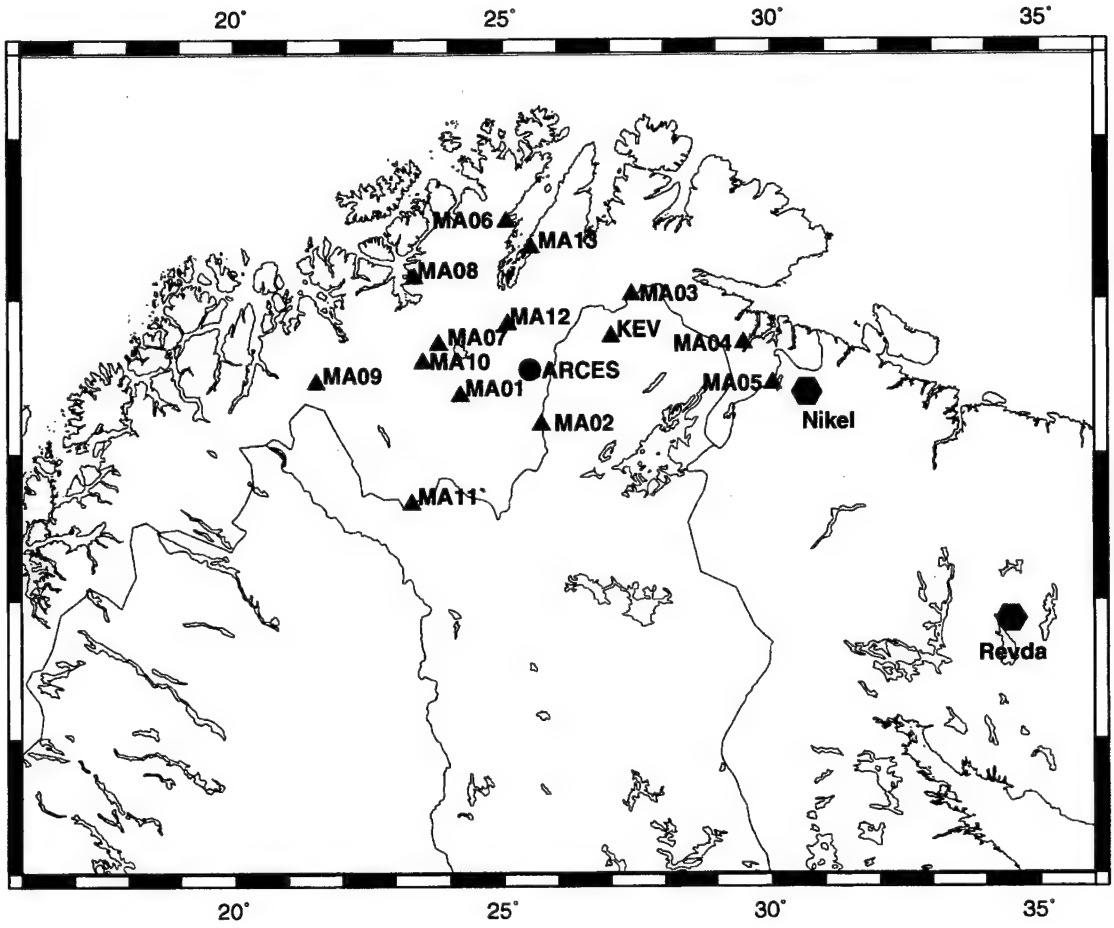

Fig. 6.2.1. Map showing the locations of the stations of the MASI network, the ARCES array, and the KEV station. Also shown are the locations of the quarry near Nikel and the epicenter of an M_s 4.2 earthquake occurring near Revda on the Kola peninsula.

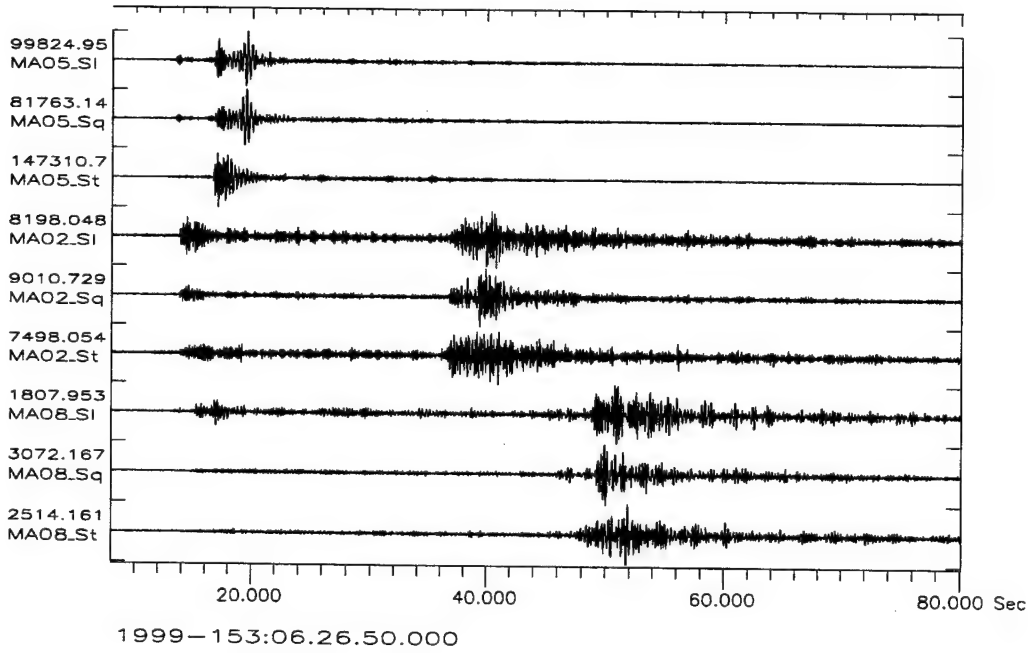

Fig. 6.2.2. Recordings of the quarry blast near Nikel (2 June1999, M_L 1.97) at three of the MASI stations. The traces were rotated into the L, Q, T components and bandpass filtered between 3 and 10 Hz.

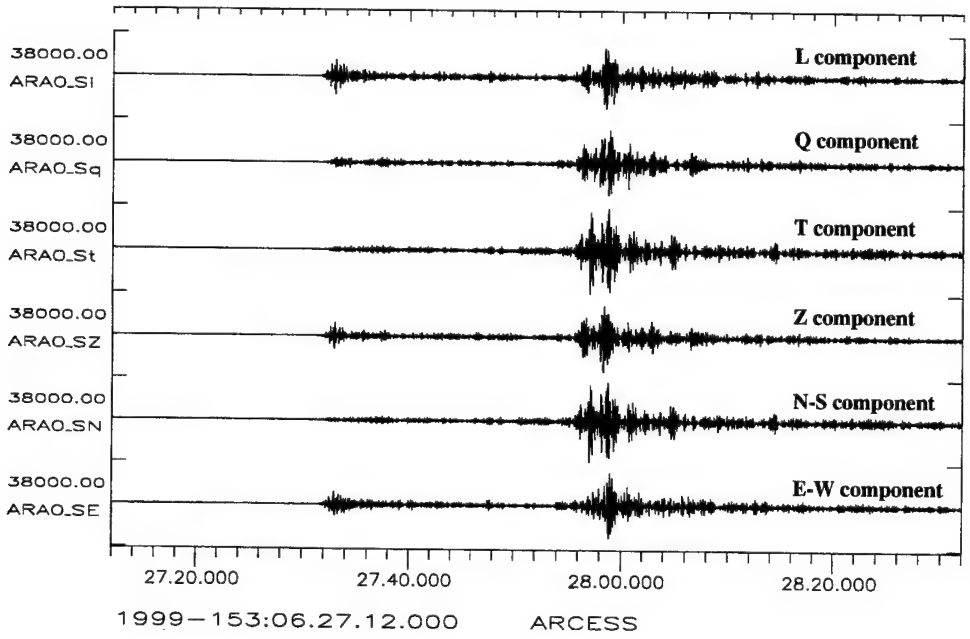

Fig. 6.2.3. Recordings of the quarry blast near Nikel (2 June1999, M_L 1.97) at ARA0, the central three-component element of the ARCES array. The upper three traces show the L, Q, T components and all traces were bandpass filtered between 4 and 10 Hz.

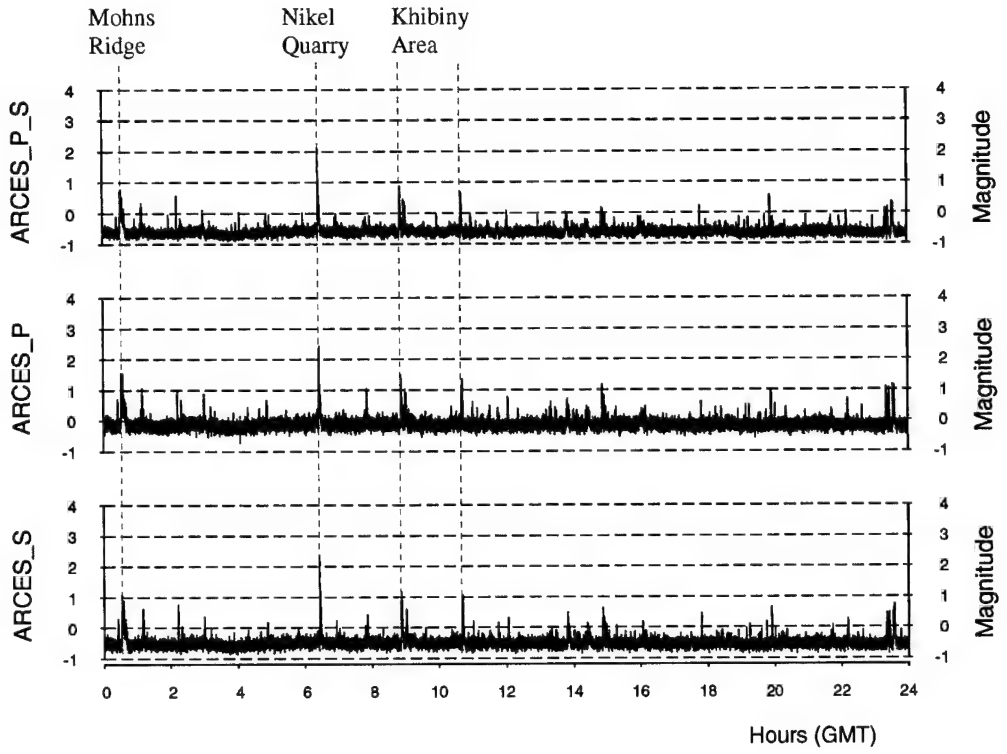

Fig. 6.2.4. Results from threshold monitoring of the quarry near Nikel for 2 June 1999, using the ARCES array. The combined P and S-phase threshold trace is shown on top, whereas the two lower traces show the thresholds for the P- and S-phases individually. The locations of the events causing the threshold peaks are given above the upper trace.

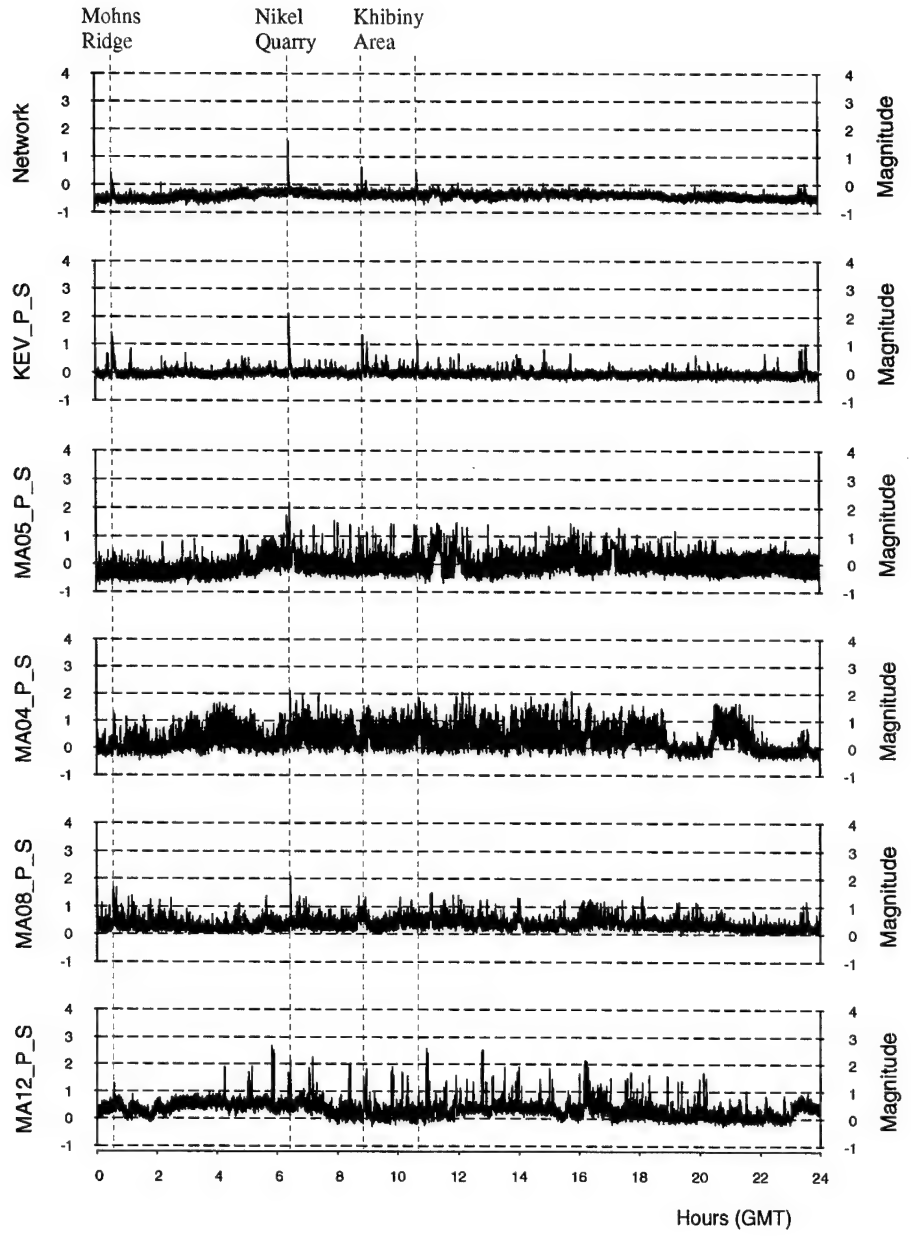

Fig. 6.2.5. Results from threshold monitoring of the quarry near Nikel for 2 June 1999, using the MASI network. The combined P and S-phase threshold trace for the network is shown on top, whereas the other traces show the combined P- and S-phase thresholds for selected stations. The locations of the events causing the threshold peaks are given above the upper trace.

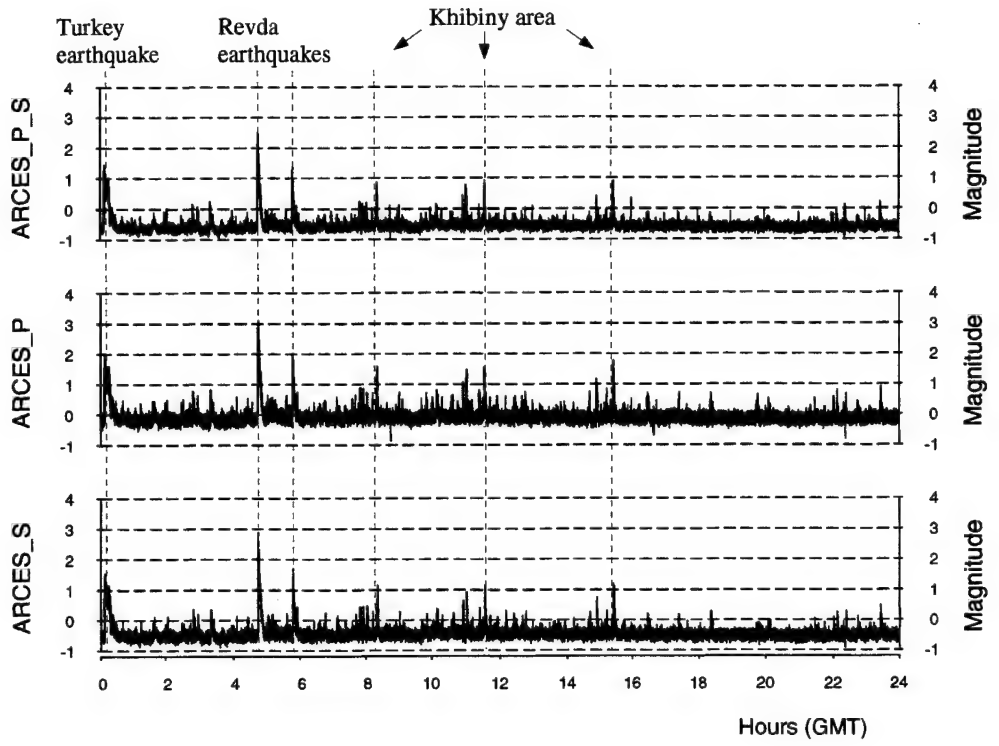

Fig. 6.2.6. Results from threshold monitoring of the quarry near Nikel for 17 August 1999, using the ARCES array. The combined P and S-phase threshold trace is shown on top, whereas the two lower traces show the thresholds for the P- and S-phases individually. The locations of the events causing the threshold peaks are given above the upper trace.

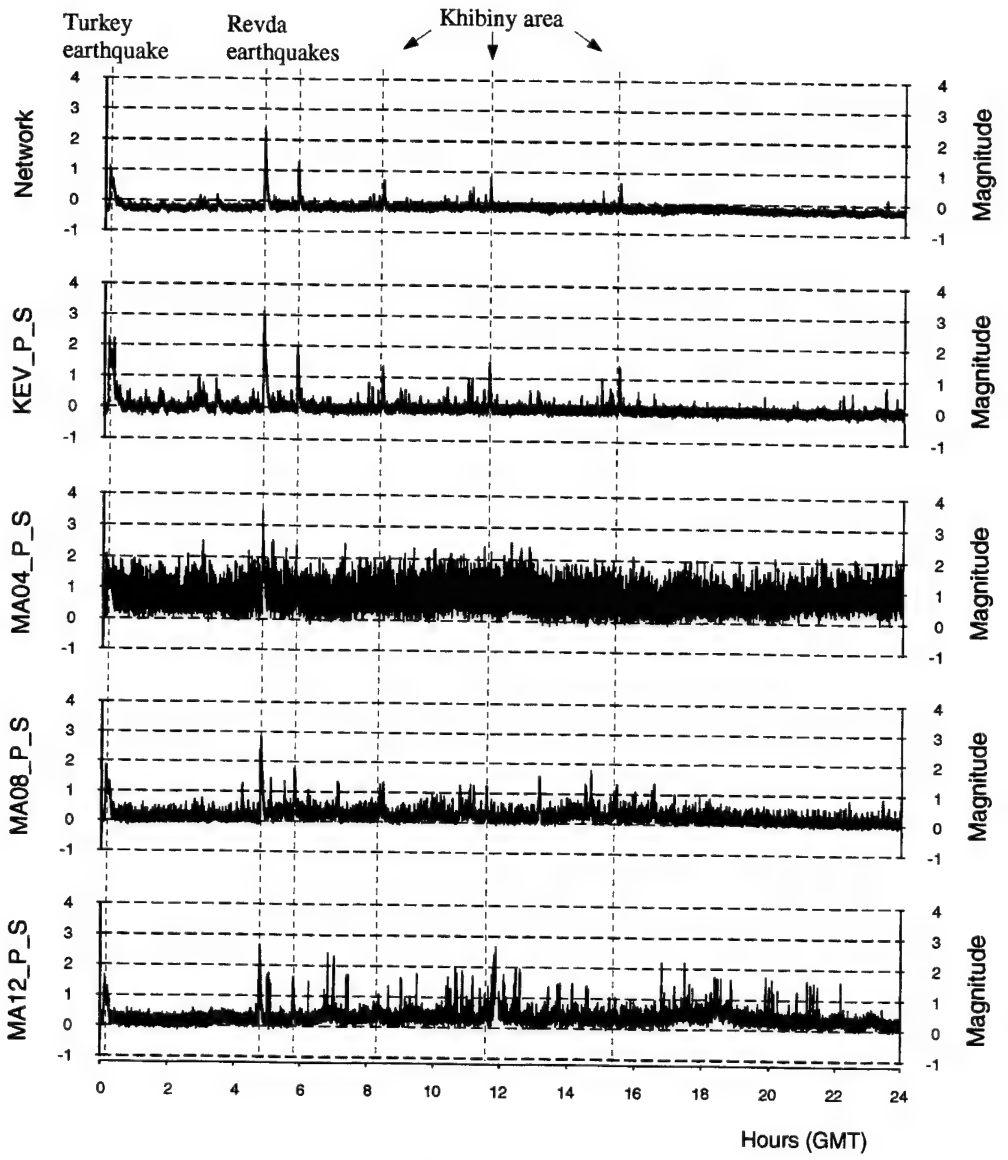

Fig. 6.2.7. Results from threshold monitoring of the quarry near Nikel for 17 August 1999, using the MASI network. The combined P and S-phase threshold trace for the network is shown on top, whereas the other traces show the combined P- and S-phase thresholds for selected stations. The locations of the events causing the threshold peaks are given above the upper trace.

6.3 Seismic events in the Barents Sea at and near the site of the Kursk submarine accident on 12 August 2000

Introduction

On 12 August 2000 signals from two presumed underwater explosions in the Barents Sea were recorded by Norwegian seismic stations. The first of these, at 07.28.27 GMT, was relatively small, measuring 1.5 on the Richter scale. The second explosion, 2 minutes and 15 seconds later, was much more powerful, with a Richter magnitude of 3.5.

It soon became clear that these seismic events were associated with the sinking of the Russian submarine "Kursk", although the exact way in which this accident occurred has not yet been determined. In any case, it is clear that the second, very large explosion must have fatally damaged the submarine.

NORSAR informed Norwegian authorities after analyzing the recordings, and published selected analysis results on the Internet through NORSAR's Web page (www.norsar.no). This paper gives a brief overview of the results of the data analysis, and also discusses some recent seismic activity in the Barents Sea near the Kursk site in September and October 2000.

Signals recorded on 12 August 2000

The large underwater explosion on 12 August 2000 in the Barents Sea were recorded on seismic stations in several countries. Among these were all the seismic arrays operated in Norway by the NORSAR institution. Using detection data from several arrays in northern Europe, the explosion was located fully automatically by NORSAR's Generalized Beamforming process (GBF) (see Fig. 6.3.1) with an estimated location only 14 km from the known position of the submarine. The GBF process is running on-line at NORSAR for the purpose of providing trial epicenters of seismic events in Europe and the European Arctic. Later interactive analysis gave a position that was as close as 5 km from the site of the accident (see Fig. 6.3.2). This high accuracy is due to the travel-time calibration available for the Barents region, as provided by the Fennoscandian/Barents velocity model.

The fact that the large explosion was preceded by a much smaller co-located event was noted by reviewing the GBF automatic output in more detail. It turned out that this smaller event was detected by at the ARCES array in northern Norway. For obvious reasons, the automatic location estimate was less accurate than that of the larger event, but still close enough to the Kursk site to be associated with the accident. The reviewed NORSAR location estimates, together with the true location, are listed in Tables 6.3.1 and 6.3.2.

Fig. 6.3.3 shows the waveforms at several stations for the largest event. A scaled-up plot for ARCES seismometers focusing on the small event is shown in Fig. 6.3.4. In this second figure, it is seen that the first event can be clearly identified (Pn, Pg and Sn phases), whereas the second event completely saturates the plot. A different perspective of the two events is shown in Fig. 6.3.5, which is a plot of estimated wave azimuth as a function of time (vespagram). The similarity of the two events is readily noticed, and the difference in size does not affect this particular figure. We note that we generated similar plots (azimuth and slowness versus time) for

the entire 24 hour period of 12 August, in order to try to detect additional explosions in the area. However, we were not able to find any such additional events.

The similarity of the kinematic parameters of the two events can also be seen in Figure 6.3.6, which shows f-k analysis results of the Pn and Sn phases of each event. It is noteworthy that the azimuth bias between the Pn and Sn phases are almost exactly the same for the two events. This confirms previous studies indicating that azimuth calibration of each phase should be done individually to obtain optimum location estimates for a given site.

Signals recorded during September-October 2000

The area in the Barents Sea where the Kursk accident occurred has no known history of significant earthquake activity. During September and October 2000, there were two sequences of seismic events in the area.The circumstances surrounding these events was initially unknown, but on 14 November 2000, the Russian authorities announced that they were small explosions set off using grenades or depth charges, with the stated purpose to protect the Kursk submarine.

Table 6.3.3 lists the origin times, estimated locations and magnitudes of those explosions detected automatically by the NORSAR GBF process. The locations in this table are based on data re-analyzed interactively, and are somewhat more accurate than the automatic results published on the Web. Note that the magnitudes have been adjusted from the NORSAR GBF values to a scale consistemt with the m_b scale currently employed by the Prototype IDC. This means that an average bias of 0.7 magnitude units has been added.

The timing patterns of the two series of explosions are rather similar, with some single explosions and some compressed sequences with explosion intervals of 1-2 minutes. The explosions are all nearly the same size, in fact the small differences in the magnitude estimates are well within the uncertainty that could be caused by variation of the shot location and depth. Comparing these magnitudes with those of the two explosions associated with the Kursk accident (Table 6.3.1), we note that the magnitude values in Table 6.3.3 are all somewhat larger than for the first (smaller) explosion on 12 August, but significantly smaller than for the second explosion that day.

Figure 6.3.7 shows a comparison of waveforms (ARCES center seismometer) for the first 6 events in the sequence. The data have been filtered in the band 2.5-8 Hz. We note that the waveforms have similar characteristics, although they are not identical. All of the events have clearly visible Pn and Sn phases at the single channel level. Analysis of the other waveforms from the sequence show similar patterns.

Concluding remarks

The recordings by seismic stations in the IMS network form the only publicly available evidence of the explosions associated with the Kursk accident. This information has been important in contributing to the study of the cause of the accident, although no definite conclusions can be drawn from these recordings alone.

The recording of numerous small explosions during September and October 2000 confirm the value of the IMS stations in monitoring seismic activity in the Barents Sea at very low magnitude levels. These explosions, although their magnitudes were only about 2.0 on the Richter

scale, were well recorded by the ARCES array (distance 500 km), but also the FINES, SPITS and NORES arrays also detected several of the events. In addition, the Apatity array station in the Kola Peninsula (not an IMS station) provided useful recordings.

We plan to follow up these analyses by applying experimental site-specific Threshold Monitoring of the Kursk site, using the regional arrays in Fennoscandia and Spitsbergen. We expect that this technique will enable us to readily detect events in this region, and may enable us to detect additional small explosions that may have been undetected by the on-line process. In addition, such a monitoring should enable easy separation of multiple events close in time. This topic will be reported at a later date.

F. Ringdal
T. Kværna
B. Paulsen

The tables below show seismic events detected and located by NORSAR during August - October 2000 in the region surrounding the site of the submarine "Kursk" accident in the Barents Sea. Table 6.3.1 lists the two presumed explosions directly associated with the accident. Table 6.3.3 shows a sequence of seismic events occurring during September and October.

Table 6.3.1. NORSAR's locations of seismic events in the Barents Sea 12 Aug 2000

Date	Time (GMT)	Latitude (N)	Longitude (E)	Richter magnitude
12.08.2000	07.28.27.0	69.70	36.80	1.50
12.08.2000	07.30.41.7	69.57	37.64	3.50

Table 6.3.2:

Location of the Kursk accident	69.62	37.58

Table 6.3.3. NORSAR's locations of seismic events in the Barents Sea Sep-Oct 2000

Date	Time (GMT)	Latitude (N)	Longitude (E)	Richter magnitude
22.09.2000	17.25.17.8	69.59	37.08	2.15
23.09.2000	06.01.08.0	69.58	37.01	2.26
23.09.2000	12.08.28.0	69.44	36.88	2.08
23.09.2000	12.10.22.0	69.59	37.48	2.16
24.09.2000	06.02.57.0	69.41	36.87	2.23
24.09.2000	08.50.37.9	69.74	37.00	1.94
27.09.2000	04.58.55.0	69.70	37.90	1.89
27.09.2000	05.00.54.8	69.73	37.79	1.96
27.09.2000	05.27.31.9	69.69	37.32	1.88
27.09.2000	05.54.46.3	69.75	37.13	1.95
27.09.2000	17.55.41.2	69.68	37.27	2.24
12.10.2000	06.41.24.2	69.74	37.23	2.14
12.10.2000	16.05.22.4	69.78	36.89	2.16
12.10.2000	16.07.34.5	69.64	37.14	2.08
13.10.2000	12.00.07.4	69.61	37.23	2.22
14.10.2000	04.31.00.2	69.58	37.29	2.21
14.10.2000	04.32.50.9	69.56	37.00	2.20
14.10.2000	04.36.29.8	69.64	36.97	2.16
17.10.2000	02.34.41.8	69.75	37.43	2.15
17.10.2000	02.35.23.2	69.61	37.82	2.10
17.10.2000	02.36.15.4	69.67	37.27	2.10
17.10.2000	02.38.32.4	69.64	37.24	2.06
17.10.2000	07.05.05.7	69.56	37.34	2.17
17.10.2000	07.05.54.8	69.68	36.95	2.20
17.10.2000	19.38.30.1	69.66	37.15	2.24
17.10.2000	19.39.28.3	69.59	37.01	2.20
18.10.2000	06.16.38.1	69.84	37.03	2.05

Table 6.3.3. NORSAR's locations of seismic events in the Barents Sea Sep-Oct 2000

Date	Time (GMT)	Latitude (N)	Longitude (E)	Richter magnitude
18.10.2000	06.17.25.6	69.74	37.11	2.04
18.10.2000	06.18.29.7	69.80	37.04	2.00
18.10.2000	09.35.20.8	69.74	37.45	2.14
18.10.2000	09.36.23.6	69.67	37.25	2.18
18.10.2000	09.54.45.2	69.70	37.61	2.03
18.10.2000	10.20.31.6	69.55	37.43	2.22
18.10.2000	10.22.12.0	69.63	37.17	2.03
18.10.2000	10.31.28.5	69.64	37.21	2.03
18.10.2000	10.34.20.1	69.68	37.07	2.00
19.10.2000	12.59.43.0	69.46	36.93	2.08

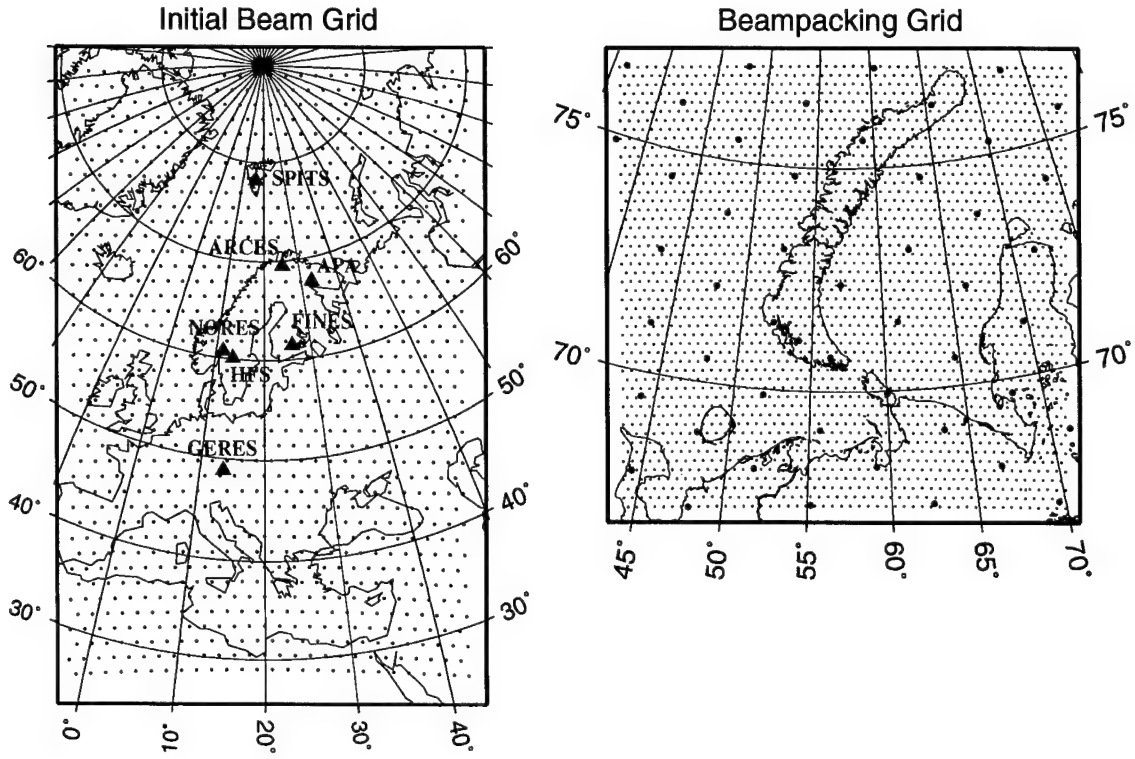

Fig. 6.3.1. Map showing the location of the seismic arrays used by NORSAR for the automatic multi-array phase association and location algorithm (Generalized Beamforming - GBF). The initial grid system used as aiming points is indicated on the left part of the figure. The right part shows a denser grid (in this example covering the Novaya Zemlya region) which is used in a second pass of the algorithm to refine the location estimates.

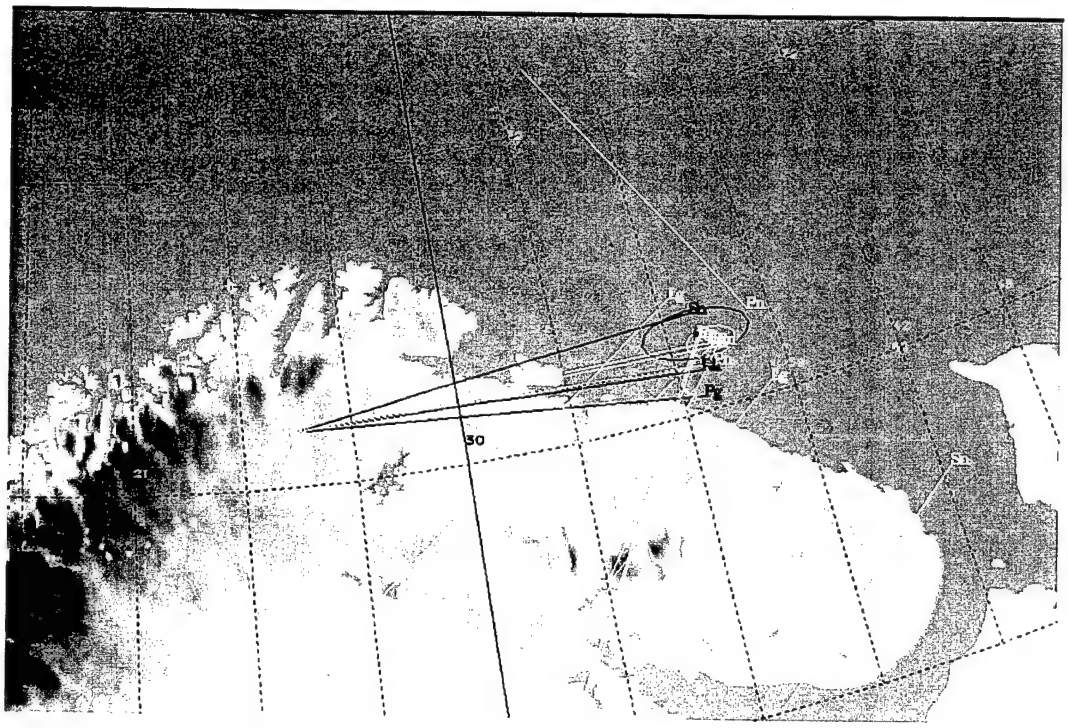

Fig. 6.3.2. Estimated location of the two seismic events in the Barents Sea on 12 August 2000. The white ellipse shows the 90% confidence area for locating the largest event, while the black ellipse corresponds to the smallest event. Estimated azimuths of phases recorded at individual stations are also shown.

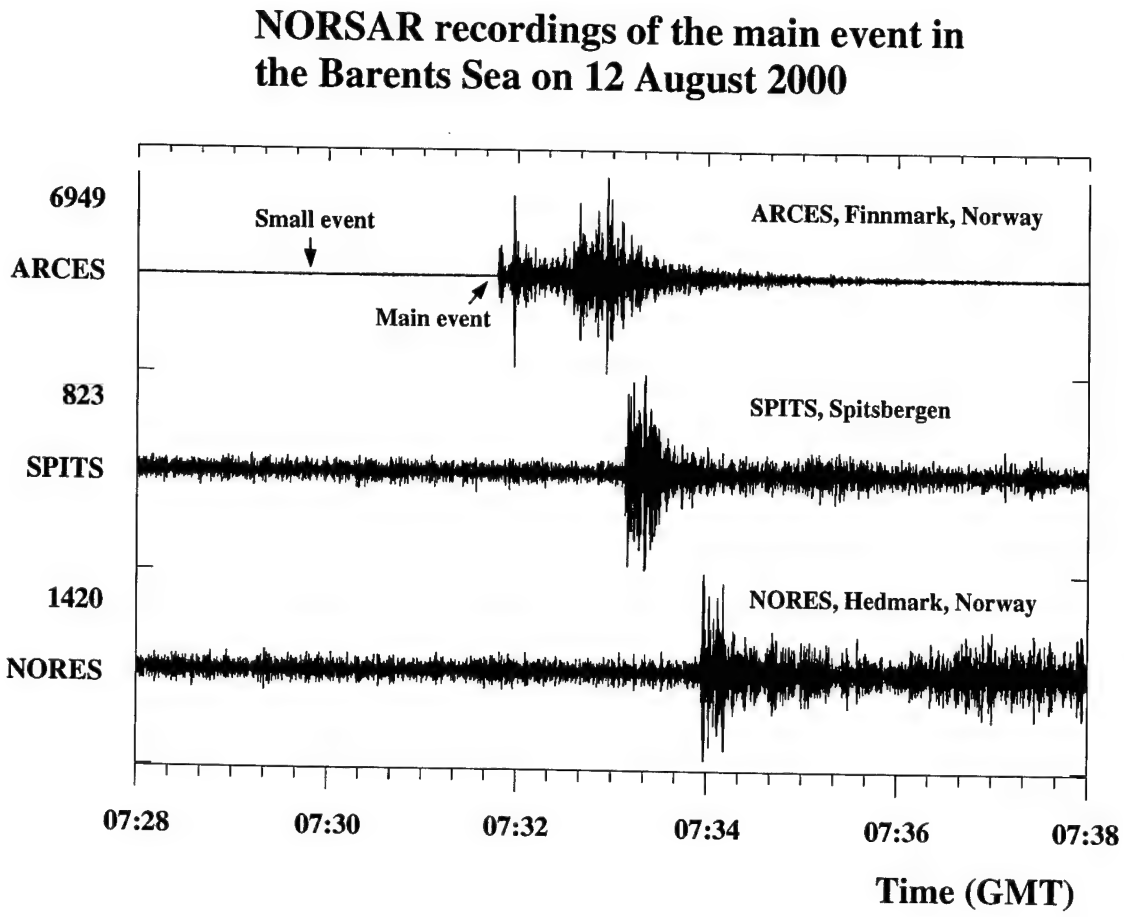

Fig. 6.3.3. Recordings by Norwegian stations of the two events in the Barents Sea on 12 August 2000. The first event is to small to be discernible on the plot, although it was detected by the ARCES array (see Fig. 6.3.4)

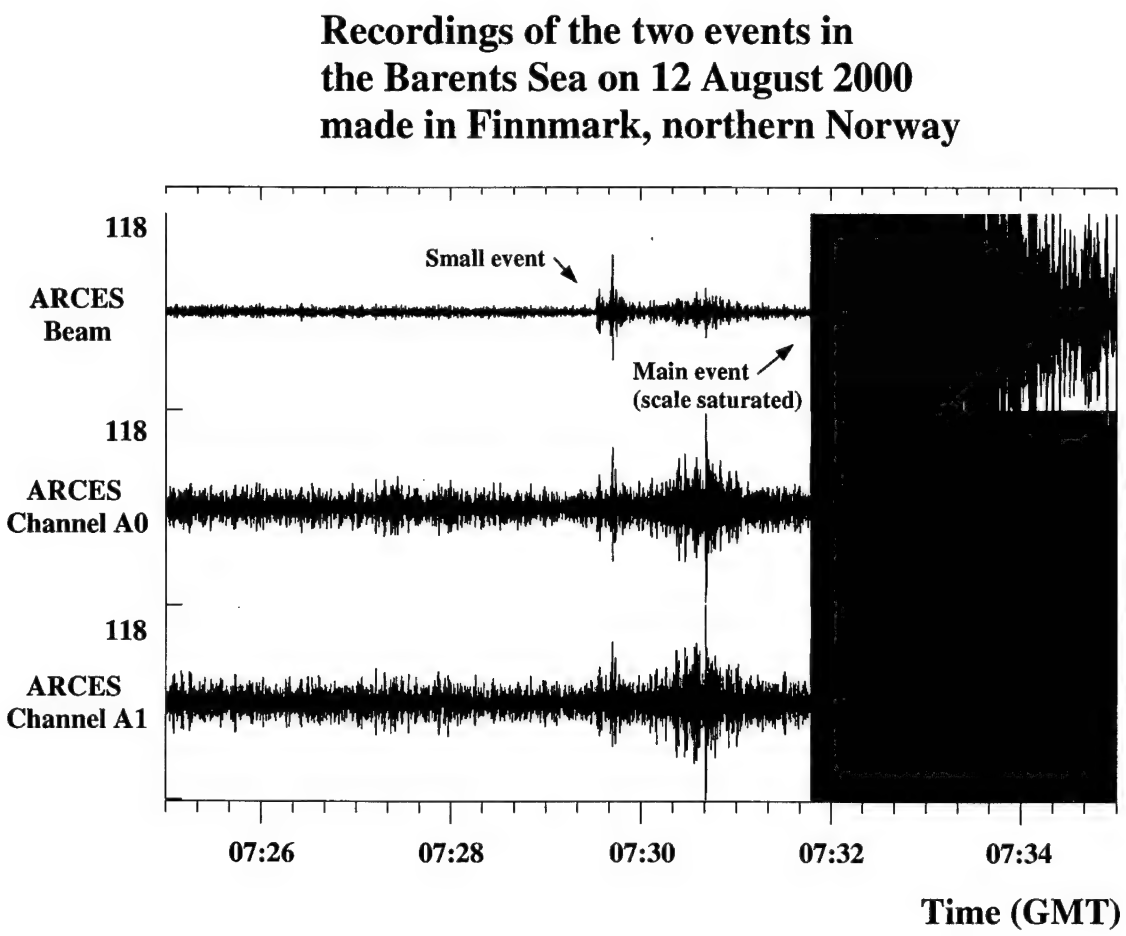

Fig. 6.3.4. Recordings of the two events in the Barents Sea on 12 August 2000 made at the ARCES array in Finnmark, northern Norway. The plot is scaled to show the smallest event, resulting in the second (larger) event being off-scale.

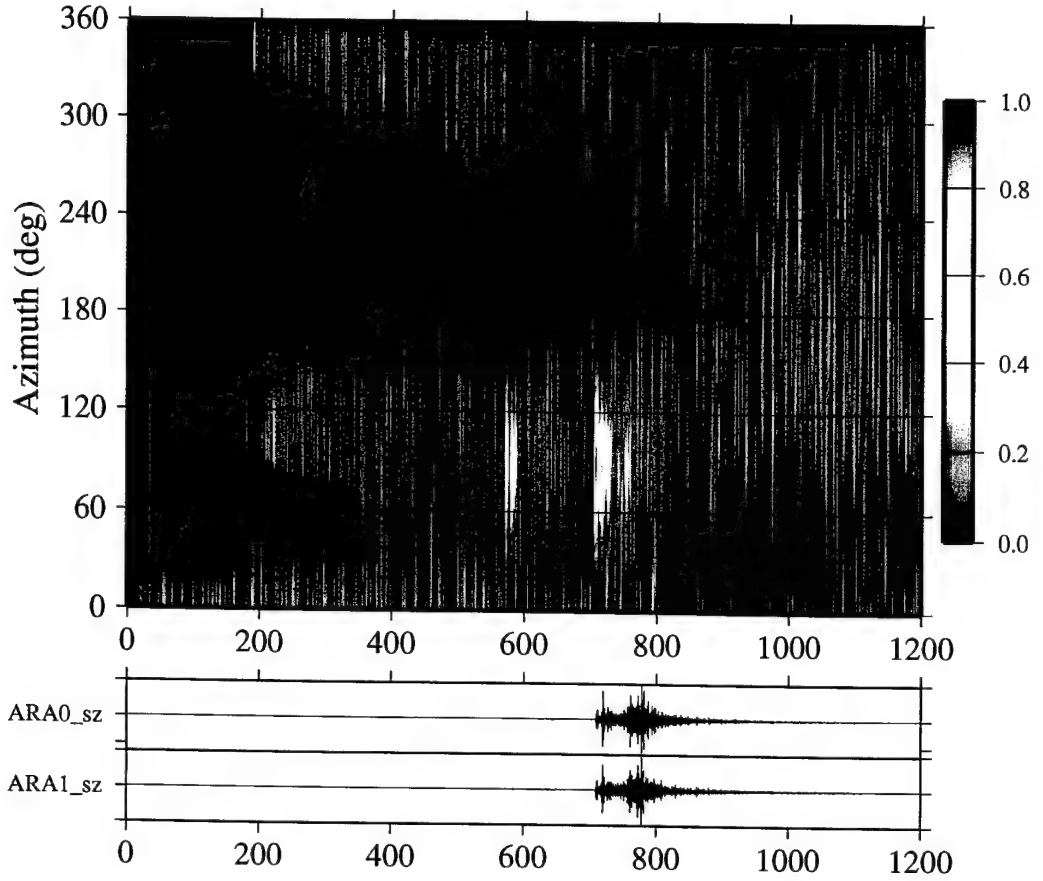

Time: 2000-225:07.20.00.000 Frequency band: 2.50 - 4.50 Hz
Window [length/step]: [3.0/ 0.5 s] Slowness: 0.125 s/km.
Isolines: dB below maximum
Channels used: ARA0_sz ARA1_sz ARA2_sz ARA3_sz ARB1_sz ARB2_sz ARB3_sz ARB4_sz ARB5_sz ARC1_sz ARC2_sz ARC3_sz ARC4_sz ARC5_sz ARC6_sz ARC7_sz ARD1_sz ARD2_sz ARD3_sz ARD4_sz ARD5_sz ARD6_sz ARD7_sz ARD8_sz ARD9_sz

Fig. 6.3.5. Plot of estimated wave azimuth at ARCES as a function of time during 20 minutes surrounding the events on 12 August.

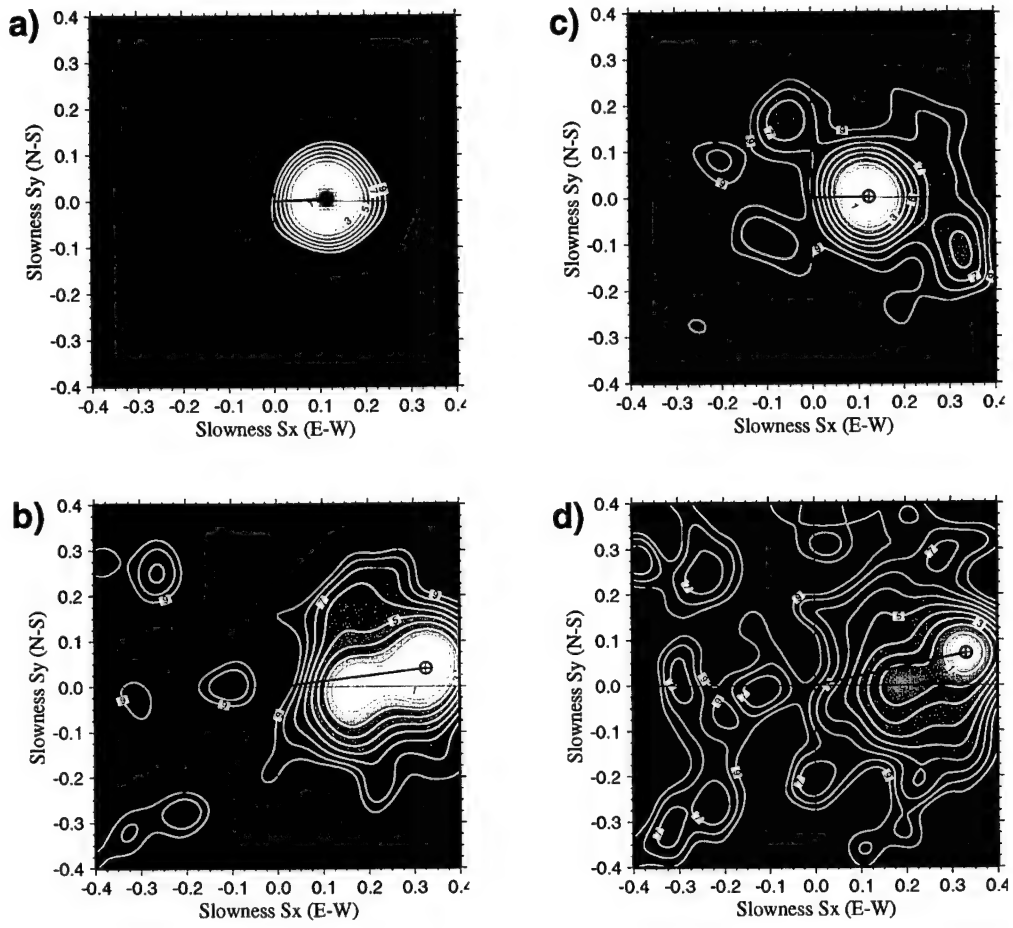

Figu. 6.3.6. Frequency-wavenumber (f-k) plots of the Pn and Sn phases at ARCES for the two events on 12 August 2000. The labels a) and b) correspond to the Pn and Sn phases for the large event, whereas c) and d) correspond to the small event. Note the similarity of the two cases. In particular, both events show the same difference between apparent P-azimuth and apparent S-azimuth.

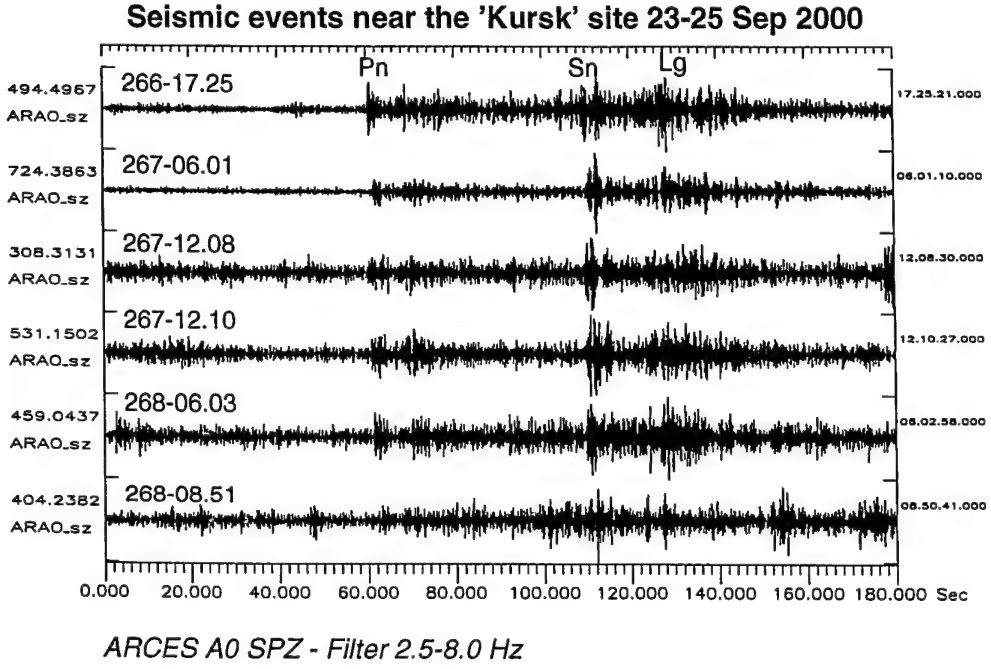

Fig. 6.3.7. Waveforms for the first 6 events in Table 6.3.3, as recorded on the center seismometer of the ARCES array in Finnmark, northern Norway. The data have been filtered in the band 2.5-8 Hz.

6.4 Synthetic travel times for regional crustal transects across the Barents Sea and the adjacent western continental margin

Introduction

The CTBT monitoring tasks have created a renewed interest for more precise estimation of local and regional travel times through a laterally varying lithosphere.

The crustal and seismic velocity structure of the Barents Sea varies significantly (Faleide, 2000):

- The thickness of the sedimentary cover varies from 0 to 20 km
- The depth to Moho varies from 20 to 45 km
- The thickness of crystalline crust varies from 10 to 45 km

If we include the western Barents Sea-Svalbard continental margin and the adjacent Norwegian-Greenland Sea, Moho rises to depths of 8 - 10 km and the thickness of the oceanic crystalline crust is typically 5 - 7 km.

The crustal heterogeneity of the Barents Sea region affects the accuracy of any seismic event location. Locating seismic events in this area with the 1D Barents Sea crustal model (Kremenetskaya and Asming, 1999) will give a location which will vary significantly in quality, depending on azimuth and distance between the seismic array (e.g. SPITS) and the earthquake (Schweitzer, 2000). The 1D Barents Sea crustal model is already known as an improvement with respect to the standard Earth model IASP91 (Kennett and Engdahl, 1991), as used at the IDC. It has a thicker crust (40 instead of 35 km), 6.9 (and 3.1)% higher P velocities in the two layered crust, and slightly higher velocities below the Moho.

In this report, we have calculated synthetic travel times for the first arrivals along four regional crustal transects across the Barents Sea and the adjacent western continental margin (Faleide, 2000) (Fig. 6.4.1) and compared these with the corresponding travel times predicted by the Barents Sea regional velocity model of Kremenetskaya and Asming (1999) which today is used to localize earthquakes in this area. Comparing these travel time curves can give some indication of how large the uncertainties tied to the localization of earthquakes with the Barents Sea model are.

Along one of the transects, between the spreading axis in the Greenland Sea and SPITS on Svalbard (Fig. 6.4.1), we have also carried out a sensitivity study where we tested the travel time effects caused by variations in the Moho topography.

Western Svalbard margin

Transect 4, across the western Svalbard margin, is the most extreme with respect to a laterally varying crustal configuration (Fig. 6.4.2). The transect is 300 km long beginning east of SPITS and heading almost directly westwards to the Knipovich Ridge (Eiken *et al.*, 1994) (Fig. 6.4.1), which is a part of the Mid-Atlantic spreading ridge system. The model consists of the main sedimentary sequences and the oceanic and continental crystalline crust separated from the mantle by the Moho discontinuity. Each unit has been assigned a velocity within the velocity ranges given by Faleide (2000) (Fig. 6.4.2).

The Moho depth is varying from 10 km under the oceanic crust to 32 - 37 km under Spitsbergen (Fig. 6.4.2). The Moho configuration is thought to be well constrained by deep seismic reflection and refraction data along the transect, however, several sensitivity tests have been performed to reveal the importance of this structure. The sediment basins are up to 10 - 12 km deep but have minor influence on the travel times for events located around the spreading ridge. On the other hand there is a high-velocity layer consisting of carbonates (V ~ 6.2 km/s) located from distance 175 km to the eastern end of the transect. This layer is always carrying the first arrivals from offsets less than ~ 70 km.

A finite difference (FD) method (Podvin & Lecomte, 1991) as implemented in the NORSAR-2D software package was used to calculate the first arrivals including head waves which are usually not included in ray tracing techniques. This method gives the theoretical first arrivals but no information about later phases, amplitudes, or other ray attributes. It should therefore be kept in mind that for larger distances the first arrivals might not always carry enough energy to be detected at a seismological station. The ray paths for the first arrivals (both from the mantle and from the crust) are shown in Fig. 6.4.3.

Because the Moho topography is the most important feature affecting the travel times and ray paths at greater distances, this has been varied in a sensitivity test with five different models (Fig. 6.4.4). The different travel time curves constructed from each model are plotted in Fig. 6.4.5. For comparison the travel time curve from the regional Barents Sea model (Kremenetskaya and Asming, 1999) is also shown. The five different tests include:

1. The Moho depth was gradually decreased from 10 km to about 7.5 km towards the Knipovich Ridge.
2. The Moho depth was gradually decreased from about 17 to 13 km between distance 50 and 110 km.
3. The Moho depth was gradually increased from about 16 to 20 km between distance 75 and 150 km.
4. The depression in the Moho topography at distance 160 km was removed, resulting in a flat and shallower Moho below the continental crust.
5. The depression in the Moho was extended to the end of the profile resulting in a flat and deeper Moho below the continental crust.

It turned out that all the different modifications of the Moho geometry only had minor influence on the travel times (Fig. 6.4.5). On the other hand, the synthetic travel time curves are quite different from that based on the Barents Sea regional velocity model of Kremenetskaya and Asming (1999). Compared to the model based on Transect 4, the Barents Sea regional model are too fast up to about 200 km but slower at offsets larger than 200 km, an effect already observed by Schweitzer (2000).

Barents Sea

Three regional profiles across the Barents Sea (Fig. 6.4.1) (Faleide, 2000), each 1100 km long, have also been modelled. In Transect 1 the source was placed at ARCES (Δ = 100 km) resulting in wave propagation from ARCES to Novaya Zemlya. In Transect 2 the source was placed at SPITS (Δ = 50 km) resulting in wave propagation from SPITS to Novaya Zemlya. Two different tests were performed on Transect 3 between northern Norway and SPITS because there is a seismic station which need to be calibrated at both ends. By reversing the survey configura-

tion (source at SPITS instead of northern Norway) the crust will be sampled in a different way, creating a different travel time curve. However, the travel times at the end of the profiles will be the same because of the principle of reciprocity.

All the layers in Transects 1 - 3 (Fig. 6.4.6 - Fig. 6.4.9) including the crystalline crust and the mantle have been assigned a gradient based on the velocity ranges given by Faleide (2000). The velocities in the sediment basins vary from 4.0 or 4.5 km/s at top to 5.0 or 5.5 km/s at the bottom (depending on which transect, usually around 15 - 20 km depth). The crystalline basement has been assigned a gradient which gives a velocity of 6.0 or 6.2 km/s at zero depth and 6.8 or 6.9 km/s at about 30 - 40 km depth. The mantle has been assigned a velocity of 8.05 km/s at 25 - 30 km depth and 8.15 km/s at 70 km depth.

Fig. 6.4.6 and Fig. 6.4.7 show the different ray paths for the theoretical first arrivals for Transects 1 and 2, and Fig. 6.4.8 and Fig. 6.4.9 show the same for the two reversed models based on Transect 3. The different travel time curves based on these ray paths are shown in Fig. 6.4.10 together with that of Transect 4 and the regional Barents Sea crustal model.

Comparing the travel time curves at various offsets (Fig. 6), three different domains can be established:

- Δ = 0 - 180 km: The Barents sea crustal model is faster compared to all the other models. The difference is greatest for Transect 3 (3.5 s at offset 100 km) and smallest for Transect 1, which is almost identical with the Barents Sea crustal model up to 200 km.
- Δ = 180 - 450 km: At about 200 km the first arrivals from the Barents Sea crustal model are coming from the third layer (Vp = 8.10 km/s), as can be seen from the slope of the curve. Transect 1 and Transect 3 are slower (~ 0.8 s) and Transect 2 and 3 (reversed) are faster (~ 0.3 - 0.5 s).
- Δ = 450 - 1100 km: The crossover distance between the Barents Sea crustal model and Transect 2, 3, and 3 reversed can be seen at an offset of 550 - 600 km. Up to this point the Barents Sea crustal model seems to represent a good average velocity compared to the different transects, but beyond 450 km where the first arrivals are coming from the fourth layer in the Barents Sea crustal model (Vp = 8.23 km/s) this velocity is relatively high with respect to the other models, as it can be seen from the slope of the curve. The average slope of the three different travel time curves above an offset of 700 km is almost identical with the slope for the Barents Sea crustal model, which indicate almost the same velocity at 50 - 70 km depth. However, the differences in the total travel times are up to two seconds.

Discussion

Depending on the offset, travel time differences of up to 2 - 3 seconds are found when comparing travel time curves from the four transects to the standard 1D model (Barents Sea crustal model). This reveals that the Barents Sea crustal model needs to be refined in order to fit the velocity structure established along the regional transects. Because most of the observed events in this region are only observable at regional distances, it will be particularly important within this context to address upper mantle velocities, as a basis for Pn travel times.

The discrepancies between the different models in the first P-onset times of up to several seconds can easily lead to systematic epicenter differences of several tens of kilometers whenever the azimuthal coverage with observing stations is low. If the azimuthal coverage is good, the actual location may be calculated quite well but we will get larger observed travel time

residuals, especially for more nearby stations. The residuals again are the base for all estimations of epicentral error ellipses. That means, unusual high residuals will generally result in lower quality locations.

This modelling is based on deep seismic reflection and refraction data observed during the last decades and is providing no explicit information about the corresponding S-velocities in this region. As long as the Vp-to-Vs ratio is constant, single array locations are mostly influenced by this ratio because they use the S-P travel-time differences as a means for estimating epicentral distance. If the Vp-to-Vs ratio is not constant, the systematic errors due to the usage of incorrect models are even more difficult to evaluate. However, especially for smaller events the usage of S onsets is essential to get a hypocentral solution. A better knowledge of S velocities is therefore needed for a successful calibration of the European Arctic.

These results show that 2D and 3D modelling of travel times for the European Arctic are both feasible and desirable, aiming at producing source-site specific corrections as used and needed by IDC/CTBTO.

As further work we plan to continue the search for ground-truth events in the European Arctic in order to obtain more and better P-phase travel time observations for the whole region. The S-phase travel times should be addressed later, building in part on the improved P-phase based locations. Tomographic studies for the whole region based on surface waves and body wave data supplemented by receiver-function studies will also be potentially useful in a further delineation of lithospheric structure for the European Arctic.

J. I. Faleide
J. Schweitzer
H. Bungum
E. Møllegaard

References

Eiken, O., editor (1994): Seismic atlas of western Svalbard - a selection of regional seismic transects. Norsk Polarinstitutt Oslo, *Meddelelser* **130**, 73 pp. and 14 enclosures.

Faleide, J. I. (2000): Crustal structure of the Barents Sea - important constraints for regional seismic velocity and travel-time models. *Semiannual Technical Report 1 October 1999 - 31 March 2000. NORSAR Sci. Report* **2-1999/2000**, Kjeller, Norway, 119-129.

Kennett, B. L. N., and E. R. Engdahl (1991): Travel times for global earthquake location and phase identification, *Geophys. J. Int.* **105**, 429-466.

Kremenetskaya, E. and V. Asming (1999): Location calibration of the Barents region. In: Workshop on IMS location calibration, IDC technical experts group on seismic event location, Oslo, 12 - 14 January 1999, Technical Documentation.

Podvin, P. and I. Lecomte (1991): Finite difference computation of traveltimes in very contrasted velocity models: a massively parallel approach and its associated tools. *Geophys. J. Int.* **105**, 271-284.

Schweitzer, J. (2000): Recent profiling experiments in the Spitsbergen area - calibration data for the SPITS array. *Semiannual Technical Report 1 October 1999 - 31 March 2000. NORSAR Sci. Report* **2-1999/2000**, Kjeller, Norway, 93-105.

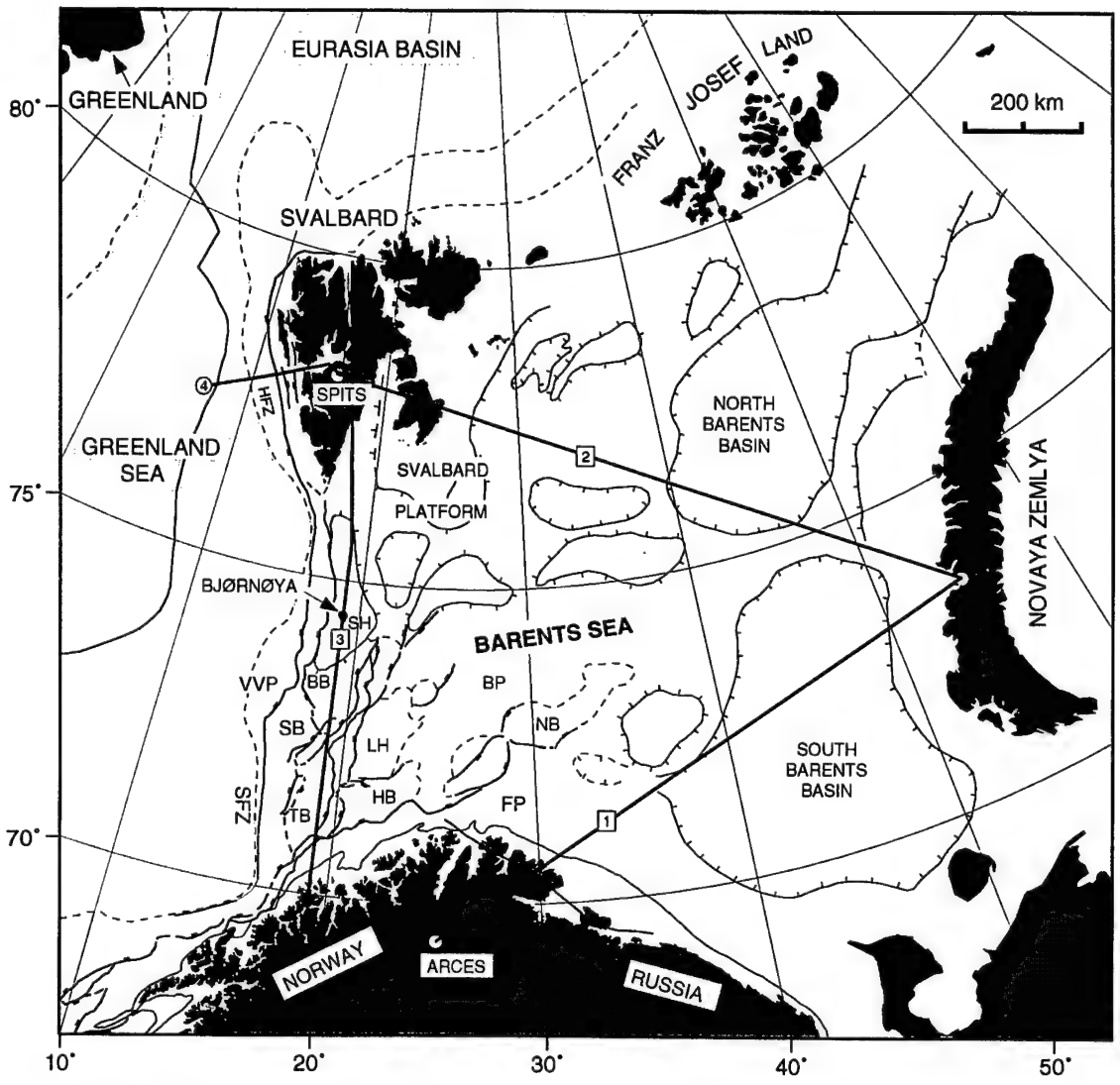

Figure 6.4.1. Regional setting - main geological provinces and structural elements in the Barents Sea and surrounding areas. Location of crustal transects and the seismic arrays SPITS and ARCES. BB = Bjørnøya Basin, BP = Bjarmeland Platform, FP = Finnmark Platform, HB = Hammerfest Basin, HFZ = Hornsund Fault Zone, LH = Loppa High, NB = Nordkapp Basin, SFZ = Senja Fracture Zone, SB = Sørvestnaget Basin, SH = Stappen High, TB = Tromsø Basin, VVP = Vestbakken Volcanic province (Faleide, 2000).

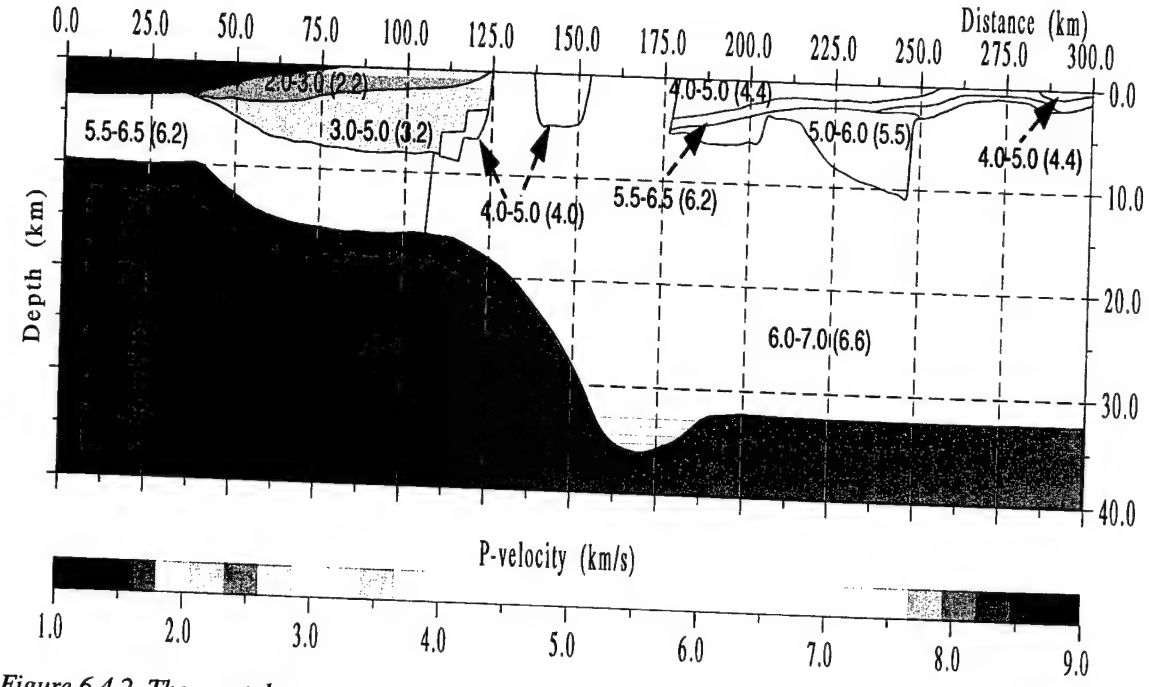

Figure 6.4.2. The crustal transect (Transect 4, Fig. 6.4.1) plotted together with the P-velocity range. A gradient has been assigned to all the layers based on the velocities in the brackets, and the gradient is varying with layer thickness. Vertical exaggeration (VE) = 3.

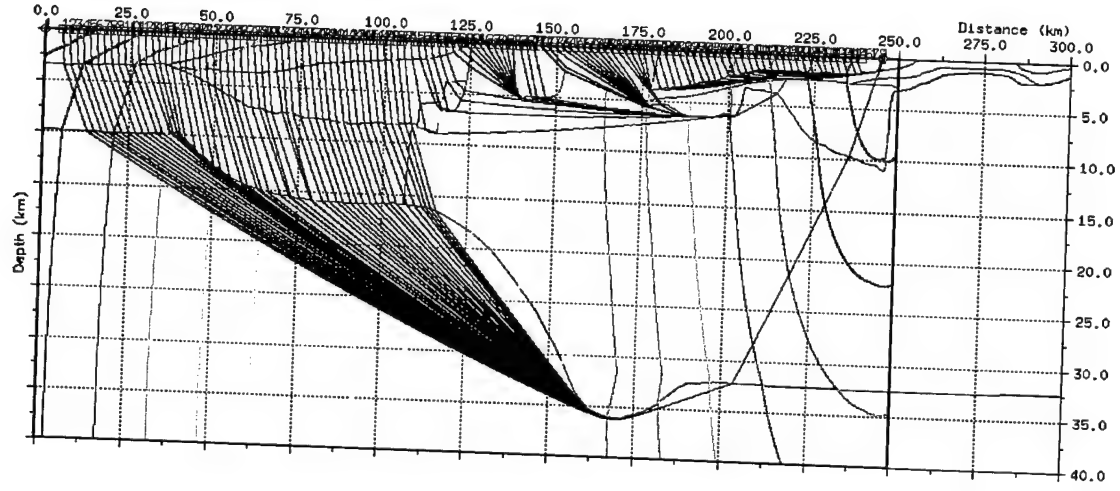

Figure 6.4.3. Ray paths from Transect 4 (Fig. 6.4.2) showing first arrivals (FD method). Wavefronts and ray paths are plotted together. VE = 3.

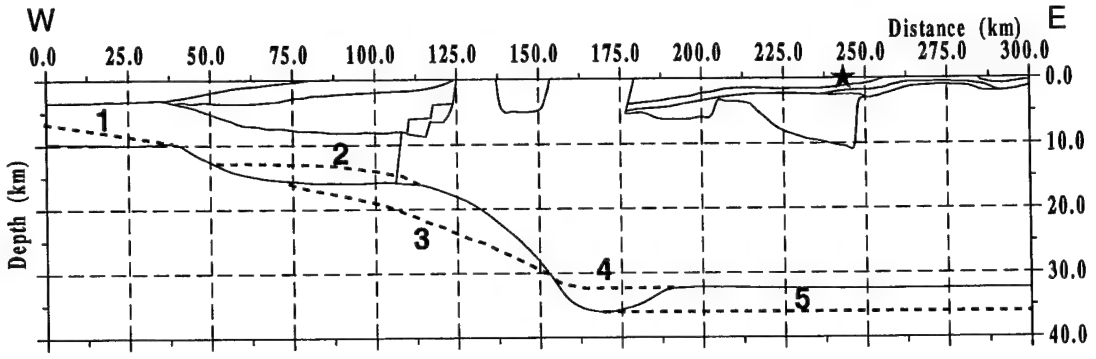

Figure 6.4.4. The different modifications of the Moho topography during the five sensitivity tests. The star indicates the location of the source.

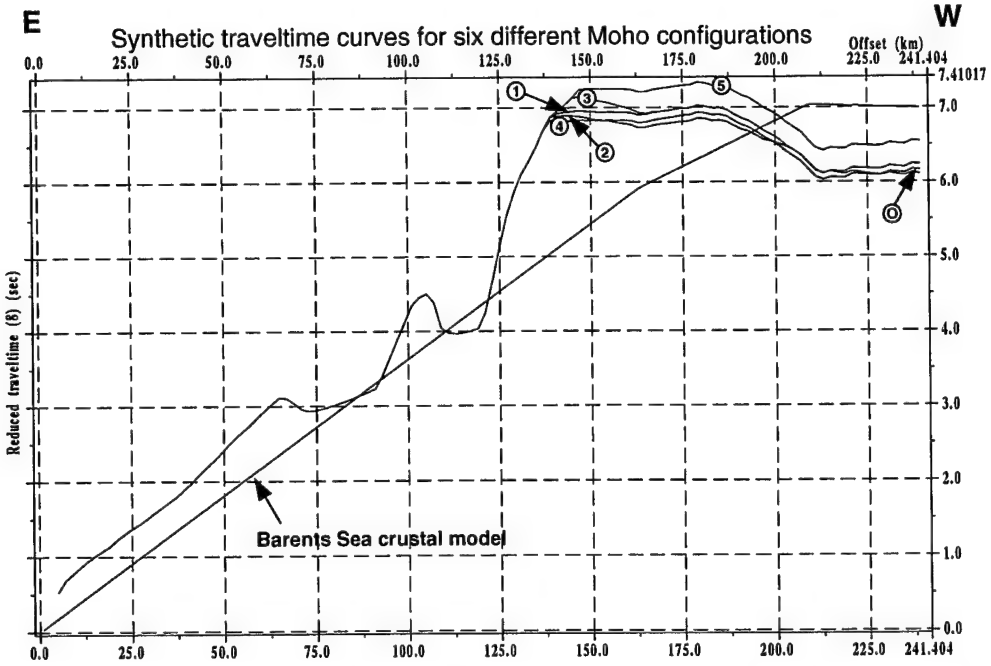

Figure 6.4.5. Synthetic travel time curves for the original Moho topography (O) and the five modifications (1 - 5), the numbers corresponds with Fig. 6.4.4. Transect 4 (Fig. 6.4.1) is shown from west to east, but the travel time curves are shown from east to west. The curves are deviating at most about 0.6 s, which indicate that the modelled details will hardly be resolvable with observed data. The travel time curve from the Barents Sea crustal model is shown for comparison.

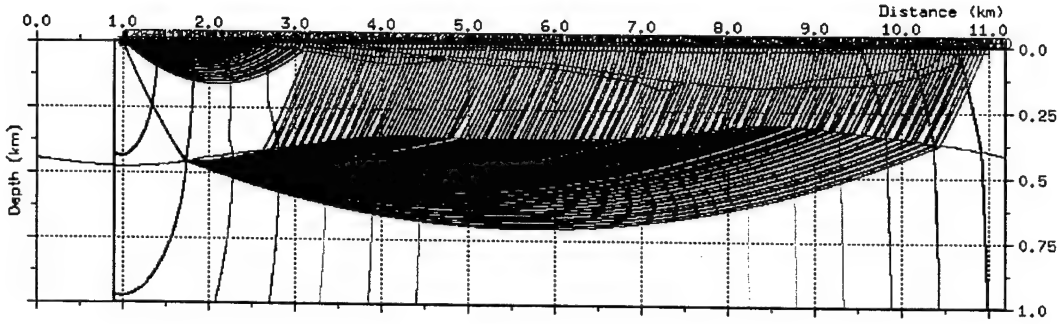

Figure 6.4.6. Ray paths for first arrivals (FD method) from ARCES to Novaya Zemlya (based on Transect 1 in Fig. 6.4.1). Source at the approximate location of ARCES. The model has been scaled down by the factor 0.01

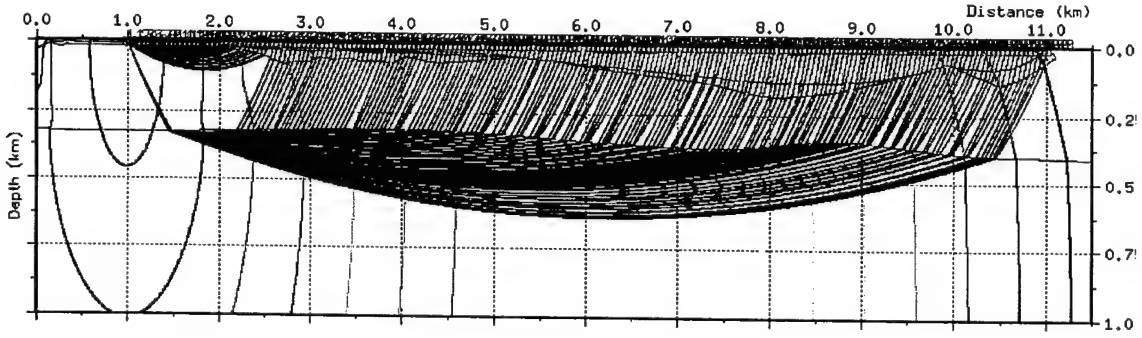

Figure 6.4.7. Ray paths for first arrivals (FD method) from SPITS to Novaya Zemlya (based on Transect 2 in Fig. 6.4.1). Source at the approximate location of SPITS. The model has been scaled down by the factor 0.01.

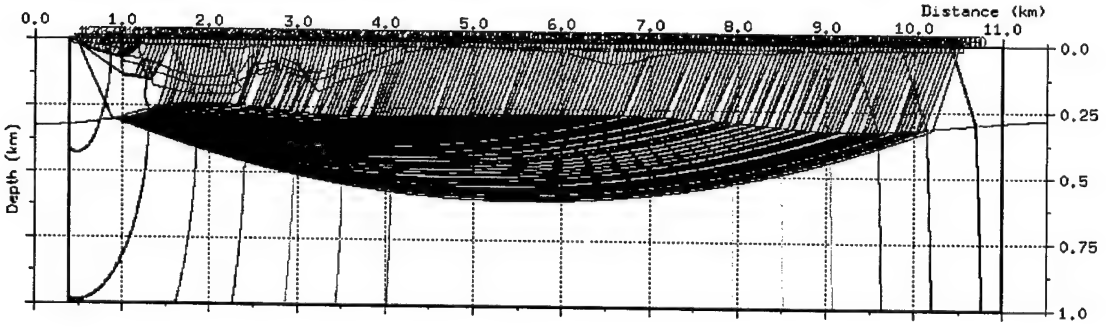

Figure 6.4.8. Ray paths for first arrivals (FD method) from northern Norway to SPITS (based on Transect 3 in Fig. 6.4.1). Source in northern Norway. The model has been scaled down by the factor 0.01.

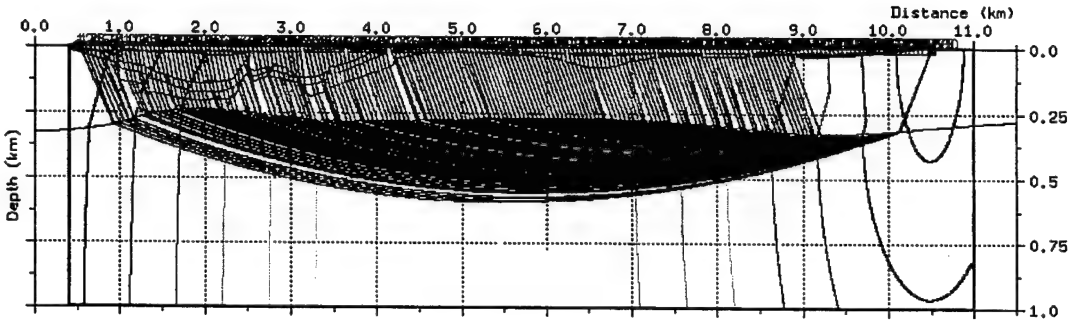

Figure 6.4.9. Ray paths for first arrivals (FD method) from SPITS to northern Norway (Transect 3, reversed survey, based on Transect 3 in Fig. 6.4.1). Source at the approximate location of SPITS. The model has been scaled down by the factor 0.01.

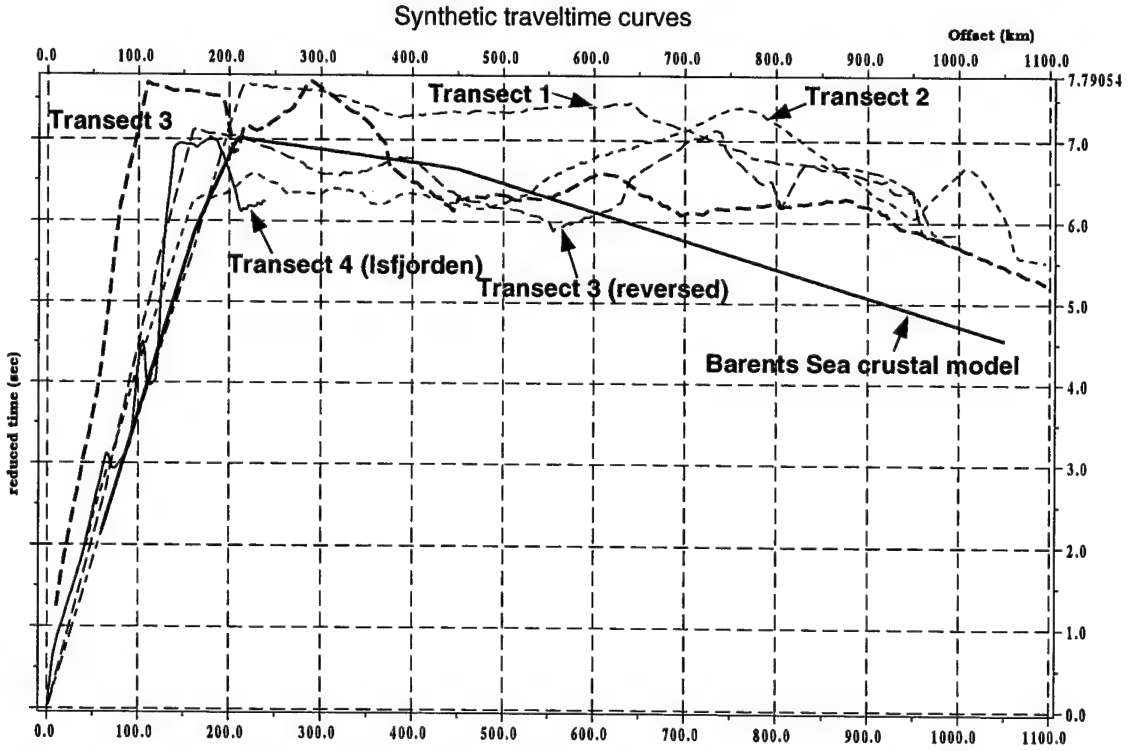

Figure 6.4.10. travel time curves from the five transects (six tests) including the Barents Sea crustal model and the Isfjord transect (Transect 4, Fig. 6.4.1). Barents Sea crustal model = thick/solid, Transect 1 = dashed/dotted, Transect 2 = dotted/thin, Transect 3 = dotted/thick, Transect 3 (reversed) = dashed/thin and Transect 4 (Isfjord) = solid/thin. Reduction velocity = 8 km/s. Note that these travel time curves are not scaled like the ray paths figures.

6.5 Threshold Monitoring Processing Parameters for IMS Stations PDYAR and ARCES

Introduction

The processing parameters for all stations to be included in the IMS Threshold Monitoring System processing need to be tuned for reliable estimation of the detection capability. We will now report on the tuning of the IMS array stations ARCES, which required retuning due to recent upgrades, and PDYAR. We follow the procedures described in the Threshold Monitoring Operations Manual (Taylor et. al., 1998). The configuration of ARCES (shown in Fig. 6.5.1) has not changed. The configuration of PDYAR is shown in Fig. 6.5.2.

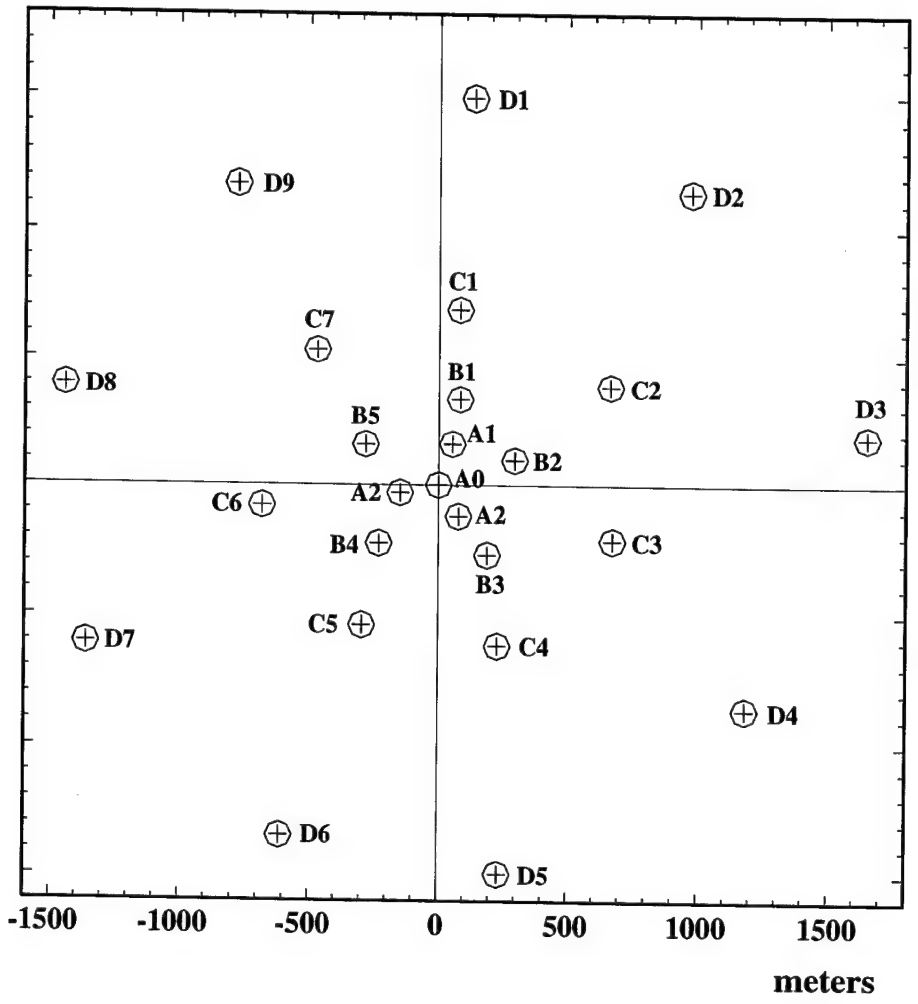

Fig. 6.5.1. Configuration of the ARCES array.

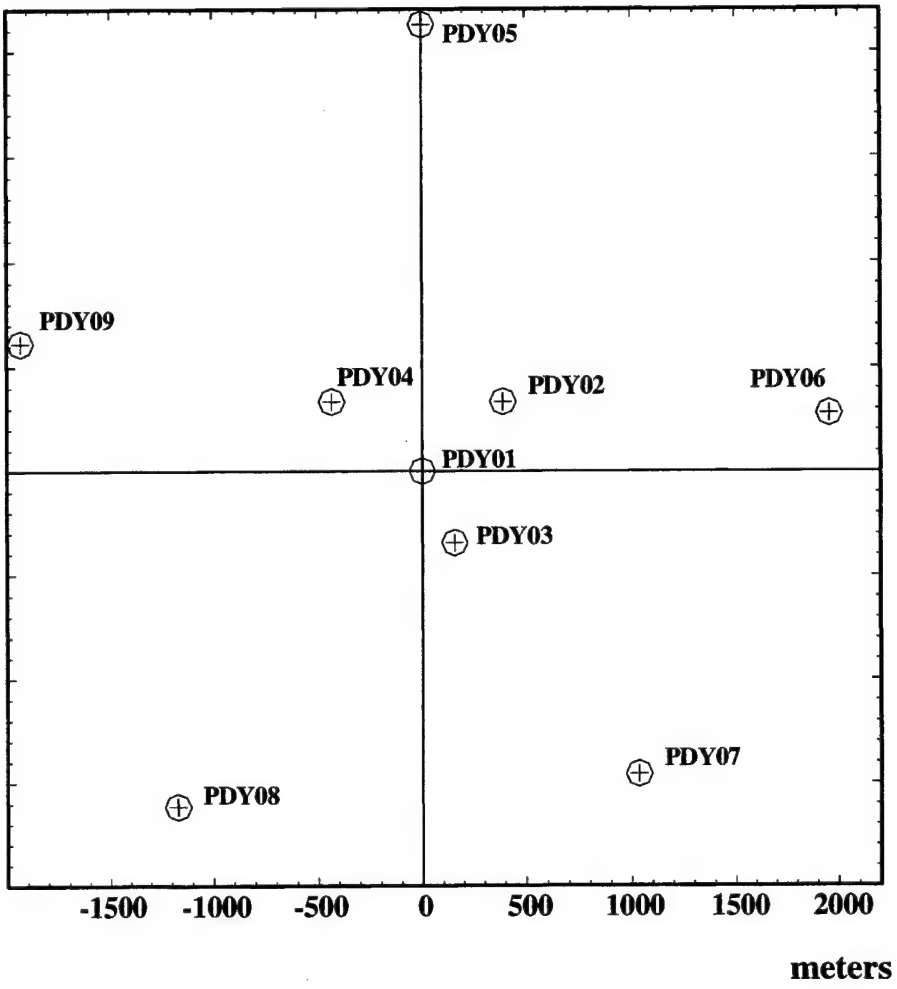

Fig. 6.5.2. Configuration of the PDYAR array.

Event Data Bases

For the tuning study we needed to find events with good SNRs, preferably occurring at various distances from the stations. This was done by searching the PIDC data base for good SNR events at various distances, and then requesting and receiving the data intervals. In order to obtain information on the background noise field, the event data segments start one minute ahead of the P arrival, with a total length of two minutes.The lists of events for PDYAR and ARCES are given in Table 6.5.1 and Table 6.5.2.

Table 6.5.1. TM tuning events for PDYAR

STA	ORID	LAT	LON	DEPTH	UTM	MB	DELTA	PHASE	SNR	AZI	VEL
PDYAR	20598919	42.3655	143.8172	43.8	1999-295:18.28.25.5	3.8	25.886	P	80.21	124.07	11.826
PDYAR	20598919	42.3655	143.8172	43.8	1999-295:18.28.25.5	3.8	25.886	PcP	4.16	128.05	42.553
PDYAR	20598947	-38.1664	-93.9545	0.0	1999-295:21.28.02.8	4.5	152.704	PKPbc	50.14	70.37	128.172
PDYAR	20600614	34.6268	-116.1812	0.0	1999-298:18.26.00.7	4.3	77.846	P	38.19	30.30	27.984
PDYAR	20600651	54.6569	-161.1353	24.6	1999-299:05.19.40.4	4.6	43.982	P	94.23	59.00	15.246
PDYAR	20600651	54.6569	-161.1353	24.6	1999-299:05.19.40.4	4.6	43.982	PcP	4.06	74.78	29.743
PDYAR	20601358	79.2520	124.0420	0.0	1999-300:05.05.07.4	4.5	20.022	P	81.15	4.60	11.863
PDYAR	20601411	52.0667	-171.3684	0.0	1999-300:08.38.48.3	3.9	41.185	P	51.69	62.81	14.473
PDYAR	20601411	52.0667	-171.3684	0.0	1999-300:08.38.48.3	3.9	41.185	PcP	3.39	78.75	20.984
PDYAR	20601517	39.4603	144.7751	0.0	1999-301:06.58.37.4	4.9	28.664	P	56.77	122.59	13.027
PDYAR	20603408	-22.8358	-69.7273	38.0	1999-302:17.13.31.9	4.2	143.179	PKP	41.22	5.07	32.542
PDYAR	20605733	19.8008	147.7117	0.0	1999-307:16.08.52.2	4.5	47.123	P	100.05	127.90	12.968
PDYAR	20605733	19.8008	147.7117	0.0	1999-307:16.08.52.2	4.5	47.123	PcP	4.51	140.89	26.483
PDYAR	20606490	51.9315	98.4437	0.0	1999-308:23.37.25.9	4.4	11.024	Pg	6.08	226.65	6.663
PDYAR	20606490	51.9315	98.4437	0.0	1999-308:23.37.25.9	4.4	11.024	Pn	168.05	230.46	9.028
PDYAR	20608186	-11.2438	114.2544	0.0	1999-309:17.03.58.5	5.0	70.673	P	60.81	198.03	11.459
PDYAR	20610056	43.8572	148.2533	0.0	1999-313:05.38.46.5	4.7	26.789	P	60.96	96.63	12.943
PDYAR	20611652	40.7401	30.2928	0.0	1999-315:14.41.23.5	5.1	52.209	P	95.15	301.80	20.052
PDYAR	20627225	.4584	125.9873	0.0	1999-332:00.53.39.4	5.1	59.971	P	63.56	181.03	13.068
PDYAR	20627237	41.5826	19.7109	0.0	1999-332:00.59.43.7	4.8	56.530	P	44.01	292.40	17.357
PDYAR	20627928	-1.2360	88.8923	0.0	1999-332:10.17.18.8	4.7	63.456	P	66.69	63.44	3.513
PDYAR	20628633	36.1573	81.2239	0.0	1999-334:10.08.05.0	4.7	30.966	P	57.46	230.66	12.321
PDYAR	20632411	32.3170	-40.1577	0.0	1999-341:02.35.48.5	4.4	85.602	P	35.91	339.37	26.215
PDYAR	20636222	-36.1486	-97.6442	0.0	1999-344:20.07.00.2	4.6	149.491	PKPbc	61.42	56.24	99.020
PDYAR	20637061	-5.7533	151.3126	0.0	1999-347:02.10.49.4	4.4	72.089	P	49.80	163.65	22.675
PDYAR	20642062	55.7126	110.2462	0.0	1999-351:12.00.21.7	4.2	4.125	Pg	48.13	191.12	7.199
PDYAR	20642062	55.7126	110.2462	0.0	1999-351:12.00.21.7	4.2	4.125	Pn	121.65	185.68	9.557
PDYAR	20654532	51.3504	-176.4437	0.0	1999-363:16.21.45.1	4.1	39.275	P	54.25	52.46	19.342
PDYAR	20654532	51.3504	-176.4437	0.0	1999-363:16.21.45.1	4.1	39.275	PcP	4.57	77.62	36.980
PDYAR	20654685	47.0925	141.9507	0.0	1999-364:14.51.44.7	3.7	21.415	P	35.64	115.67	19.080
PDYAR	20654792	18.2315	-101.3410	48.3	1999-363:05.19.45.8	5.5	97.654	P	78.24	37.90	20.562
PDYAR	20655891	36.9270	69.8463	0.0	2000-001:06.26.00.8	4.4	35.424	P	60.98	262.95	13.040
PDYAR	20667265	43.7660	-128.8626	0.0	2000-019:20.23.18.1	3.9	65.342	P	40.38	51.48	12.866

Table 6.5.2. TM tuning events for ARCES

STA	ORID	LAT	LON	DEPTH	UTM	MB	DELTA	PHASE	SNR	AZI	VEL
ARCES	20748712	67.1724	21.6042	0.0	2000-096:16.47.28.5	-999.0	2.779	Pn	66.40	209.60	7.981
ARCES	20642591	67.2049	20.7676	0.0	1999-352:10.51.18.2	-999.0	2.925	Pg	21.28	215.67	6.397
ARCES	20642591	67.2049	20.7676	0.0	1999-352:10.51.18.2	-999.0	2.925	Pn	92.01	216.10	7.870
ARCES	20689326	67.0984	21.0218	0.0	2000-046:17.10.33.1	-999.0	2.960	Pg	8.51	214.94	7.762
ARCES	20689326	67.0984	21.0218	0.0	2000-046:17.10.33.1	-999.0	2.960	Pn	48.66	214.51	8.026
ARCES	20655723	67.6755	33.3921	0.0	1999-365:11.25.03.5	-999.0	3.441	Pg	15.75	115.07	7.091
ARCES	20655723	67.6755	33.3921	0.0	1999-365:11.25.03.5	-999.0	3.441	Pn	90.71	122.49	7.524
ARCES	20624125	73.9421	13.1160	0.0	1999-328:19.54.07.6	3.6	5.884	Pn	87.36	325.68	9.892
ARCES	20657653	72.7508	4.6900	0.0	2000-005:21.08.27.2	3.2	7.450	Pn	41.48	309.94	10.037
ARCES	20689380	72.7741	4.6605	0.0	2000-046:18.37.21.0	3.5	7.464	Pn	58.76	307.29	9.455
ARCES	20656603	76.4794	8.1999	15.1	2000-002:11.10.59.0	3.7	8.570	Pn	57.92	331.22	9.419
ARCES	20637912	77.8335	7.5103	0.0	1999-347:21.34.22.2	3.6	9.680	Pn	28.97	322.96	9.519
ARCES	20731076	59.0957	18.5772	0.0	2000-074:09.57.29.6	-999.0	10.892	Pn	43.32	200.16	8.275
ARCES	20617789	81.2118	-4.1285	0.0	1999-320:19.06.56.1	3.7	13.593	Pn	13.93	8.15	14.386
ARCES	20628623	84.4093	1.7543	0.0	1999-334:09.24.01.7	4.4	15.598	Pn	21.55	358.00	10.968
ARCES	20671000	51.5575	16.2164	0.0	2000-022:20.30.58.1	3.9	18.564	P	20.50	197.15	9.634
ARCES	20667369	48.0585	26.8734	41.7	2000-019:23.09.43.5	3.6	21.552	P	20.17	180.50	9.094
ARCES	20654598	80.4997	121.9986	0.0	1999-364:06.46.55.4	4.5	23.581	P	45.57	36.78	11.391
ARCES	20654598	80.4997	121.9986	0.0	1999-364:06.46.55.4	4.5	23.581	PcP	12.52	34.82	49.270
ARCES	20753648	45.7120	26.4893	134.2	2000-097:00.10.40.0	4.6	23.894	P	76.69	181.82	9.832
ARCES	20627237	41.5826	19.7109	0.0	1999-332:00.59.43.7	4.8	28.181	P	12.98	183.75	10.273
ARCES	20615746	40.9257	31.3416	33.9	1999-316:16.57.24.9	5.5	28.838	P	113.05	162.61	27.029
ARCES	20611652	40.7401	30.2928	0.0	1999-315:14.41.23.5	5.1	28.969	P	47.35	171.73	13.862
ARCES	20622226	39.6134	20.7906	0.0	1999-328:03.38.49.8	4.6	30.089	P	35.24	186.25	9.790
ARCES	20631578	35.8479	22.1214	0.0	1999-340:01.28.27.5	4.0	33.794	P	51.13	188.13	11.522
ARCES	20651185	55.7226	110.1668	0.0	1999-362:01.19.44.3	4.1	37.778	P	42.01	67.55	12.848
ARCES	20633388	42.2840	76.9051	21.3	1999-340:07.33.10.1	4.9	37.784	P	79.03	101.73	12.638
ARCES	20610083	35.6821	61.2042	0.0	1999-312:21.37.20.5	5.3	39.093	P	57.05	136.35	12.537
ARCES	20610083	35.6821	61.2042	0.0	1999-312:21.37.20.5	5.3	39.093	PcP	2.78	102.28	27.928
ARCES	20610083	35.6821	61.2042	0.0	1999-312:21.37.20.5	5.3	39.093	PP	4.95	132.35	12.125
ARCES	20617150	36.9184	69.8054	0.0	1999-319:19.05.01.5	4.7	40.393	P	73.69	115.86	15.136
ARCES	20628633	36.1573	81.2239	0.0	1999-334:10.08.05.0	4.7	44.748	P	52.57	98.60	15.819
ARCES	20701883	60.3979	-145.9958	18.9	2000-058:02.22.15.0	4.6	50.216	P	66.07	4.41	14.431
ARCES	20639628	54.6320	-160.9635	35.7	1999-350:23.51.29.9	5.0	56.051	P	66.71	18.41	15.196
ARCES	20639628	54.6320	-160.9635	35.7	1999-350:23.51.29.9	5.0	56.051	PcP	2.53	29.83	27.242
ARCES	20665029	25.7086	101.1317	0.0	2000-014:23.37.04.8	5.2	61.142	P	22.96	79.15	14.386
ARCES	20622113	9.6720	57.1961	0.0	1999-327:14.37.56.7	5.3	63.172	P	54.92	144.62	17.466
ARCES	20667321	19.7346	101.3614	0.0	2000-019:20.59.24.0	4.9	66.723	P	22.44	86.12	25.381
ARCES	20604467	23.3651	121.6230	39.8	1999-305:17.53.02.5	5.4	70.445	P	33.23	62.05	15.262
ARCES	20647972	16.5885	119.1092	0.0	1999-358:22.53.52.2	4.7	75.853	P	18.11	78.99	22.135
ARCES	20636414	15.7492	119.8326	19.5	1999-345:18.03.36.2	5.9	76.882	P	116.84	77.94	28.050
ARCES	20636414	15.7492	119.8326	19.5	1999-345:18.03.36.2	5.9	76.882	PKKPbc	4.74	273.12	37.443
ARCES	20616307	-1.3429	88.9331	0.0	1999-319:05.42.42.9	5.8	82.213	P	58.22	104.45	55.813
ARCES	20739324	15.8981	147.3181	0.0	2000-085:04.47.55.0	4.3	85.616	P	52.62	60.72	19.002
ARCES	20628689	3.1374	126.6989	0.0	1999-335:05.29.07.7	5.2	90.990	P	38.41	77.33	17.021
ARCES	20669588	-1.0589	127.3430	0.0	2000-022:19.42.13.0	4.8	95.124	P	11.46	62.59	15.358

Table 6.5.2. TM tuning events for ARCES

STA	ORID	LAT	LON	DEPTH	UTM	MB	DELTA	PHASE	SNR	AZI	VEL
ARCES	20642632	-2.4472	139.7918	0.0	1999-352:17.44.54.2	5.7	100.616	P	28.55	67.74	18.463
ARCES	20642632	-2.4472	139.7918	0.0	1999-352:17.44.54.2	5.7	100.616	PKiKP	6.63	104.81	47.469
ARCES	20708431	-6.7413	144.1117	0.0	2000-063:22.22.40.6	5.8	106.046	Pdiff	17.25	64.57	19.172
ARCES	20708431	-6.7413	144.1117	0.0	2000-063:22.22.40.6	5.8	106.046	PKiKP	3.69	74.36	24.059
ARCES	20682978	-5.8018	151.1546	27.0	2000-037:11.33.53.0	6.2	107.334	Pdiff	8.85	47.12	17.338
ARCES	20682978	-5.8018	151.1546	27.0	2000-037:11.33.53.0	6.2	107.334	PKiKP	88.11	106.38	67.308
ARCES	20682978	-5.8018	151.1546	27.0	2000-037:11.33.53.0	6.2	107.334	PKKPab	5.12	220.23	99.187
ARCES	20682978	-5.8018	151.1546	27.0	2000-037:11.33.53.0	6.2	107.334	PKKPbc	10.01	256.08	63.391
ARCES	20657541	-11.4416	165.5249	0.0	2000-005:12.12.04.1	4.7	116.661	PKP	21.78	98.09	172.096
ARCES	20690379	-13.7422	167.7477	0.0	2000-047:22.11.20.1	4.0	119.418	PKP	48.33	75.47	50.840
ARCES	20626420	-16.3801	168.2151	0.0	1999-330:19.36.05.6	5.2	122.070	PKP	34.15	89.85	67.309
ARCES	20672510	-17.2153	-173.8116	0.0	2000-026:13.26.46.5	5.6	126.340	PKP	20.04	15.44	73.672
ARCES	20647915	-56.2004	146.6543	0.0	1999-358:19.26.05.7	5.2	151.396	PKPbc	49.74	126.43	98.126
ARCES	20720795	-62.8570	146.0535	0.0	2000-065:23.57.03.4	5.8	156.041	PKP	4.71	308.86	38.180
ARCES	20720795	-62.8570	146.0535	0.0	2000-065:23.57.03.4	5.8	156.041	PKPab	23.49	99.59	29.682

Signal-to-noise ratio vs. distance

We would like the TM procedure for estimating the network detection capability to resemble the IDC procedure for estimating m_b. At the IDC, a third order Butterworth filter with a passband between 0.8 and 4.5 Hz is applied to the data prior to the estimation of signal amplitude and period. The same prefilter should ideally be applied prior to the generation of the STA envelopes, but we also have to take into consideration the frequency band where we expect the highest SNR.

In Figs. 6.5.3 and 6.5.4 we have plotted the average log(STA) for all noise segments preceding the P-phases versus frequency to see if there are noise peaks that should be avoided. To find the frequency range in which we expect the highest SNR, we have plotted the SNR (STA/LTA) measured in narrow frequency bands vs. the distance to the events in Figs. 6.5.5 and 6.5.6. For each event we have normalized the maximum SNR to 50 dB. For ARCES we see that the frequency with the maximum SNR changes significantly with distance, and we will therefore generate separate tuning parameters for the regional (0 - 15 degrees) and teleseismic (15 - 180 degrees) cases. The best SNR for PDYAR is more consistent, being below 3.0 Hz at all distances.

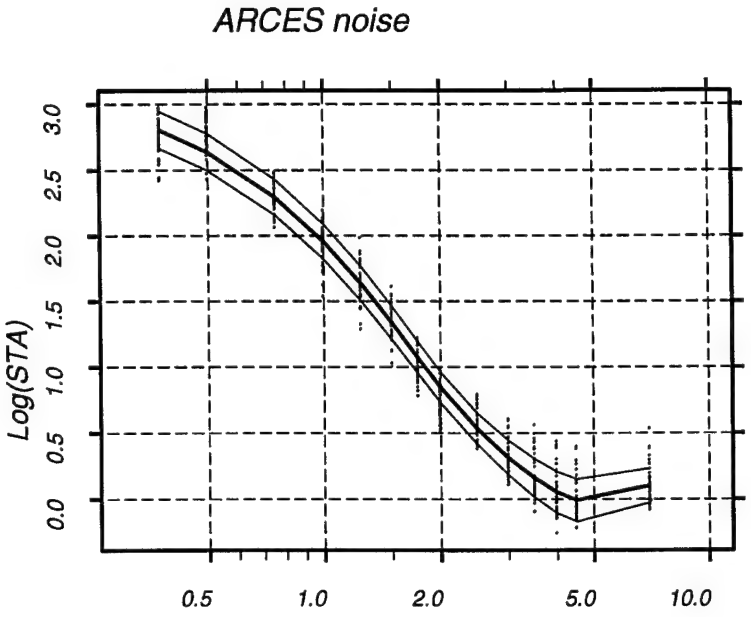

Fig. 6.5.3. Average narrowband log(STA) of the ARCES noise segments plotted versus frequency. Lines ±1σ around the mean are also shown.

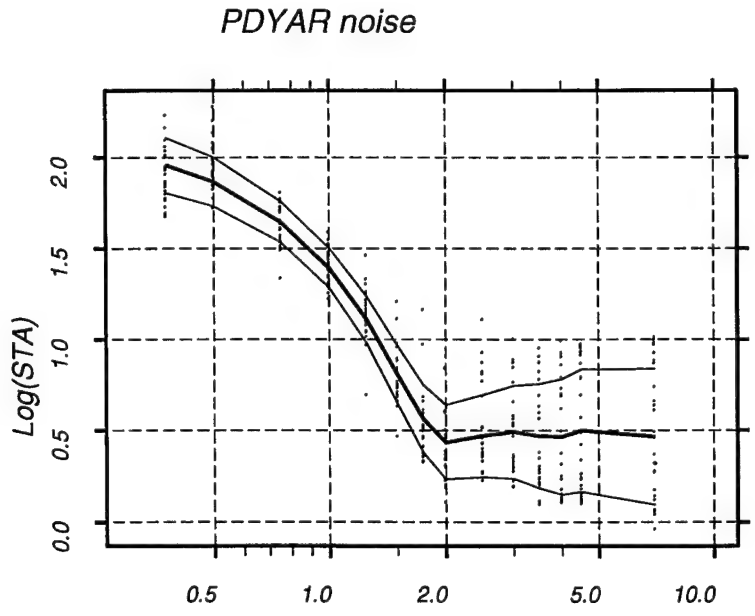

Fig. 6.5.4. Average narrowband log(STA) of the PDYAR noise segments plotted versus frequency. Lines ±1σ around the mean are also shown.

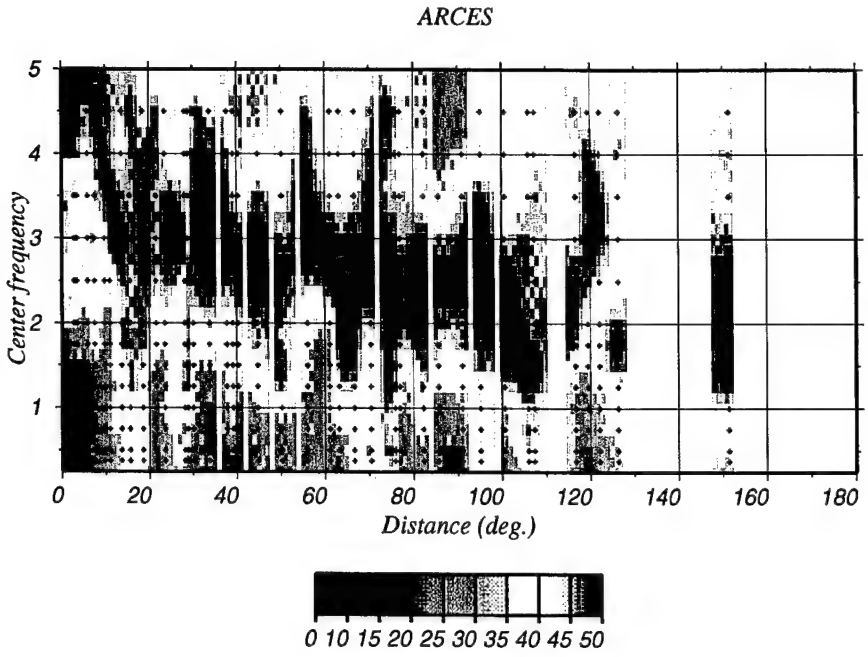

Fig. 6.5.5. SNR (STA/LTA) versus distance for events recorded at ARCES. The maximum SNR is normalized to 50 dB.

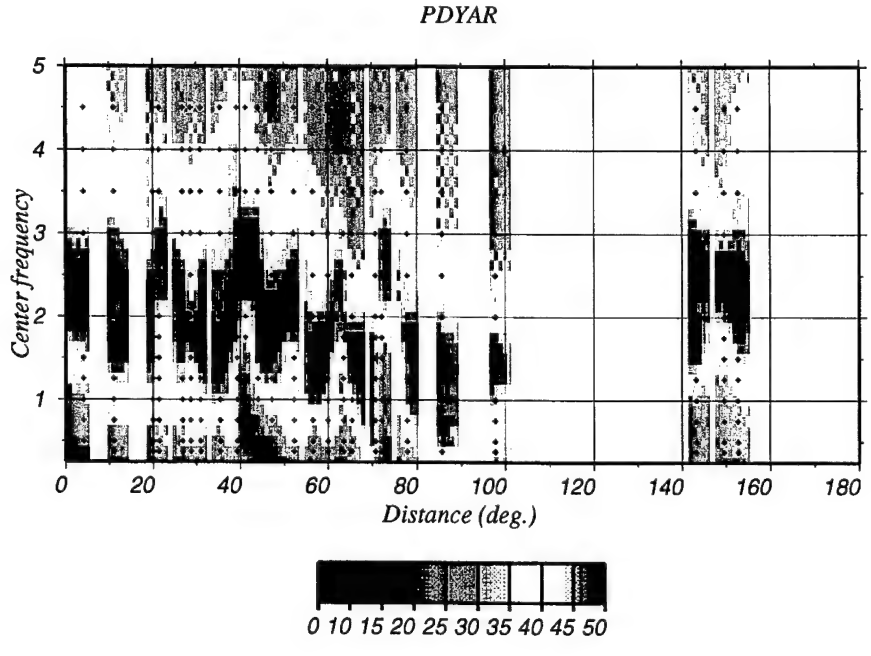

Fig. 6.5.6. SNR (STA/LTA) versus distance for events recorded at PDYAR. The maximum SNR is normalized to 50 dB.

Prefiltering

When choosing the prefilter cutoffs from the tuning events, we try to balance low amplitudes during noise conditions with a good recovery of the signal amplitudes. The frequencies may be different from those used for routine magnitude estimation.

To be able to relate the log(STA) estimates used by the TM system to the log(A/T) estimates used for magnitude estimation at the IDC, we manually measure log(A/T) of the tuning events. A/T is measured on beams steered with the azimuths and slownesses of the P-phases, and filtered between 0.8 and 4.5 Hz. The A/T measurements are made on the maximum amplitude occurring within 8 seconds of the first arrival.

Based on the average noise characteristics (see Figs. 6.5.3 and 6.5.4) and the frequency range with the highest SNR (see Figs. 6.5.5 and 6.5.6), we will test a series of filters for subsequent use in the TM system. For PDYAR, the frequency ranges with maximum SNR show no significant distance dependent trend, and we therefore propose to use the same prefilter for all distances. ARCES, on the other hand, will require separate prefilters for the regional and teleseismic cases.

For ARCES (regional and teleseismic) and PDYAR we show in Figs. 6.5.7, 6.5.8, and 6.5.9 results from comparing the reference measurements in the 0.8 - 4.5 Hz filter band with the $\log((\pi/2) \cdot STA \cdot calib)$ measurements in three different filter bands (several other filters have also been tested). This average difference is later referred to as ATcomp. Mean and Median (ATcomp) give the average difference for the events. St.dev. gives the standard deviation of the differences and Noise gives the average STA level of the preceding noise.

For PDYAR we see that for STAs measured in the 0.8 - 4.5 Hz filter band (upper panel) there is, as expected, a very good correspondence with the reference A/T values. The median difference is -0.05 with a standard deviation of 0.05 and average noise value of -0.59 (all values given in m_b units). As expected, the best filter band for ARCES at regional distances (2.5 - 8.0 Hz, median -0.07 mb, standard deviation 0.203 m_b, and average noise value -1.12 m_b) is higher in frequency than that for teleseismic distances (1.5 - 6.0 Hz, median 0.21 m_b, standard deviation 0.176 m_b, and average noise value -0.427 m_b).

When deciding which prefilter to use, we find that the filter bands described above best combine low amplitudes during noise conditions with a good and stable recovery of the signal amplitudes for the three cases. When processing data in these frequency bands we should subtract the relevant median values (ATcomp) from the estimates to make them compatible with the magnitude estimation procedure at the IDC.

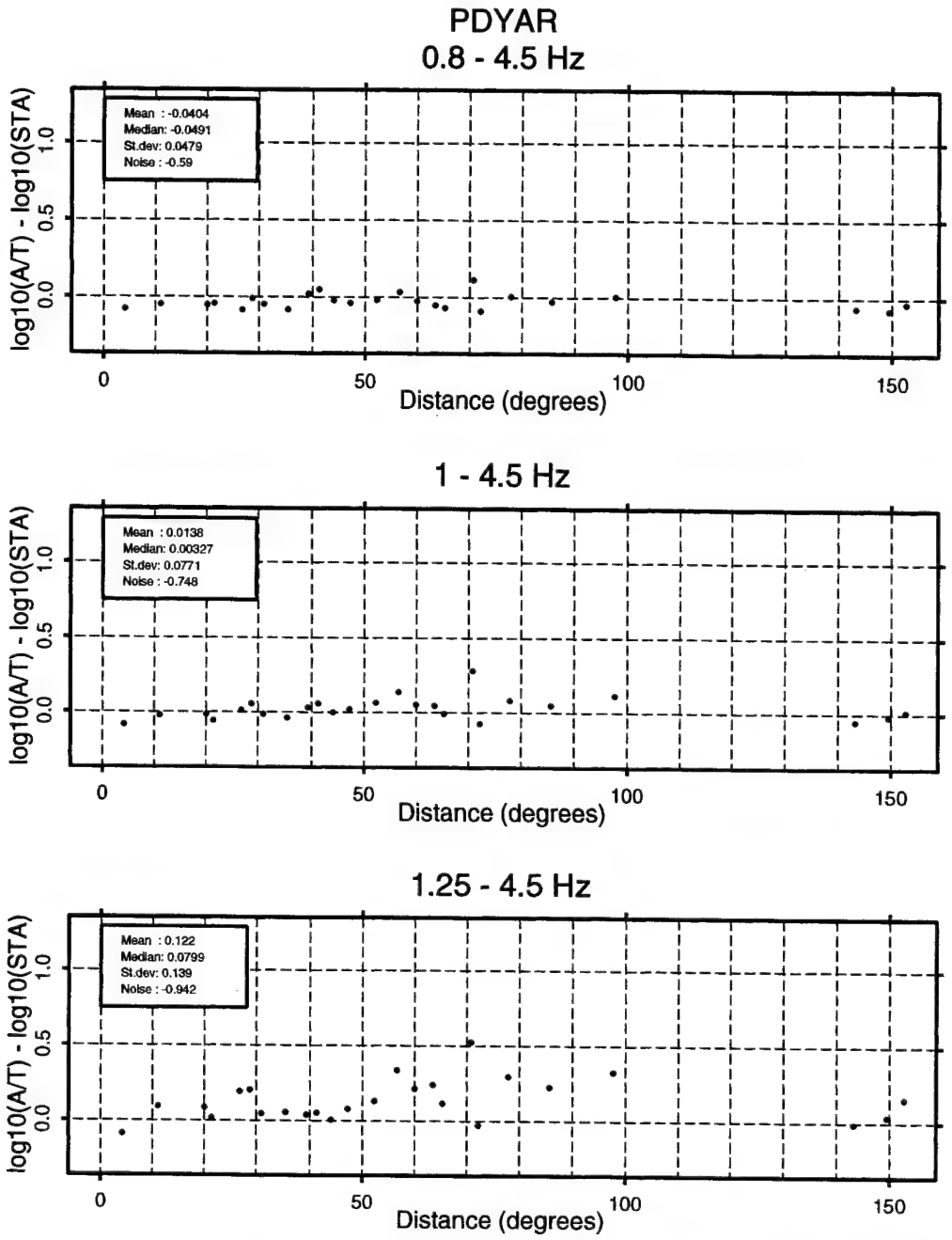

Fig. 6.5.7. Panels showing the differences between the reference $\log(A/T)$ *measurements (0.8-4.5 Hz) and* $\log((\pi/2) \cdot STA \times calib)$ *measured in three different filter bands. All tuning events at PDYAR have been considered. The mean and median differences and standard deviations are shown for the events along with the average STA level of the preceding noise.*

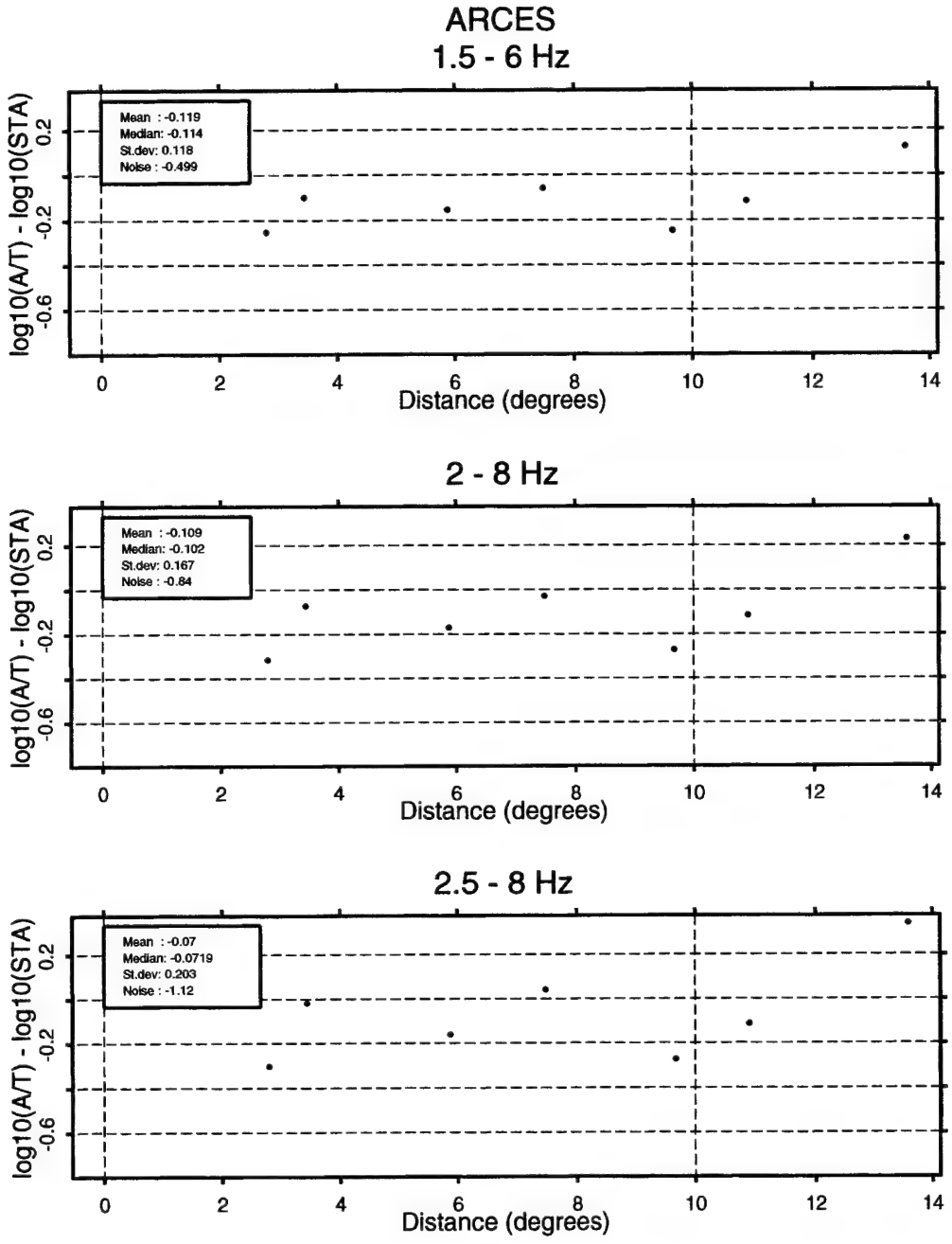

Fig. 6.5.8. Panels showing the differences between the reference $\log(A/T)$ *measurements (0.8-4.5 Hz) and* $\log((\pi/2) \cdot STA \times calib)$ *measured in three different filter bands. All regional tuning events at ARCES have been considered. The mean and median differences and standard deviations are shown for the events along with the average STA level of the preceding noise.*

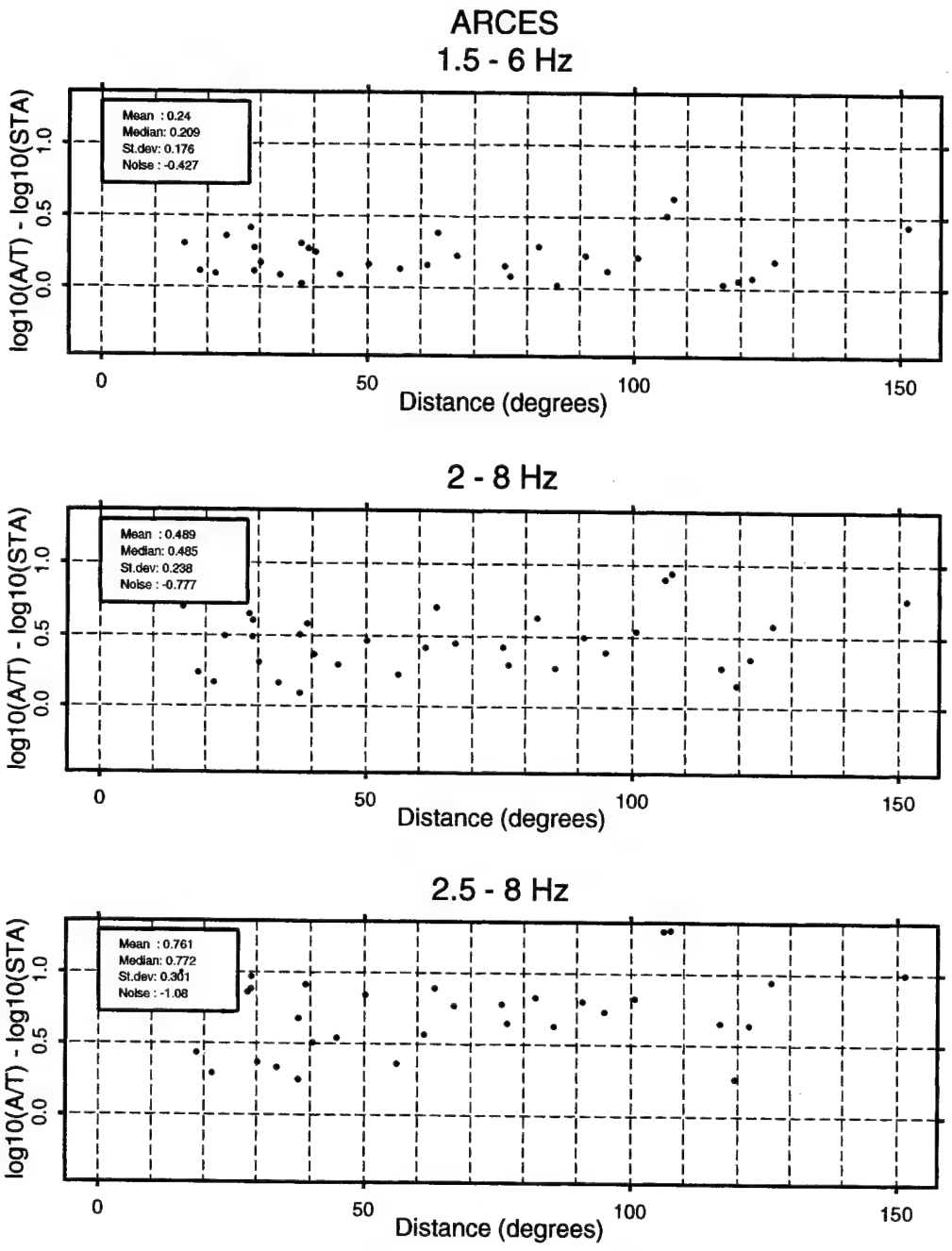

Fig. 6.5.9. Panels showing the differences between the reference $\log(A/T)$ *measurements (0.8-4.5 Hz) and* $\log((\pi/2) \cdot STA \times calib)$ *measured in three different filter bands. All teleseismic tuning events at ARCES have been considered. The mean and median differences and standard deviations are shown for the events along with the average STA level of the preceding noise.*

Signal Loss and Mis-steering

As outlined in the Threshold Monitoring Operations Manual (Taylor et. al., 1998), we need to have available estimates of the expected beamforming signal loss as a function of the mis-steering of the beams for each array. This is done by measuring the signal loss as a function of the mis-steering of the filtered beams, according to the relation:

sloss=(beam STA)/(Average STA of individual sensors)

where STA is taken to be the maximum within 8 seconds of the first arrival.

In Fig. 6.5.10 we show the signal loss as a function of mis-steering for all regional ARCES events. As discussed in the preceding section, the prefilter passband 2.5 - 8.0 Hz was applied to the data. We see from the figure that the average signal loss for correct beam steering is 1.37 dB, and that an additional 3 dB signal loss is expected to be found at a mis-steering of 0.0432 s/km.

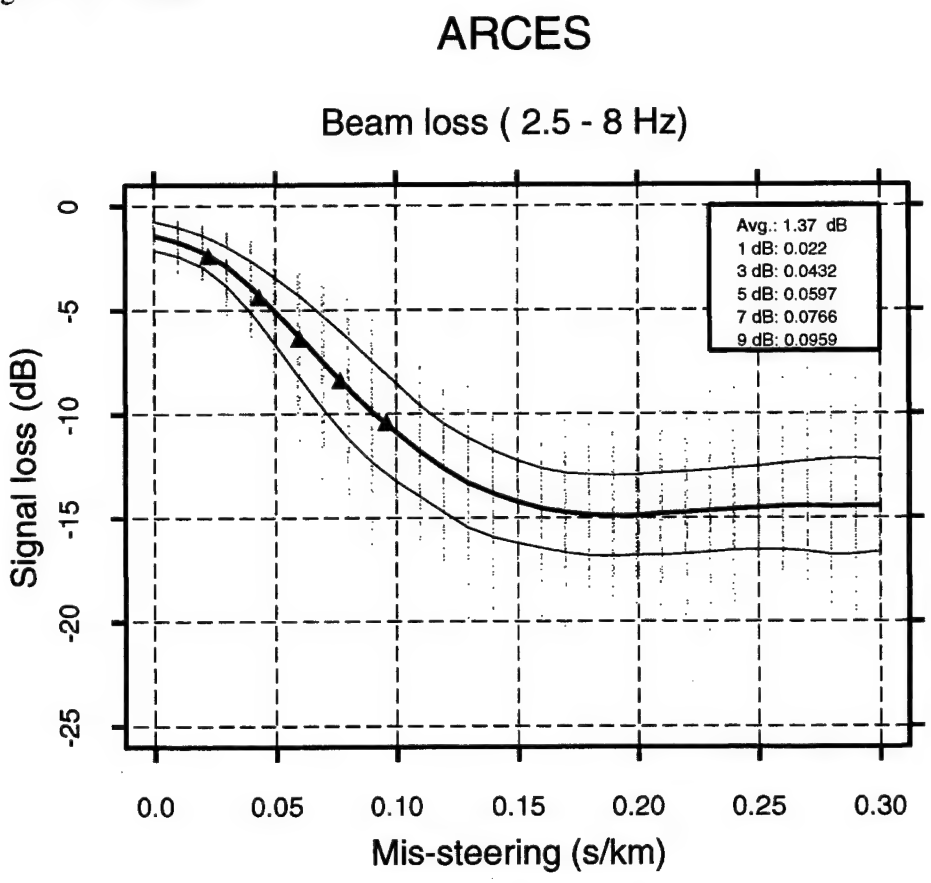

Fig. 6.5.10. Signal loss for ARCES regional events prefiltered in the passband 2.5-8.0 Hz. The three lines show the average and the 1 σ levels of the signal loss. For no mis-steering the average signal loss is 1.31 dB. An additional 3 dB signal loss is expected at a mis-steering of 0.0432 s/km.

In Fig. 6.5.11 we show the signal loss as a function of mis-steering for all teleseismic ARCES events for beams filtered in the passband 1.5 - 6.0 Hz. The average signal loss for correct beam steering is 0.541 dB, and an additional 3 dB signal loss is expected to be found at a mis-steering of 0.106 s/km.

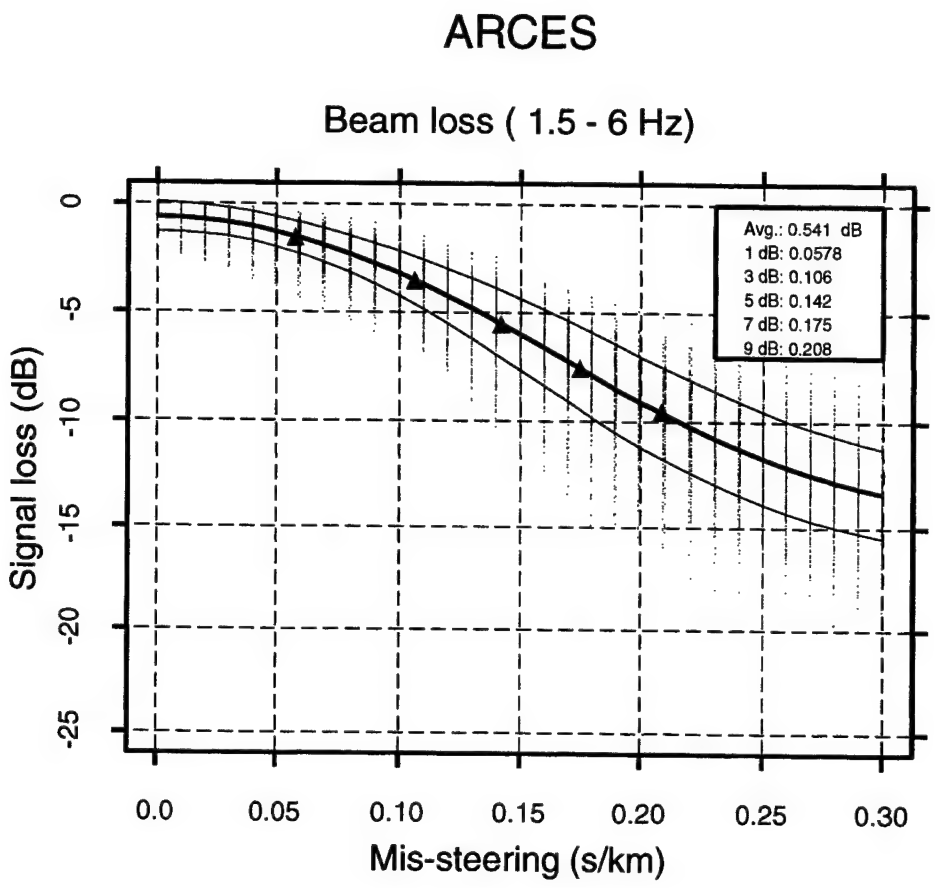

Fig. 6.5.11. Signal loss for ARCES teleseismic events prefiltered in the passband 1.5-6.0 Hz. The three lines show the average and the 1 σ levels of the signal loss. For no mis-steering the average signal loss is 0.541 dB. An additional 3 dB signal loss is expected at a mis-steering of 0.105 s/km.

In Fig. 6.5.12 we show the signal loss as a function of mis-steering for all PDYAR events for beams filtered in the passband 0.8 - 4.5 Hz. The average signal loss for correct beam steering is 1.28 dB, and an additional 3 dB signal loss is expected to be found at a mis-steering of 0.0962 s/km.

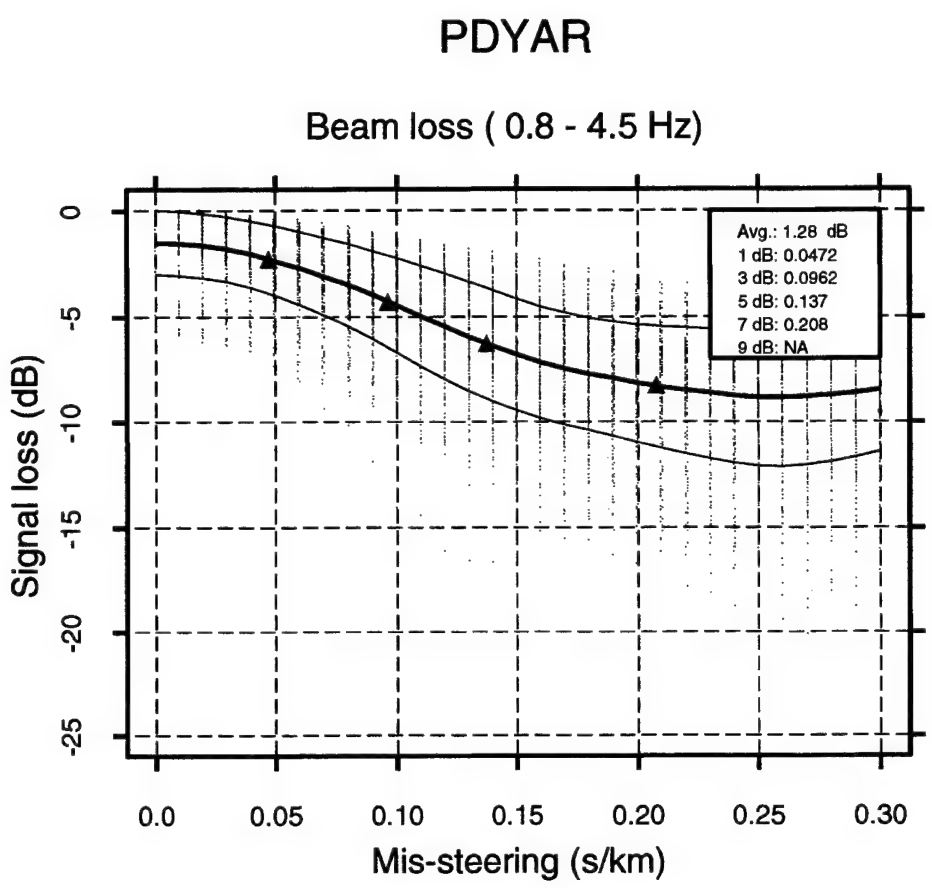

Fig. 6.5.12. Signal loss for PDYAR events prefiltered in the passband 0.8-4.5 Hz. The three lines show the average and the 1 σ levels of the signal loss. For no mis-steering the average signal loss is 1.28 dB. An additional 3 dB signal loss is expected at a mis-steering of 0.0962 s/km.

Beam Deployment

According to the IASP91 travel-time tables, the P phases used for estimation of network detection thresholds span the slowness range 0.0 - 0.124 s/km. This range corresponds to the distance range (0 - 180 degrees) appropriate for PDYAR. For ARCES, we divide this range into two parts corresponding to the regional (0 - 15 degrees, 0.098 - 0.124 s/km) and teleseismic (15 - 180 degrees, 0.0 - 0.098 s/km) cases. Beams must be deployed such that no part of the relevant slowness range will experience more than a 3 dB signal loss.

For ARCES regional beams we expect the 3 dB signal loss at a mis-steering of 0.0432 s/km (see **Fig.** 6.5.10). The procedure for deploying the beams is illustrated in Fig. 6.5.13, where the dashed circles with radii of 0.0432 s/km (3 dB level) cover the slowness range 0.098 - 0.124 s/km. The center points of the small circles correspond to the steering parameters of the beams.

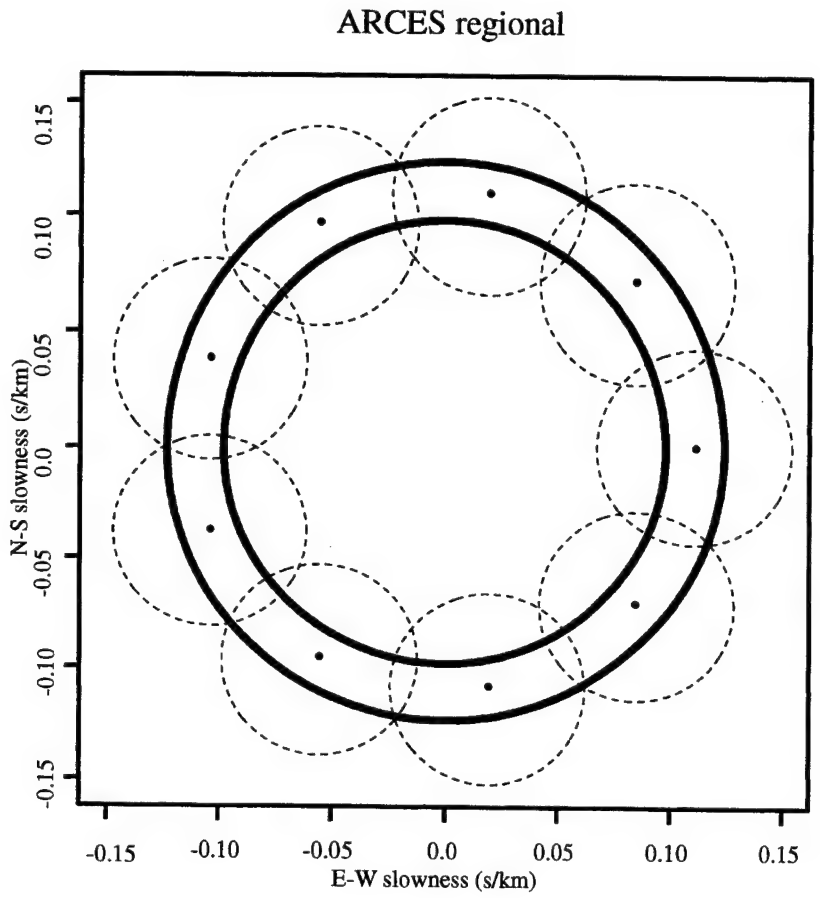

Fig. 6.5.13. Regional ARCES beam deployment used in the TM system for assessing the detection capability in the distance range 0-15 degrees. The area between the solid circles corresponds to the expected slowness range of P-phases from surface events in this distance range. In order to ensure complete coverage within the 3 dB level, it was necessary to deploy 9 beams, represented by the centers of the dashed circles. The radius of each small circle is 0.0432 s/km, corresponding to the expected mis-steering associated with the 3 dB signal loss.

For ARCES teleseismic beams we expect the 3 dB signal loss at a mis-steering of 0.106 s/km (see Fig. 6.5.11). The procedure for deploying the beams is illustrated in Fig. 6.5.13, where the dashed circles with radii of 0.106 s/km (3 dB level) cover the slowness range 0.0-0.098 s/km. The center points of the small circles correspond to the steering parameters of the beams.

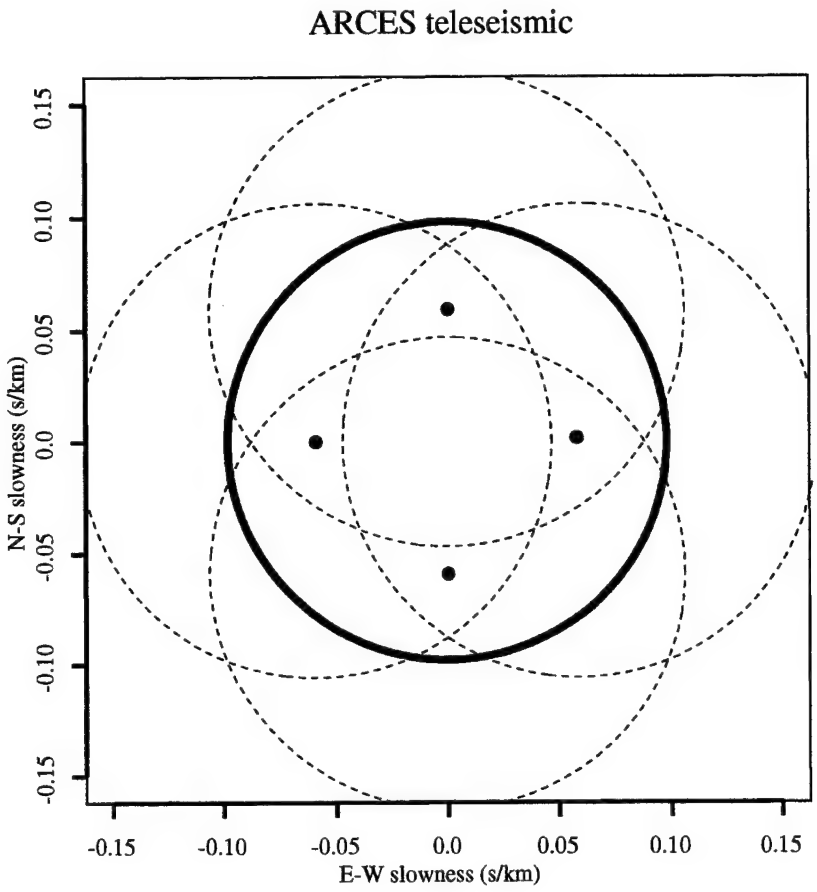

Fig. 6.5.14. Teleseismic ARCES beam deployment used in the TM system for assessing the detection capability in the distance range 15-180 degrees. The area within the solid circle corresponds to the expected slowness range of P-phases from surface events in this distance range. In order to ensure complete coverage within the 3 dB level, it was necessary to deploy 4 beams, represented by the centers of the dashed circles. The radius of each small circle is 0.106 s/km, corresponding to the expected mis-steering associated with the 3 dB signal loss.

For PDYAR beams we expect the 3 dB signal loss at a mis-steering of 0.0962 s/km (see Fig. 6.5.12). The procedure for deploying the beams is illustrated in Fig. 6.5.15, where the dashed circles with radii of 0.0962 s/km (3 dB level) cover the slowness range 0.0-0.124 s/km. The center points of the small circles correspond to the steering parameters of the beams.

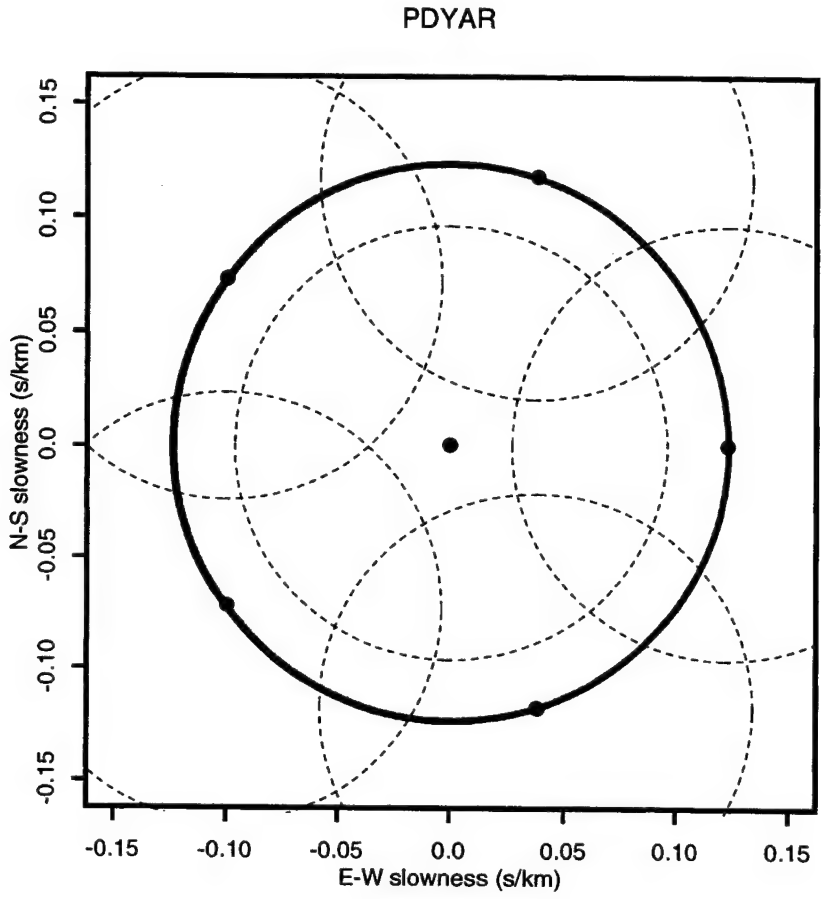

Fig. 6.5.15. PDYAR beam deployment used in the TM system for assessing the detection capability in the distance range 0-180 degrees. The area within the solid circle corresponds to the expected slowness range of P-phases from surface events in this distance range. In order to ensure complete coverage within the 3 dB level, it was necessary to deploy 6 beams, represented by the centers of the dashed circles. The radius of each small circle is 0.0962 s/km, corresponding to the expected mis-steering associated with the 3 dB signal loss.

Details on the tuned processing parameters for ARCES and PDYAR are given in Tables 6.5.3-6.5.5 below.

Table 6.5.3: Definitions of Array Configurations

Array	Configuration	sta_chan
ARCES	vertical	ARA0_sz ARB1_sz ARB2_sz ARB3_sz ARB4_sz ARB5_sz ARC1_sz ARC2_sz ARC3_sz ARC4_sz ARC5_sz ARC6_sz ARC7_sz ARD1_sz ARD2_sz ARD3_sz ARD4_sz ARD5_sz ARD6_sz ARD7_sz ARD8_sz ARD9_sz
PDYAR	vertical	PDY01_sz PDY02_sz PDY03_sz PDY04_sz PDY05_sz PDY06_sz PDY07_sz PDY08_sz PDY09_sz

Table 6.5.4: TM Tuning Parameters

Array	Distance interval (deg)	Config.	Frequency band (Hz)	A/T correction (m_b units)	Signal loss (dB)	3 dB level (s/km)	Number of beams
ARCES	0-15	vertical	2.5 - 8.0	–0.072±0.203	1.370	0.043	9
ARCES	15-180	vertical	1.5 - 6.0	0.209±0.176	0.541	0.106	4
PDYAR	0-180	vertical	0.8 - 4.5	–0.049±0.048	1.280	0.096	6

Table 6.5.5: Beam Steering Parameters

Array	Distance interval (deg)	Azimuth (deg) and slowness (s/km) of beams					
ARCES	0-15	0.0, 0.111	40.0, 0.111	80.0, 0.111	115.0, 0.111	160.0, 0.111	150.0, 0.111
		240.0, 0.111	280.0, 0.111	315.0, 0.111			
	15-180	0.0, 0.059	90.0, 0.059	180.0, 0.059	270.0, 0.059		
PDYAR	0-180	0.0, 0.0	0.0, 0.123	72.0, 0.123	144.0, 0.123	216.0, 0.123	288.0, 0.123

References

Taylor, L., T. Kværna, and F. Ringdal (1998). Threshold Monitoring Operations Manual. NORSAR Contribution No. 639.

T. Kværna
L. Taylor

6.6 Source properties and focal depth of the M_S 4.2 Revda (Lovozero) earthquake of August 17, 1999

Introduction

Between mid May and end of September,1999, 13 Lennartz MARSlite data loggers equipped with three-component LE-3D/5s broad band seismometers with a sampling rate of 125 Hz were in operation over an area of about 200 km NS and 350 km EW in Finnmark (see Fig. 6.6.1). The purpose of the experiment, which was conducted in cooperation with the University of Potsdam, was partly to study possible earthquakes along the prominent postglacial Stuoragurra fault in Masi (Olesen 1988; Bungum and Lindholm, 1996; Dehls et al., 2000), and partly to study regional seismicity and associated source and attenuation characteristics, including events from mines on the Kola peninsula.

More details about this experiment can be found in Schweitzer (1999).

Fig. 6.6.1 shows the Masi-1999 stations together with the background seismicity from this region (based on Bungum and Lindholm, 1996), including available focal mechanisms. The red circle with a focal mechanism is a local earthquake at the Stuoragurra fault on August 22, 1999, recorded during this experiment, while the Revda earthquake of August 17, 1999 can be seen with a focal mechanism in the southeastern corner of the map. Both of these events are analyzed in this report, the former for anelastic attenuation (Q) and the latter for source properties and focal depth.

The Revda earthquake - observed data from the Masi-1999 network

This Revda (Lovozero) earthquake at M_L 3.9 and M_S 4.2-4.3 (Schweitzer, 1999) was the strongest of the local and regional earthquakes observed during the Masi-1999 field experiment. Fig. 6.6.2 shows the Masi recordings of this event, together with an indication of the regional phases observed, including Pn, Sn, Lg and Rg. The data plotted are corrected for frequency response and bandpass filtered between 0.01 and 50 Hz. The distance range is from 286 to 553 km as seen in the figure.

To present the character and the potentials of the broadband data more clearly we have in Fig. 6.6.3 included the original (vertical) record for channel MA06 (distance 472 km) on top, while further below we have filtered the recording sequentially with one octave wide bandwidth filters between 0.05 and 50 Hz. The contribution of the different wave groups to the seismic signal becomes obvious from this display, in that:

- for frequencies up to 1 Hz the surface wave Rg is dominant,
- between 1 and 8 Hz the signal is mainly composed by the Lg and Sn wave group, and
- for frequencies above 8 Hz the signal is dominated by scattering.

The low-frequency Rg wave is sensitive to the velocity-depth distribution of the upper part of the crust. The arrival time for Rg increases with frequency indicating both a pronounced dispersion and a corresponding strong velocity gradient within the crust. With increasing fre-

quency the seismic waves become sensitive to 2D and 3D small-scale heterogeneities within the crust resulting in multiple scattering.

Fig. 6.6.4 shows the displacement spectra of the Revda earthquake for 12 of the Masi stations, corrected for the instrument response. The signal amplitude spectra are drawn as solid lines, and the corresponding noise spectra as computed for a 120 s time window preceding the signal onset are indicated by dotted lines. For all stations, the signals are above the noise for frequencies higher than 0.1 Hz, going at least up to 10 Hz.

The displacement spectra in Fig. 6.6.4 are relatively flat up to about 0.7 Hz and then decay with a slope of about -3 with frequency. For frequencies larger than 1 Hz the stations MA02, MA03, MA09, MA10 and MA12 exhibit frequency peaks which have been identified unambiguously as station effects, tied to the fact that all of these stations are installed on soil sites. Typically these stations are located on top of thin (up to 10 m) sedimentary layers consisting of moraines, which are known to have strong tuning effects for frequencies at about 10Hz (NORSAR and NGI, 1998). The spectra for stations located on solid rock, MA04, MA06, MA07, MA08 and MA13, are all characterized by a relatively simple shape.

Q estimation based on the Masi M_L 2.7 earthquake of August 22, 1999

The purpose of the Masi-1999 experiment with respect to the earthquakes that we hoped to get from the Stuoragurra faults was fulfilled in that several, albeit small, events were recorded over the four months of operation (about what one statistically should expect). The largest of these was a M_L 2.7 earthquake on August 22, 1999, used in the following for estimation of anelastic attenuation (Q).

The response corrected spectra for the Masi event all show similar characteristics as just described for the Revda event, in particular with respect to soil versus rock sites. The rock station spectra are relatively flat up to 10 Hz, which is to be expected since the corner frequency should be expected to be at least at that level for a M_L 2.7 earthquake.

In consequence of this the spectra of the rock stations were analyzed for an average Q in the frequency range between 1 and 10 Hz. The analysis is based on an iterative method, which adjusts Q and station corrections simultaneously in order to match the average level of the amplitude spectra, making the procedure independent of assumptions on geometrical spreading. The result is a relatively high Q of about 1400. Furthermore, it turned out that the station correction for the rock stations are almost negligible.

Fig. 6.6.5 displays the Q-corrected spectra of the rock stations. The spectra now have almost the same level between 1 and 10 Hz, reducing significantly the Q-related roll-off at high frequencies.

The derived Q corrections are also applied to the spectra of the non-rock (moraine) sites. The difference of these spectra from the average level of the rock sites provides frequency-dependent station corrections which will be used in the subsequent analysis of the August 17, 1999, Revda (Lovozero) earthquake in order to compensate for the tuning (soil response) effects.

Full waveform modelling of the Revda earthquake

Full waveform modelling of this event has been conducted using two different methods, a precise frequency-wavenumber (f-k) method as coded by Ray Haddon, and the reflectivity method (Müller, 1985). Both methods compute complete seismograms for 1D velocity models. One difference between the two methods is the implementation of the source. The f-k method computes synthetic seismograms for specified distributions of slip over spatially extensive source regions. In the implementation of the program that we have been using, the particular specified slip distributions are kinematic representations that very closely represent the classical exact elastodynamic dislocation solutions for a circularly symmetric crack in a homogeneous elastic medium for constant stress drop (see, e.g., Madariaga, 1976). For numerical integration purposes, the perfectly continuous slip distribution was discretized. For the modelling with the reflectivity method we used a moment tensor point source with a source function describing a smooth increase of the seismic moment (Brüstle and Müller, 1983).

The main target of the modelling has been the dispersed surface waves and the goal was to resolve the 1D crustal shear wave velocity model and the source depth of the Revda event. In the following we present a few selected modelling results pointing out the effect of different source depths (Fig. 6.6.6) and crustal structure (Table 6.6.1).

Fig. 6.6.6 shows firstly the focal mechanism solution used as a starting point for the synthetics. To this end we used first motion readings from altogether 28 stations, including the MASI-1999 stations and stations from Kola, Finland, Sweden and Norway (denoted as circles and filled squares), resulting in a number of possible solutions. The shaded fault plane solution is the final double-couple solution obtained through a systematic search over mechanism parameter space during the waveform modelling. As a part of this, the seismic moment, the source radius and stress drop were obtained by detailed matching of the source spectrum, which in turn was estimated by averaging all observed spectra after applying the station- and Q-corrections inferred from the analyses of the August 22, 1999, earthquake mentioned above.

We considered various velocity models in order to fit the observed waveforms; Table 6.6.1 shows two of them. Model 1 is a simple two layered crustal model with the Conrad discontinuity at 15 km depth and the Moho discontinuity at 40 km. Model 2, which represents our final model, has the same major discontinuities, but contains additionally a velocity gradient within the uppermost three kilometers. The P-wave velocities and densities are considered to be proportional to the S-wave velocity by a factor $\sqrt{3}$ and 0.7, respectively.

Fig. 6.6.7 shows the comparison of the observed data and the synthetics computed with the f-k method for the crustal model containing the velocity gradient (model 2) for stations MA04, MA06, MA07 and MA09. The results for the other stations are similar and therefore we omit displaying the corresponding plots. In order to match the spectra at the low-frequency end we assumed a circular fault plane with 1.6 km radius and a complete stress drop of 45 bars. The source depth in this case was 5 km. It is seen from the figure that the amplitude spectra of the observed data (solid lines), could be fitted quite well by the synthetics (dashed lines). The absolute values as well as the spectral shape of the individual components (green: vertical, blue: radial, red: transversal) could be modelled successfully within the frequency range from 0.1 to at least 1 Hz. The misfit for frequencies above about 1.5 Hz is a result of chosen discretization.

A better fit at least up to 6 Hz can be achieved by a refinement of the discretization. However, the refinement is associated with additional computational efforts, and the main purpose of this study was to model the low-frequency surface waves.

The bottom part of Fig. 6.6.7 displays the fit of the waveforms. The seismograms are bandpass-filtered between 0.1 and 0.5 Hz and the components are shifted vertically for a better comparision. The synthetics (black) and the observed data (color coded) are scaled in the same way and the lineup is according to the absolute time. The arrival times, the amplitudes and the dispersion of the radial (blue) and vertical (green) component (containing the Rg contribution) are well matched by the synthetics. The fit of the transverse (red) component (containing mainly the Lg-wave group) is sufficient for station MA04, but for the more distant stations (MA06, MA07 MA09) there is a phase shift of about 1.5 s. Such a misfit was consistently present in our modelling results. It was not possible to match the arrival times of Rg and Lg simultaneously using a 1D-velocity model.

Figs. 6.6.8 to 6.6.11 illustrate the effects of different velocity models and of variations in source depth. The synthetics in these cases were computed using the reflectivity method. Fig. 6.6.8 represents the results for the simple two-layered crustal model. The spectra could be modelled reasonably well for frequencies up to 1 Hz. The differences for higher frequencies are seen to be somewhat larger in this case as compared to the f-k method, which is mainly due to the somewhat simpler source function used in the reflectivity modelling. The duration of the source function was chosen as 1 s which results in the lack of high frequency energy. This, however, does not affect our waveform modelling, where we primarily are interested in matching the surface waves in the observed seismograms at low frequencies.

The bottom part of Fig. 6.6.8 again shows the fit of the observed (colored) and synthetic (black) waveform components. Generally the fit is unsatisfactory, because the synthetics exhibit no dispersion. This is of course due to the simple crustal velocity model, which in this case consists of only two homogeneous layers. In order to model the dispersion of the observed data it is necessary to include a velocity variation with depth. We performed various numerical experiments to this end and concluded with a model containing a fairly strong velocity gradient (model 2, Table 6.6.1) as the one which gave the best fit to the observations.

Figs. 6.6.9 and 6.6.10 show the results for crustal model 2 and a focal depth of 2.5 and 7.5 km, respectively. The main effect of a change of the source depth is on the spectra. At the first order, a decrease of the source depth by a factor two results in a frequency doubling of the spectral peak of Rg. This is clearly illustrated in Fig. 6.6.9, where the amplitude spectra of the synthetics are shifted to higher frequencies and the fit between modelled and observed data becomes worse. For a focal depth at 7.5 km (Fig. 6.6.10) the spectra are shifted to lower frequencies, and the observed spectra are slightly underestimated.

The effect of the focal depth on the waveforms is mainly expressed in the duration of the surface wave groups. For the shallow source the synthetics exhibit a multi-cyclic behavior with a gradual decay within a time window of about 15 s. In the case of a source depth of 7.5 km, the synthetics appear to be less dispersive.

Fig. 6.6.11 shows the results for our preferred model 2 with a source depth of 5 km. This results are comparable to those displayed in Fig. 6.6.7, because the same velocity model was used in the two cases. Differences are due to the source models.

The waveform fit of the Rg wave (radial and vertical component) is almost perfect in Fig. 6.6.11, reproducing both the arrival times, the amplitudes and the dispersion characteristics of the observations. The discrepancies for the transverse component remain to be explained. Timing differences between the transverse and radial/vertical components is, however, a common and well known problem for structural modelling using Lg and Rg waves. Anisotropy is often suggested as a possible cause for this phenomenon, but a velocity shift related to small-scale lateral heterogeneities (Müller et al., 1992; Roth et al., 1993) may also contribute to such effects.

From the waveform modelling of the surface waves of the Revda earthquake we conclude that the source depth of the event was deeper than 2.5 km, probably between 4 and 7 km, and that there must be a relatively strong velocity gradient in the uppermost crust.

M. Roth
H. Bungum
R.A.W. Haddon

References

Brüstle, W. and G. Müller (1983): Moment and duration of shallow earthquakes from Love-wave modelling for regional distances. *Phys. Earth Planet. Inter.*, 32, 312-324.

Bungum, H. and C. Lindholm (1997): Seismo- and neotectonics in Finnmark, Kola, and the southern Barents Sea, Part 2: Seismological analysis and seismotectonics. *Tectonophysics*, 270, 15-28.

Dehls, J.F., O. Olesen, L. Olsen and L.H. Blikra (2000): Neotectonic faulting in northern Norway; the Stuoragurra and Normannvikdalen postglacial faults. *Quat. Sci. Rev.*, 19, 1447-1460.

Madariaga, R. (1976): Dynamics of an expanding circular fault. *Bull. Seism. Soc. Am.*, 66, 639-666.

Müller, G. (1985): The reflectivity method: a tutorial. *J. Geophys.*, 58, 153-174.

Müller, G., M. Roth and M. Korn (1992): Seismic-wave traveltimes in random media. *Geophys. J. Int.*, 110, 29-41.

Olesen, O. (1988): The Stuoragurra fault, evidence of neotectonics in the Precambrian of Finnmark, northern Norway. *Nor. Geol. Tidsskr.*, 68, 107-118.

Roth, M., G. Müller and R. Snieder (1993): Velocity shift in random media. *Geophys. J. Int*, 115, 552-563.

Schweitzer, J. (1999). The MASI-1999 field experiment. *In* F. Ringdal (ed.): *Semiannual Technical Report 1 April - 30 September 1999*. NORSAR Sci. Report 1-1999/2000, Kjeller, Norway, pp. 91-101.

Schweitzer, J., F. Krüger, G. Richter, E. Hicks, C. Lindholm and H. Bungum (2000). The 1999 Finnmark seismic field experiment. *In* J. Dehls and O. Olesen (eds.): *Neotectonics in Norway, Annual Technical Report 1999*. NGU (Norwegian Geological Survey) Report 2000.001, pp. 89-97.

Table 6.6.1: Crustal models used in the waveform modeling. Model 1 represents a simple two-layered crust, whereas model 2 includes a strong velocity gradient approximated by thin constant velocity layers. The P-wave velocities and densities are related to the S-wave velocity (β) via the factor 3 and 0.7, respectively.

Crustal Model 1		Crustal Model 2	
Depth (km)	β (km/s)	Depth (km)	β (km/s)
0 - 15	3.65	0 - 0.75	3.25
15 - 40	3.80	0.75 - 1.5	3.35
> 40	4.65	1.5 -2.25	3.45
		2.25 - 3	3.55
		3 - 15	3.65
		15 - 40	3.80
		> 40	4.65

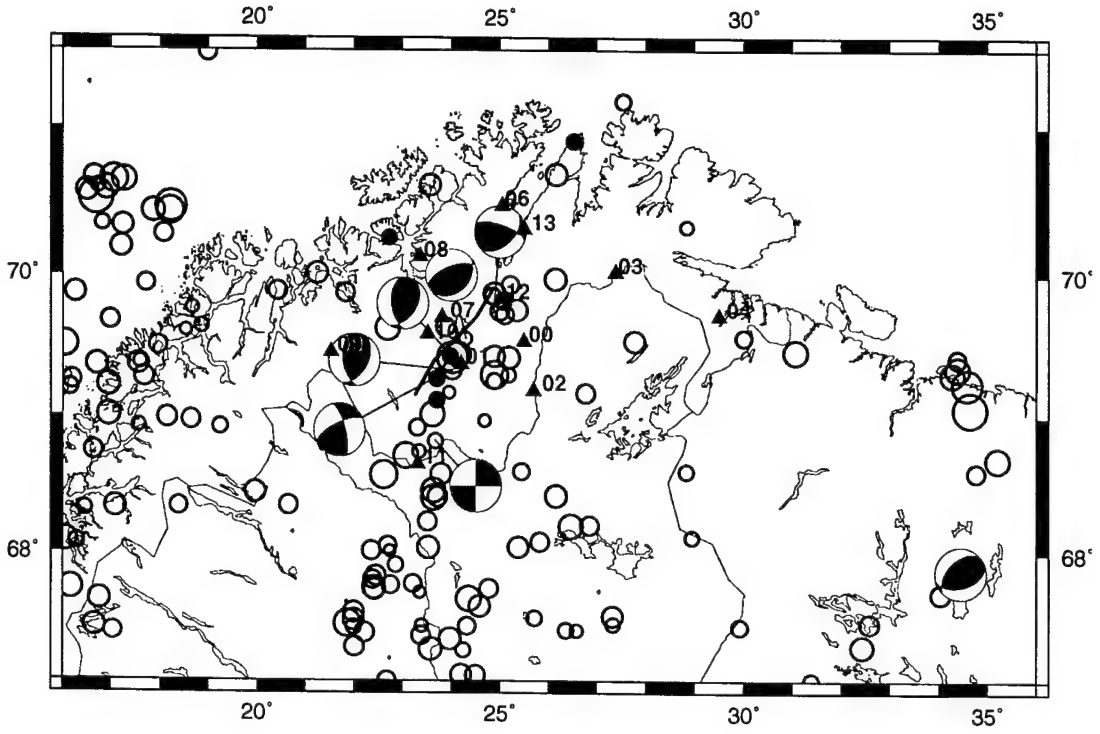

Fig. 6.6.1. The Masi-1999 stations (blue triangles with numbers) together with previous earthquakes in Finnmark for the time period 1979-1992 (Bungum and Lindholm, 1996), updated with earthquakes for the time period 1993-1999 (all with open circles) and preliminary locations from the Masi-1999 network (red circles). Available focal mechanism solutions are also shown, including the M_L 2.7 Masi earthquake of August 22, 1999 (69.276N. 23.685E), used in this study for estimation of Q, and the August 17, 1999, Revda earthquake (67.865N, 34.454E) at the Kola peninsula, which is the focus of the present study. Redrawn from Schweitzer et al. (2000).

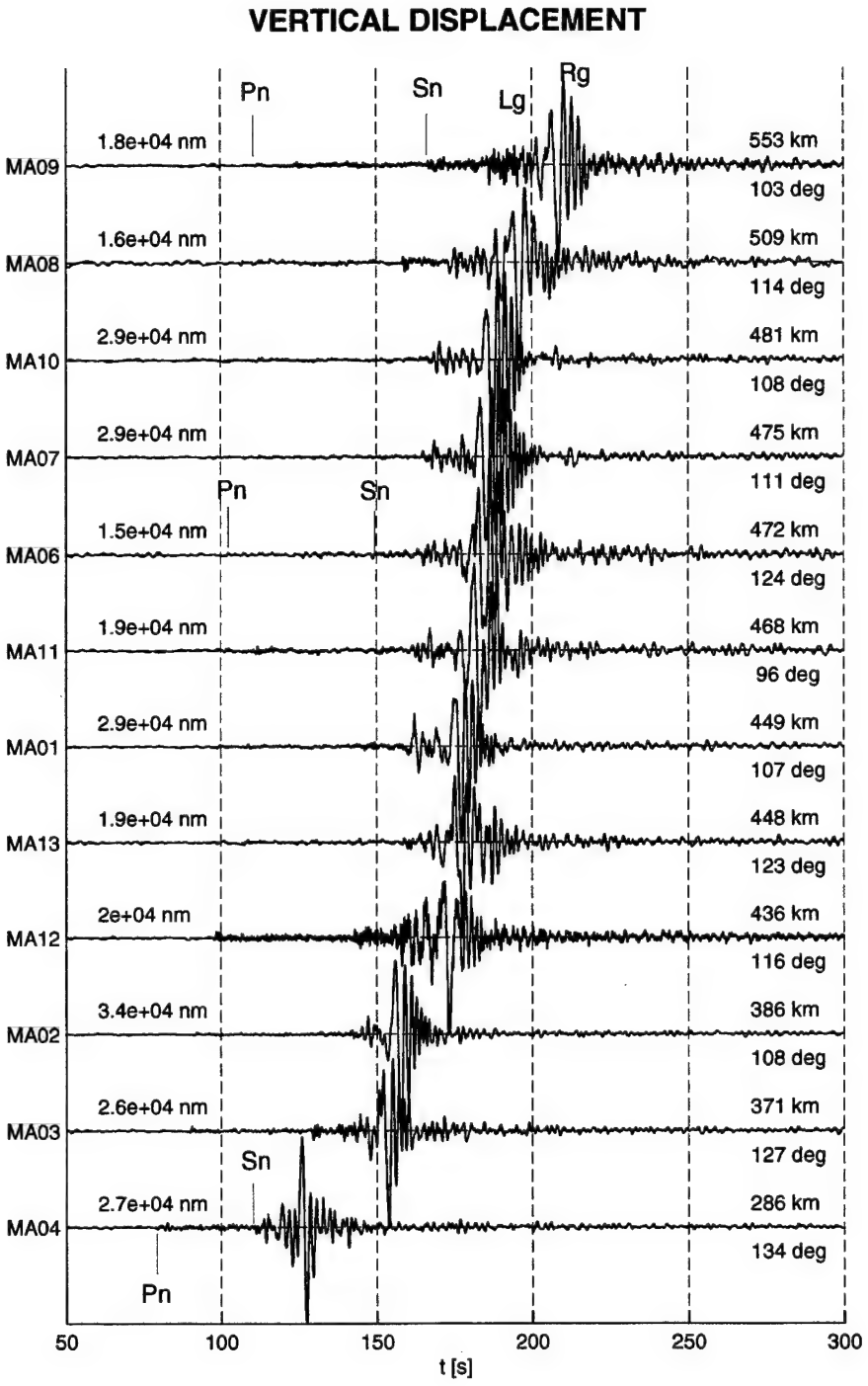

Fig. 6.6.2. Vertical displacement recorded at the stations of the MASI-1999 network for the Revda earthquake. The seismograms are corrected for the instrument response and bandpass filtered between 0.01Hz and 50Hz. The time axis starts at 4:44:50. On the right hand side the epicentral distances and back azimuths are annotated, on the left hand side the trace maximum in units of nm.

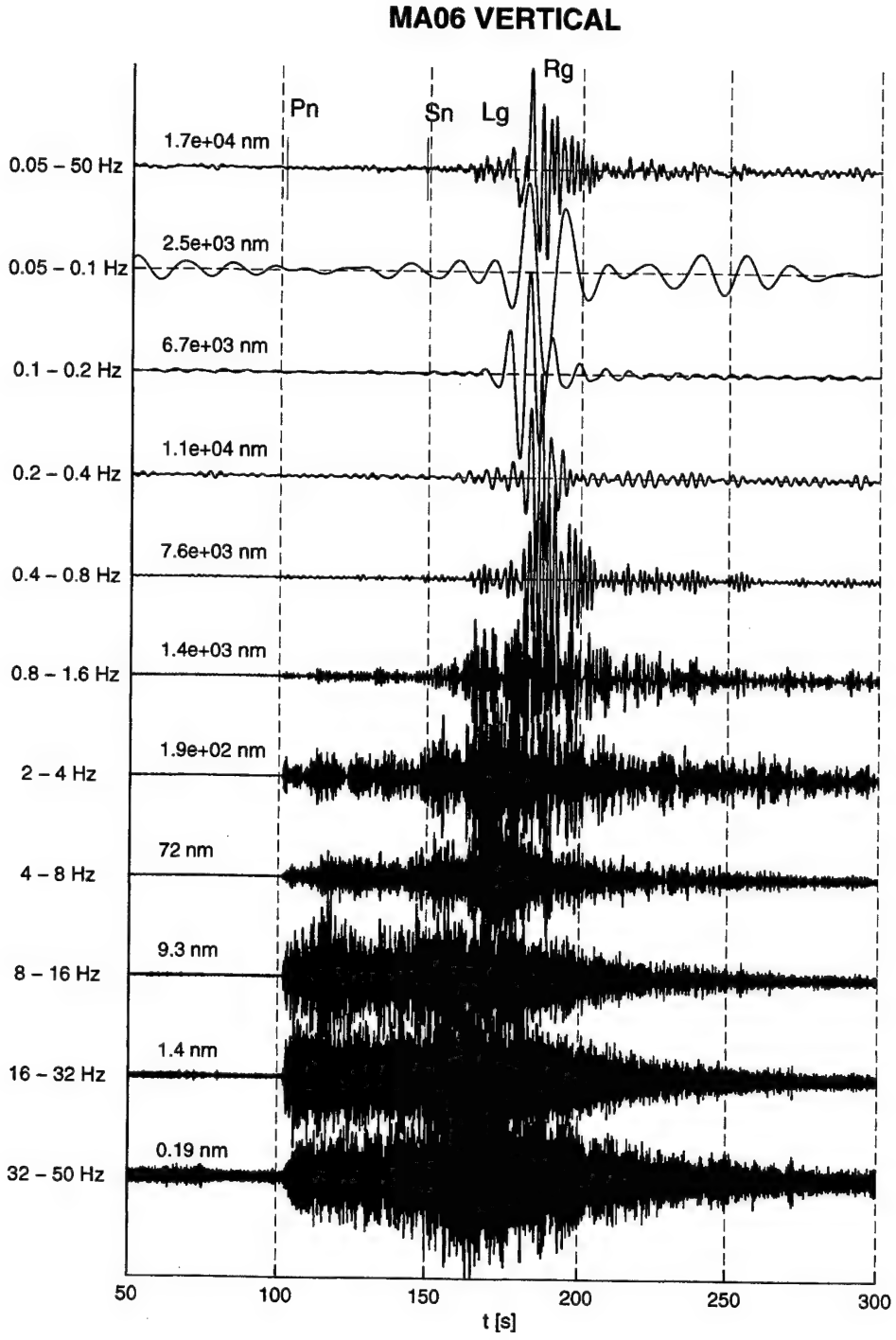

Fig. 6.6.3. Displacements recorded at station MA06 for different frequency bands. See the main text for more details and discussion.

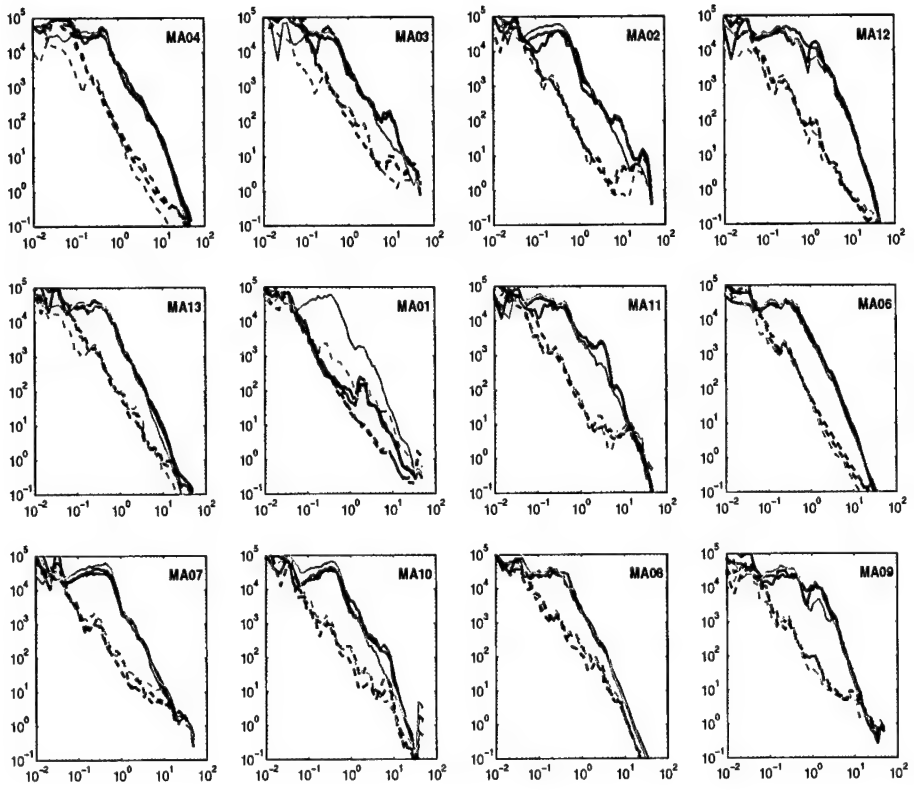

Fig. 6.6.4. Signal (solid lines) and noise (dashed lines) amplitude spectra of the Revda event. The spectra of the three components (vertical: green, radial: blue, transverse: red) are plotted in units of [nm s] versus frequency in [Hz]. The spectra indicate a good signal-to-noise ratio between 0.1 and 10 Hz. The corner frequency of the event is at about 0.7 Hz.

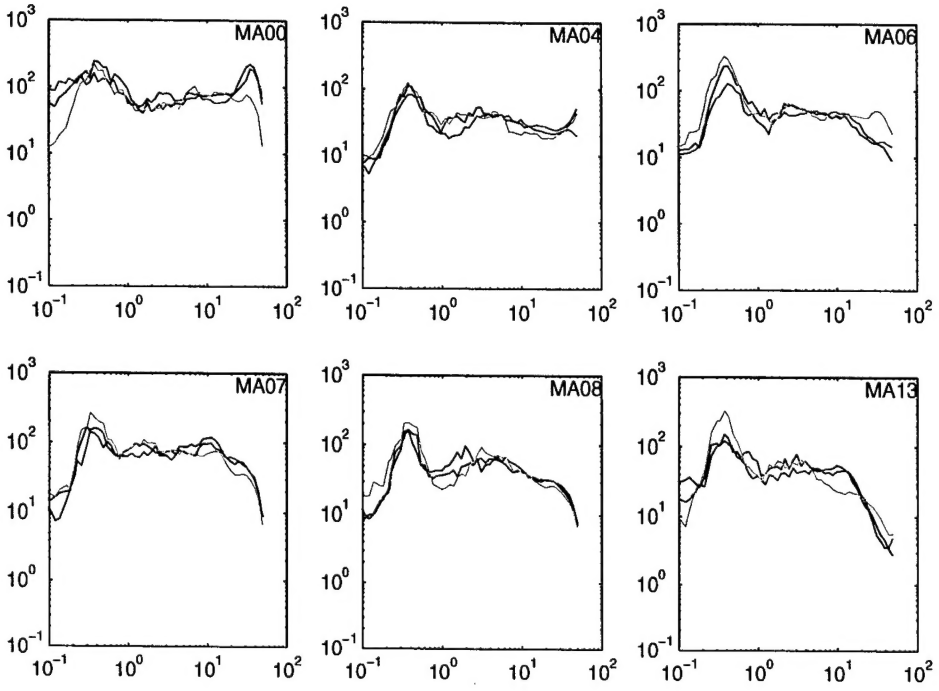

Fig. 6.6.5. Q-corrected spectra for the August 22, 1999, Masi earthquake at the rock sites. The spectra of the three components (red: transverse, blue: radial, green: vertical) are plotted in units of [nm s] versus frequency in [Hz].

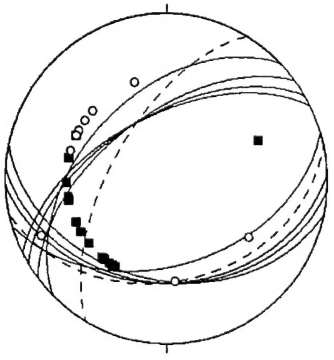

$M_0 = 6x10^{22}$ dyn-cm ($M_W = 4.5$)

Strike = 240°, dip = 60°, rake = 70°

Focal depth = 2.5, 5, 7.5 km

Source radius = 1.6 km (rupture area 8 km^2)

Stress drop $\Delta\sigma$ = 45 bars

Fig. 6.6.6. This figure shows the initial focal mechanism solution for the Revda event derived from 28 first motion readings from Fennoscandia (filled symbols are compressions, open symbols dilatations), with several possible solutions (courtesy of Erik Hicks), used as starting solution for the waveform modelling. The shaded solution is the final one following a systematic search over mechanism parameter space. The parameters for the final solution are shown to right.

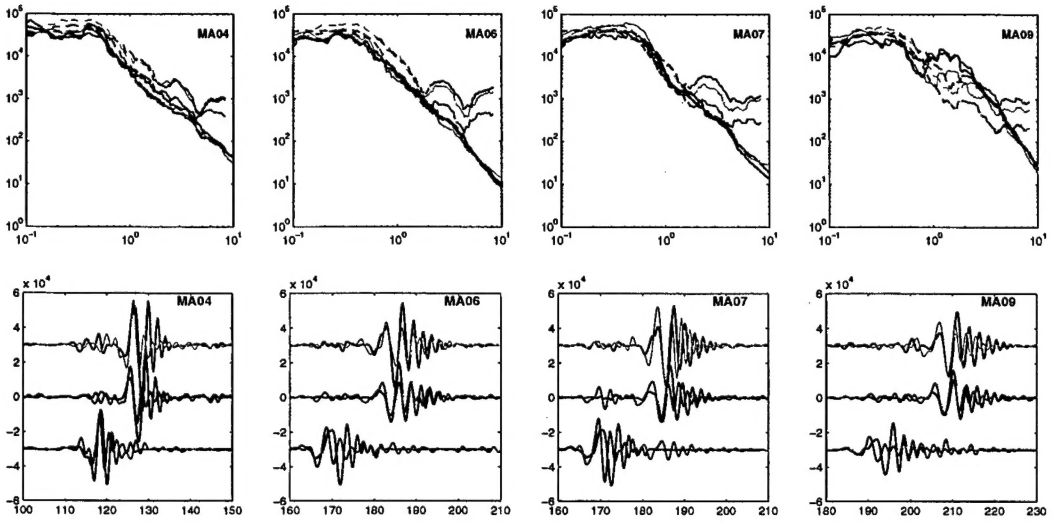

Fig. 6.6.7. Observations and synthetics for model 2 and a source depth of 5 km computed with the f-k method. Top: signal (solid) and modelled (dashed) amplitude spectra (in [nm s]) for the frequency range between 0.1 and 10 Hz, Green, blue and read are the vertical, radial and transverse component, respectively. Bottom: Observed displacement (color coded as above) and modelled displacement (black)

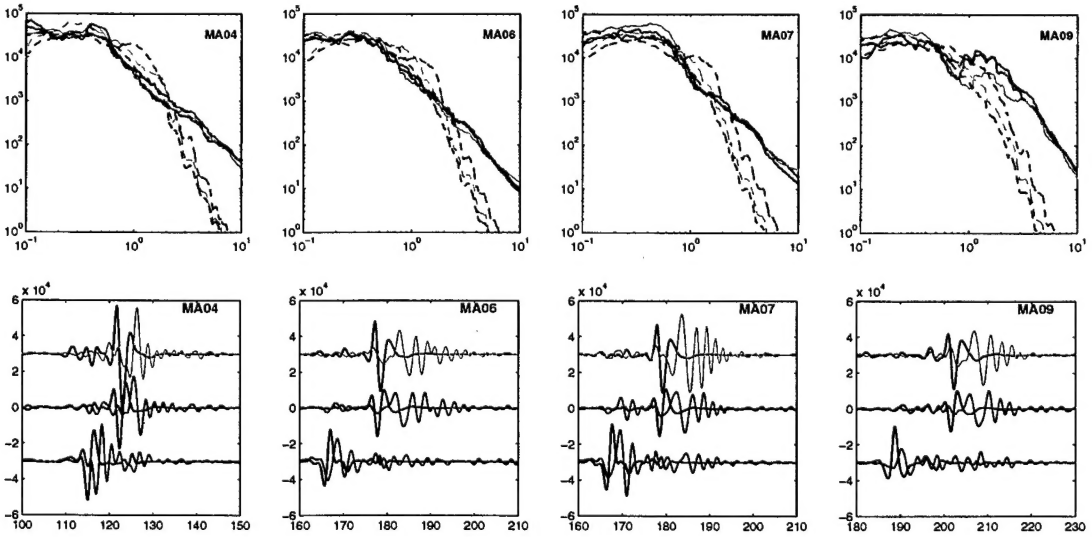

Fig. 6.6.8. Observations and synthetics for model 1 with 5km source depth computed with the reflectivity method (color coding as in Fig. 6.6.7).

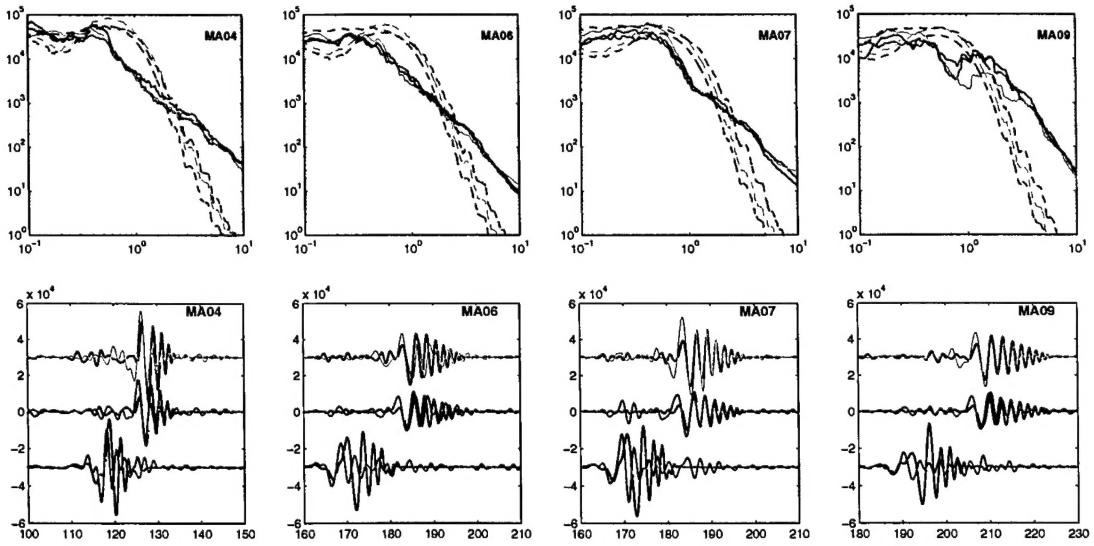

Fig. 6.6.9. Observations and synthetic for crust model 2 and a source depth of 2.5 km computed with the reflectivity method (color coding as in Fig. 6.6.7).

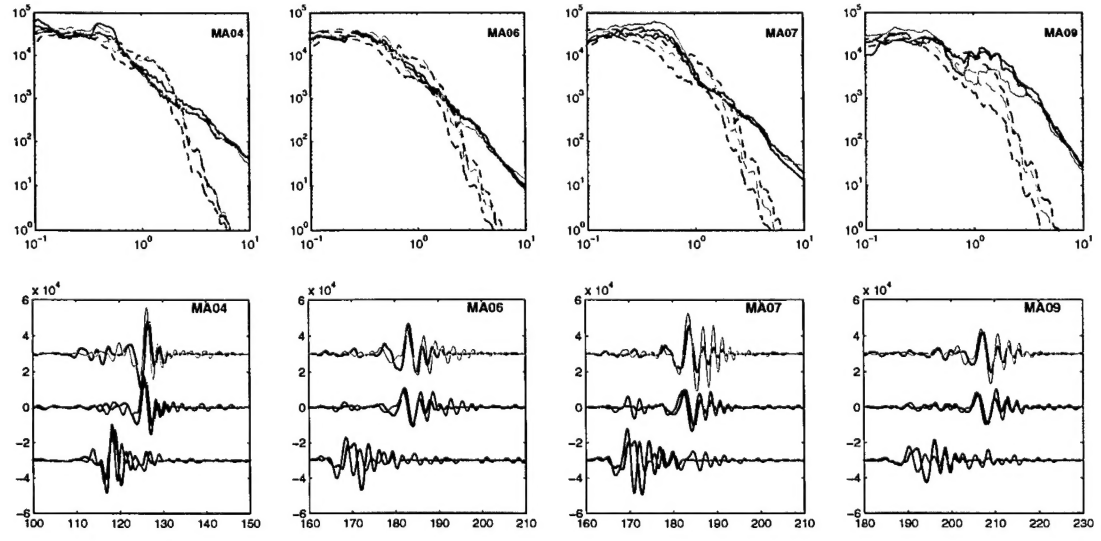

Fig. 6.6.10. Observations and modelling for crust model 2 and a source depth of 7.5 km computed with the reflectivity method (color coding as in Fig. 6.6.7).

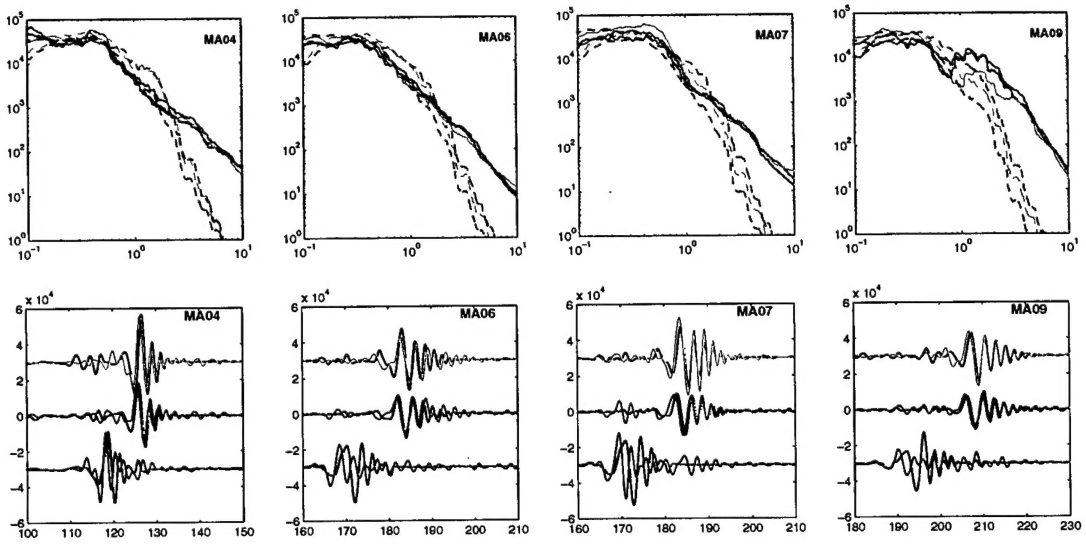

Fig. 6.6.11. Observations and synthetics for model 2 and 5km source depth computed with the reflectivity method (color coding as in Fig. 6.6.7).